2018

Heparan Sulfate, A New Target for Platinum in Metastatic TNBC

Samantha J. Katner
Virginia Commonwealth University

Heparan Sulfate, A New Target for Platinum in Metastatic TNBC

A dissertation submitted in partial fulfillment of the requirements for the degree of Doctor of Philosophy at Virginia Commonwealth University

Author:
Samantha Katner
B.S. Biochemistry, 2011, St. Lawrence University

Principal Investigator:
Dr. Nicholas Farrell
Professor
Chemistry Department

Committee Members:
Dr. Jennifer Koblinski
Dr. Matthew Hartman
Dr. John Ryan
Dr. T.A. Cropp

Virginia Commonwealth University
Richmond, Virginia

April 26, 2018

Acknowledgements

My PhD program has been exciting and intense. I have learned so much and have made life-long connections. I have so many people to thank for this wonderful opportunity. I will attempt to convey my gratitude for them here.

Dr. Nicholas Farrell, thank you for being a supportive and patient mentor. Your encouragement and useful critiques helped me so much in my PhD journey and in preparing for my career.

To my current and former lab mates: Dr. Zhifeng Du, Dr. Angelica Gramin, Dr. Raphael Paiva, Dr. Victor Bernardes, Dr. Daniel Lee, Dr. A. Gerald Daniel, Erica Peterson, David Hampton, Eric Ginsburg, Jamie Beaton, Wyatt Johnson, and Thomas Wells, thank you all for your discussions, and the friendly work environment.

Dr. Jennifer Koblinski, thank you for allowing me to attend your lab meetings, and teaching me all about *in vivo* models. To Dr. Hu, thank you for helping me with the *in vivo* experiments. To Megan Sayyad, thank you for collaborating with me on the *in vitro* BBB assays.

Dr. Matthew Hartman, thank you for allowing me to start my graduate career in your lab and your extraordinary mentorship that continued on. I truly appreciate all that I have learned from you.

To my husband Michael, thank you for your support, encouragement, and taking care of me. I'm very happy and lucky to have you in my life. Peter Rabbit, thank you for making me smile and listening to my practice talks.

Mom and Dad, thank you both for your unwavering support and encouragement all the way from Vermont. All of my accomplishments and success is because of you both.

Table of Contents

Abbreviations, Acronyms, and Frequently Used Terms

Carboplatin	*cis*-diammine(1, 1-cyclobutanedicarboxylato)platinum(II)
CD	Circular dichroism
CHO	Chinese hamster ovary cells
CS	Chondroitin sulfate
Cisplatin	*cis*-diamminedichlorophlatinum(II)
CT-DNA	Calf thymus DNA
DMSO	Dimethyl sulfoxide
EtBr	Ethidium bromide
FBS	Fetal bovine serum
FPX	Fondaparinux
GAG	Glycosaminoglycan
HS	Heparan sulfate
HSPG	Heparan sulfate proteoglycans
IC	Intracardiac injection
ICP-MS	Inductively coupled plasma mass spectrometry
IP	Intraperitoneal injection
IV	Intravenous injection
IVIS	*In vivo* imaging system
MTT	3-4,5-dimethlythiazol-2-yl)-2,5-diphenyltetrazolium bromide
MTD	Maximum tolerated dose
NC	noncovalent
NSG mice	NOD-SCID-IL2R-Gamma null (NSG) mice
PBS	Phosphate buffered saline
PPC	Polynuclear platinum complex
P/S	Penicillin/streptomycin
SPR	Surface plasmon resonance
TAMRA-R_9	Nonaarginine peptide (R_9) coupled to the TAMRA fluorescent label 5-(6)-carboxytetramethylrhodamine
TNBC	Triple negative breast cancer
TPA	*trans*-platinum planar amine
wt	Wild type

List of Figures and Tables

Abstract

HEPARAN SULFATE, A NEW TARGET FOR PLATINUM IN METASTATIC TNBC

Author: Samantha J. Katner, Ph.D.
A dissertation submitted in partial fulfillment of the requirements for the degree of Doctor of Philosophy
Virginia Commonwealth University, 2018
Advisor: Dr. Nicholas Farrell, Professor, Chemistry Department

Heparan sulfate proteoglycans (HSPGs), composed of the linear polysaccharide heparan sulfate (HS) conjugated to a protein core, are located on the cell surface and extracellular matrix. The HS chains display varying degrees of sulfation, which constitutes the molecular recognition motif for many HS-protein interactions. HSPGs, associated growth factors, and heparanase promote tumor progression by facilitating invasion, angiogenesis, and metastasis.[1] Sulfate clusters on the glycan backbone also mediate the interaction of polynuclear platinum complexes (PPCs) with HSPG through a "sulfate clamp." Such PPC-HS interactions can be conceptualized as "polyarginine" mimics. Strong HS-PPC binding protects the oligosaccharide against sulfate loss through metalloshielding.[2] The biological consequences of metalloshielding will in principle affect HS interactions with relevant enzymes and proteins such as heparanase and growth factors, similar in concept to the inhibition of DNA-protein binding through modification of DNA structure and conformation. The end-point of functional modulation of HS interactions is inhibition of angiogenesis and metastasis.

PPCs are dual-function agents through their interactions with both nucleic acids and HS. The novel Pt-HS interactions open up new areas of metalloglycomics and potential anti-angiogenic activity. Here, we report PPC interactions with HS-like models: Fondaparinux (FPX)[3] and heparin[4]. We demonstrate TriplatinNC high affinity to heparin in biophysical studies and compare

HS interactions with DNA and HS using competition assays.[3,4] these approaches may be extended to a range of metal-ammine compounds.[4]

The biological consequences of PPC-HS interactions include modulation of heparanase cleavage of FPX,[3] growth factor binding to HS, and growth factor-induced migration and signaling in breast cancer and endothelial cells, as potential anti-metastatic and anti-angiogenic effects *in vivo*. We report proof-of-principle of strong *in vivo* anti-metastatic activity of PPCs in triple negative breast cancer (TNBC) models.[5–7] Already, PPC-HS interactions have major biological consequences in the aggressive metastatic TNBC mouse models. Impressively, PPCs reduce overall tumor metastases with emphasis in lung, bone, and liver locations in both immunocompetent and immunosuppressive mouse models. PPCs demonstrated permeability through the blood brain barrier (BBB) implying further applications for PPCs. PPCs represent a novel class of intrinsically dual-function agents combining platinum cytotoxicity through DNA targeting with anti-angiogenic effects through glycan targeting. Together, these results suggest that strong PPC-HS interactions have a significant role in the inhibition of breast cancer metastases, particularly in metastatic TNBC patients.

1. Peterson, E. J. *et al.* Antiangiogenic platinum through glycan targeting. *Chem. Sci.* **8,** 241–252 (2017).
2. Mangrum, J. B. *et al.* A new approach to glycan targeting: enzyme inhibition by oligosaccharide metalloshielding. *Chem. Commun. (Camb).* **50,** 4056–8 (2014).
3. Gorle, A. K. *et al.* Substitution-Inert Polynuclear Platinum Complexes as Metalloshielding Agents for Heparan Sulfate. *Chem. Eur. J* (2018). doi:10.1002/chem.201706030
4. Katner, S. J., Johnson, W. E., Peterson, E. J., Page, P. & Farrell, N. P. Comparison of Metal–Ammine Compounds Binding to DNA and Heparin. Glycans as Ligands in Bioinorganic Chemistry. *Inorg. Chem.* acs.inorgchem.7b03043 (2018). doi:10.1021/acs.inorgchem.7b03043
5. Katsuta, E., Peterson, E. J., Katner, S. J., Farrell, N. P. & Takabe, K. Triplatin preferably suppress lung metastasis of breast cancer, and peritoneal carcinomatosis of colon and pancreatic cancer. *Proc. AACR Washingt. D.C.* Abstract #5117 (2017).
6. Katner, S. J. *et al.* Heparan sulfate , a new target for platinum in metastatic TNBC. *Proc. AACR Chicago,* Abstract #3941 (2018).
7. Katner, S. J. *et al.* Anti-metastatic platinum through glycan targeting in breast cancer. *Proc. AACR Washingt. D.C.* Abstract #17 (2017).
8. Silva, H. *et al.* Heparan sulfate proteoglycan-mediated entry pathway for charged tri-platinum compounds. Differential cellular accumulation mechanisms for platinum. *Mol. Pharmacol.* **9,** 1795–1802 (2012).
9. Peterson, E. J. *et al.* Nucleolar targeting by platinum: P53-independent apoptosis follows rRNA inhibition, cell-cycle arrest, and DNA compaction. *Mol. Pharm.* **12,** 287–297 (2015).

Chapter 1. Introduction

Polynuclear platinum complexes (PPCs) interact with DNA and heparan sulfate proteoglycans (HSPG) resulting in cytotoxic and anti-angiogenic/metastatic profiles. The focus of my thesis was to determine PPC interactions with heparan sulfate (HS) like models and to investigate the biological consequences of PPC-HS interactions resulting in anti-angiogenic/metastatic activities in metastatic breast cancer and triple negative breast cancer (TNBC). Therefore, our hypothesis was that strong PPC-HS interactions can result in the inhibition of breast cancer metastases.

1.1 Treatments in breast cancer.

In the United States alone, breast cancer is estimated to be the most common form of cancer to occur with 29% of new cancer cases and the leading cause of cancer-related deaths in women ages 20 to 59 for 2016.[1] There exist three main molecular markers in breast cancer that can dictate the patient's treatment regimen and estimate their prognosis: estrogen receptor-alpha (ERα), progesterone receptor (PR), and human epidermal growth factor receptor 2 (HER2).[2] Therefore, treatment options for breast cancer patients can be grouped into ERα+/PR+ with 70%, HER2+ with 15-20%, or lacking all three molecular markers, triple negative breast cancer (TNBC), with 15% of all breast cancers.[3] Endocrine therapies such as aromatase inhibitors (reduce estrogen levels), anti-estrogens (block estrogen signaling), and luteinizing-hormone releasing hormone (LHRH) (reduce estrogen levels from ovaries) target ERα+ and or PR+ tumors.[3] HER2-targeted therapies: Herceptin® (antibody against HER2), Lapatinib (tyrosine kinase inhibitor), and HER2 dimerization inhibitors have been developed to treat HER2+ breast cancers. Endocrine therapies for some HER2+ tumors also expressing ERα+/PR+ are also available.[3] Unfortunately, the TNBC

group has no molecular-targeted therapies available thereby relying on chemotherapy for drug treatment options.

Breast tumors have heterogeneity within and among tumors at the cellular level with different cell types, at the molecular level having different expression of markers like HER2, and at the epigenetic/genetic level such as constitutively active ERα in the absence of ligand or BRCA1/2 gene mutation.[3–5] For instance, ERα+ tumors can have ERα- cells, and metastatic patients with ERα+ primary tumors can have ERα- circulating tumor cells.[6] This tumor heterogeneity contributes to a reduced response from endocrine therapies as do *de novo* or acquired resistance from a loss of function or tumor dependency,[3] in which case chemotherapies are employed. Endocrine therapies target a whopping 70% of breast cancers however, of these breast cancers there is only a 50% benefit on ERα+, a 75% benefit on ERα+/PR+, and a 40% benefit on ER-/PR+ breast cancer subtypes.[3] Also, metastatic breast cancer has only a 26% five-year relative survival rate in the United States in 2005 to 2011[1] and a median survival from the first relapse has only improved by 7 months (26 to 33 months) over the past 2 decades.[7] Therefore, a therapeutic strategy is needed to fill these disparities.

For breast cancer, chemotherapy is used to treat tumors having *de novo* or acquired resistance to molecular-targeted therapies, TNBC tumors, and metastatic tumors. TNBCs have a higher incidence of mutations involving the homologous recombination that repairs damaged DNA (BRCA1/2) than other breast cancers, which makes them particularly sensitive to DNA damaging agents such as platinum-based agents.[8] In clinical trials, there have been some responses to platinum-based agents in TNBC patients with BRCA mutation,[5] and to androgen receptors (AR)

antagonists for AR+ TNBC patients.[9] However, TNBC tumors are diverse with having +/- expression of AR, homologous recombination mutations, or other mutations (TP53, PIK3CA, and PTEN) and thus will likely require multiple therapeutic approaches. Other approaches have been developed to treat TNBC by targeting VEGF[10] and EGFR[11] noted to be highly expressed in TNBC, however immunotherapies against these factors had minimal responses.[12,13] Hence a therapeutic strategy with specificity to allow for minimal side effects, but simultaneously capable of targeting multiple sites to attack the disease on several levels and evade resistance formation would be optimal for TNBC and metastatic breast cancer.

1.2 Platinum complexes.

The occurrence of resistance in chemotherapy can be *de novo* or acquired resistance which are both generally multifactorial. The usual suspects for resistance to platinum-based chemotherapy are the following: inactivation by sulfur containing nucleophiles (glutathione in cells, and human serum albumin in blood), modification in the cell uptake/efflux profile, and recognition and repair of Pt-DNA adducts.[14,15]

In preclinical studies, the polynuclear platinum complex (PPC) Triplatin (BBR3464) was active in both cisplatin sensitive and resistant cells,[16] and mutant p53 cells.[17] BBR3464 (Figure 1.1) is more effective at lower doses and has a different pattern of cytotoxicity signifying a different mechanism of action than cisplatin.[18] Also, BBR3464 has a broad-spectrum anti-tumor activity with a better overall response across breast cancer cell lines.[18] In a phase I dose escalation study for BBR3464 in combination with 5-fluorouracil (5-FU), the only breast cancer patient in the trial exhibited a response noted by the authors to likely be attributed to BBR3464 since the patient previously had

a 5-FU regiment.[19] This response was observed in the patient's lung metastases. Prior to the BBR3464 treatment, the breast cancer patient had surgery and was heavily pretreated with hormone therapies, Herceptin, CMF (cyclophosphamide, methotrexate, & 5-FU), Adriamycin & cyclophosphamide, capecitabine & docetaxel, and vinorelbine.[19]

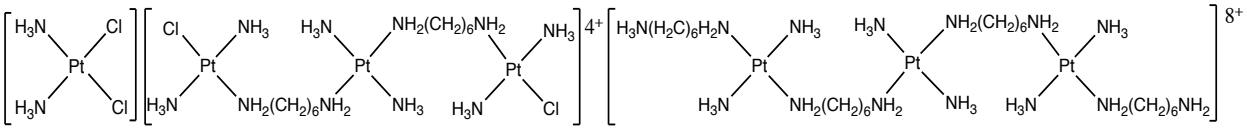

Figure 1.1. Evolution of platinum-based anticancer agents. Cisplatin (left) is the first platinum-based anticancer agent and is still used today for treating metastatic testicular cancer, and ovarian cancer. The other two FDA-approved drugs, oxaliplatin and carboplatin contain the same basic structure *cis*-[$PtX_2(amine)_2$]. Triplatin (BBR3464, center) is a Polynuclear Pt compound (PPC) and the first, and still the only "non-cisplatin" platinum analog to enter human clinical trials. TriplatinNC (right) replaces the Pt-Cl bond with "inert" Pt-amine for non-covalent (NC) association with biomolecules and greater metabolic stability.

Unfortunately, due to company takeovers and BBR3464's pharmacokinetics, BBR3464 did not progress after phase II clinical trials. BBR3464's deactivation by sulfur nucleophiles such as glutathione and human serum albumin[20] led to an exploration of structure activity relationships in PPCs identifying TriplatinNC as an anti-tumor agent[21,22] with greater metabolic stability. TriplatinNC (Figure 1.1) is a noncovalent derivative of BBR3464 with inert dangling amine (hexanediamine) ligands in place of the chloride ligands creating an increase in charge from 4+ to 8+. TriplatinNC binds noncovalently to DNA through electrostatic and hydrogen bond interactions, while BBR3464 pre-associates electrostatically with its 4+ charge and then covalently

form Pt-DNA coordinations.[23] More specifically, the square-planar tetra-am(m)ine Pt(II) coordination units in TriplatinNC (and other PPCs) form phosphate clamps on the DNA by a bidenate NH---O---HN (amine-phosphate-ammine) complex (Figure 1.2).[23,24] Using these phosphate clamps, TriplatinNC binds to the DNA *via* novel backbone tracking and grooving spanning interactions.[23] Such phosphate clamps are similar to the arginine fork, generally employed by DNA and RNA-binding-proteins, involving the arginine's guanidino groups forming hydrogen bonds to the DNA phosphate backbone.[24,25]

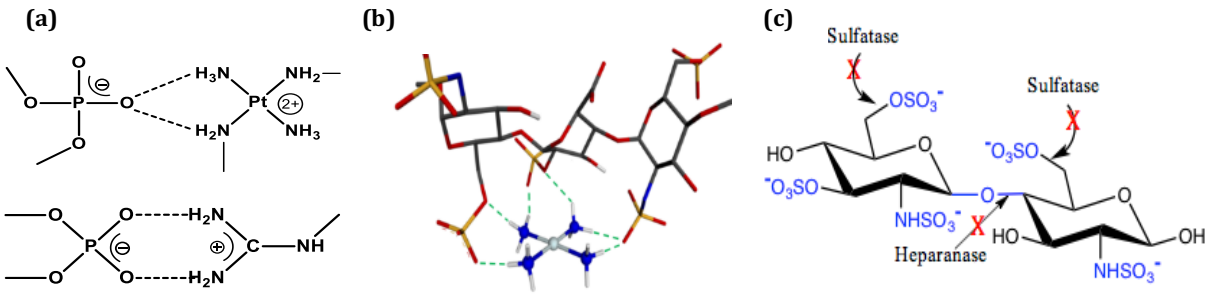

Figure 1.2. PPC interactions with HS. (a) The PPC phosphate clamp (top) is compared to the arginine fork (bottom) interaction with DNA. The phosphate clamp to DNA is analogous to the sulfate clamp to HS. (b) The square-planar tetra-am(m)ine Pt(II) coordination units in PPC (modeled with $[Pt(NH_3)_4]^{2+}$ unit) form extended hydrogen-bonding network along the HS sulfate cluster protecting the sulfate groups. (c) PPCs protect HS from heparanase degradation and when sulfatase levels are low, PPCs can bind to HS and compete with growth factor binding.

1.3 PPC-Glycan interactions.

Polycationic protein translocation domains utilize their electrostatic and hydrogen-bonding interactions to penetrate the cellular membrane with polyarginines being the most effective.[26]

Polyarginine cellular uptake is mediated by heparan sulfate proteoglycans (HSPG) located on the cell surface.[27] HSPGs are protein cores (proteoglycan, PG) with negatively charged polysaccharide glycosaminoglycan (GAG) chains (heparan sulfate, heparin, etc.). Heparan sulfate (HS) and heparin are composed of repeating IdoA2S-GlcNS6S disaccharides with varying degrees of sulfation (fully-sulfated, non-sulfated, or under-sulfated units), and chain length.[28] The conceptualization of PPCs as "polyarginine mimics" led to the discovery of PPC-HSPG interactions showing a novel cellular internalization pathway for platinum-based agents.[29] Thus began the saga of PPC-HSPG interactions.

Specifically, PPCs bind to sulfated regions of heparan sulfate (HS) chains creating a sulfate clamp analogous to the PPC phosphate clamp on the DNA phosphate backbone.[30–32] The PPC-HSPG interactions inhibited the cellular uptake[29] and nucleolar localization of the fluorescently-labeled nona-arginine (TAMRA-R_9).[33] Unlike other platinum-based agents, PPCs uniquely benefit from this internalization mechanism for selective uptake in tumors with high levels of HSPG.[29] GAG-protein interactions result from electrostatic interactions between the fully-sulfated regions of the polysaccharide and the basic amino acids of the protein, as well as van der Waals and hydrogen bonding.[34] Consequently, when PPCs bind to HS, the PPCs form a metalloshield that blocks sulfate loss and protein recognition to the HS.[30,32] HS facilitates fibroblast growth factor (FGF)-induced dimerization and subsequently activation of FGFRs (a tyrosine kinase receptor) *via* autophosphorylation of the kinase domain.[35] FGF/FGFR signaling is implicated in many cancers particularly FGF2 promoting tumor progression.[35] FGF2, like other HS-binding pro-angiogenic factors directly stimulate tumor and endothelial cell proliferation, migration, and survival.[28] Therefore, FGF2 is an attractive anti-cancer target for providing multi-targeted therapies by

inhibiting tumor growth and angiogenesis. PPCs bind to HSPG and competitively block FGF2 and FGF/FGFR signaling.[30] Vascular endothelial growth factors (VEGF)-A also bind to HSPG on endothelial cells and create a complex with its receptor VEGFR2 for VEGF/VEGFR2 pro-angiogenic signaling promoting tumor angiogenesis.[28]

PPC-metalloshielding protects the heparan sulfate from mammalian heparanase[30] and bacterial heparinase cleavage significantly more so than the polyarginine TAMRA-R_9.[32] Heparanase is an endo-β-D-glucuronidase that cleaves HS chains of HSPGs on the cell surface and extracellular matrix.[36] In noncancerous cells, heparanase expression is suppressed by promoter inhibition from methylation and p53 binding.[37] High heparanase expression associates with large tumor size and greater metastatic potential in breast cancer.[38] Heparanase inhibitors are an intriguing therapy from the potential to have high selectivity for tumor cells since noncancerous cells typically do not express heparanase.[36,39] Heparanase inhibitors also have the potential for low resistance considering only one functional mammalian heparanase exists which means there are no redundant enzymes to cause HS cleavage.[36,39] Several heparanase inhibitors are currently in clinical trials, most notably sulfated oligosaccharide HS-like-mimetics (PI-88, PG545, SST0001, etc.), but have anticoagulant side effects.[36,39] Given that heparanase has a high abundance in many tumors[40] and has a positive correlation of metastatic potential,[41] compounds that block heparanase activity are desirable.

PPCs have potential efficacy and tumor selectivity for TNBC tumors. TNBC overexpress HSPGs while reduced presence of sulfatases provides an abundant available binding sites for PPCs (Table 1.1). Moreover, HSPG-binding proteins such as growth factors, growth factor receptors, and

heparanase exhibit high expression levels in TNBC (Table 1.1) all of which may be influenced by PPC-HSPG interactions.

Table 1A. TNBC samples with high levels of sulfated GAGs		
High levels of cell surface GAGs due to:	Sample type:	Ref.
↑ expression of Syndecan-1/CD138	Clinical, MDA-MB-468	4
↑ expression of Syndecan-4	MDA-MB-468, MDA-MB-231, MDA-MET	4
↓ activity of HSulf -1/-2 sulfatase	Clinical	5
↓expression of HSulf-1 sulfatase	Clinical, MDA-MB-231, MDA-MB-468	5
Table 1B. TNBC samples overexpressing GAG-binding angiogenic factors		
Increased cell migration/invasion signaling due to:	Sample type:	Ref.
↑ expression of HPSE	Clinical, MDA-MB-231BR	3
↑ expression of FGF/FGFR	Clinical, MDA-MB-231, MDA-MB-453, 4T1	2,6
↑ expression of HBEGF/EGFR	Clinical, MDA-MB-231, MDA-MB-231BR	7
↑ expression of VEGFA/VEGFR2	Clinical, MDA-MB-231BR	8

2. Chiodelli P. et al., Molecules 20 (2015)
3. Gomes A.M. et al., BioMed Res Int, 2013:852093 (2013)
4. Barbareschi, M. et al., Cancer, 2003, 98, 474-483(2003) ; Cooney, C.A., et al., Breast Cancer Research, 13, R58 (2011)
5. Gill, R.M. et al., Cell Biol., 146, 431-444 (2016)
6. Dey, J.H. et al., Cancer Res., 70, 4151-4162 (2010)
7. Bos, P.D. et al., Nature, 459, 1005-1009 (2009) ; Yotsumoto, C. et al., Inter. J. Cancer 127: 2707-2717 (2010)
8. Linderholm, B. et al., Annals of oncology, 2009mdp062 (2009)

Table 1.1. TNBC samples with high levels of sulfated GAGs and overexpressing GAG-binding angiogenic factors.

1.4 Summary.

TriplatinNC is a dual-functional agent from cytotoxic to anti-angiogenic and anti-metastatic profiles (Figure 1.3). As a cytotoxic agent, TriplatinNC localizes to the nucleolus,[42] inhibits rRNA transcription for cells in G_1 phase, and prevents DNA re-condensation for cells in S/G_2 phase causing G_1 arrest and eventual apoptosis.[33] As an anti-angiogenic and anti-metastatic agent, TriplatinNC blocks heparanase cleavage and competes with FGF2 interactions on HS chains influencing FGF/FGFR signaling.[30] Since heparanase and HSPG overall are overexpressed in

many tumors creates a potential for PPC-tumor selectivity.[43] Furthermore, low sulfatase expression can increase growth factor binding to HS further stimulating tumor progression.[43] Also, reduced sulfatase expression present in TNBC (Table 1.1) facilitates more available binding sites (sulfate clusters) for PPCs. Overall the HS interatome creates a niche for PPCs.

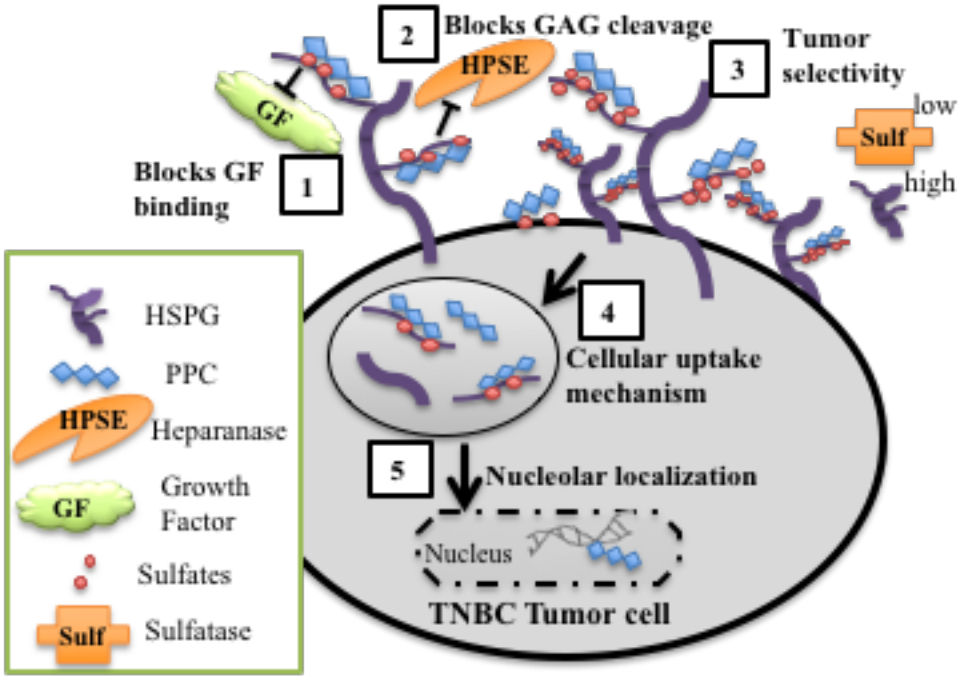

Figure 1.3. PPC interactions with tumor cells. (1) Sulfatase (Sulf)-high expressing cells reduces HS sulfates and thus reduces growth factor (GF) and PPC binding to HSPG. In Sulf-low expressing cells, PPCs metalloshield the HSPG to (2) block GF binding and (3) inhibit heparanase (HPSE) cleavage ultimately reducing tumor invasion, migration, and growth.[25] (4) PPC-HSPG interaction also provides a GAG-mediated cellular uptake mechanism for PPCs.[29] Once inside the cell, (5) PPCs localize to the nucleolus, decrease rRNA transcription, and cause G_1 cell cycle arrest with eventual apoptosis.[32]

Here, we report PPC interactions with HS-like models: Fondaparinux (FPX)[44] (Chapter 2) and heparin[45] (Chapter 3). We demonstrate TriplatinNC high affinity to heparin in biophysical studies and compare HS interactions with DNA and HS using competition assays.[44,45] these approaches may be extended to a range of metal-ammine compounds[45] (Chapter 3). The biological consequences of PPC-HS interactions include modulation of heparanase cleavage, growth factor binding to HS, and growth factor-induced migration and signaling in breast cancer and endothelial cells (Chapter 4), as potential anti-metastatic and anti-angiogenic effects *in vivo*. We report proof-of-principle of strong *in vivo* anti-metastatic activity of PPCs in triple negative breast cancer (TNBC) models[46–48] (Chapter 5). Impressively, PPCs reduce overall tumor metastases with emphasis in lung, bone, and liver locations in both immunocompetent and immunosuppressive mouse models (Chapter 5). PPCs demonstrated permeability through the blood brain barrier (BBB) implying further applications for PPCs (Chapter 6), while other platinum compounds demonstrate *in vivo* efficacy (Chapter 7). PPCs represent a novel class of intrinsically dual-function agents combining platinum cytotoxicity through DNA targeting with anti-angiogenic effects through glycan targeting. Together, these results suggest that strong PPC-HS interactions have a significant role in the inhibition of breast cancer metastases, particularly in metastatic TNBC patients.

Chapter 2. HS-model Interactions with PPCs

2.1 Rationale.

Almost half of all cancer patients will receive a platinum-based anticancer agent during their treatment regimen. Cisplatin is the first platinum-based drug to be FDA-approved as an anticancer agent in 1978 and is still used today in testicular and other cancer treatments. Since 1978, the anticancer platinum era has developed cisplatin analogs to address *de novo* or acquired resistance, improve the metabolic stability and tolerability, and expand the clinical profile. The result, two more FDA-approved platinum agents (carboplatin and oxaliplatin) were developed. The template that guided these developments was a mononuclear *cis*-[$PtX_2(amine)_2$] chemotype (X = leaving group, amine = neutral or carrier group) based upon structure-activity relationships and DNA as the target for such agents.[31]

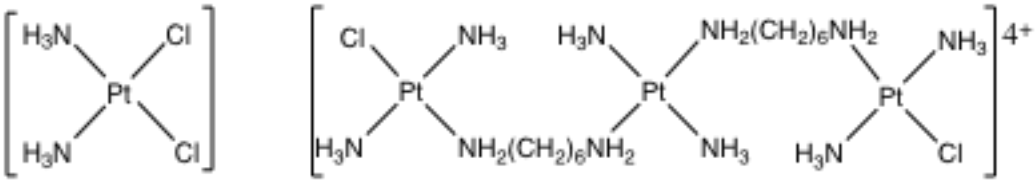

Figure 2.1. Structures of cisplatin (left) and Triplatin (BBR3464, right).

Currently, BBR3464 is the only platinum-based non-cisplatin analog to be in clinical trials.[31] As a trinuclear, tetrapositive agent, its DNA adducts were structurally different than those of the monoclear drugs which challenged the previous structure-activity relationships.[49–51] Creating unique DNA-Pt adducts can be therapeutically advantageous by influencing alternative cellular signaling pathways apart from cisplatin. The concept that BBR3464 was efficacious enough to

extend into phase II clinical trials gave proof-of-principle to further challenge the accepted structure-activity relationships giving rise to new chemotypes based on a polynuclear platinum complex (PPC) formation.

The new class of platinum agents, PPCs, were also structurally intriguing due to BBR3464 central coordination sphere (and overall 4+ charge) contributing to its DNA affinity through electrostatic and hydrogen-bonding interactions. To further explore these noncovalent interactions, a new series of PPCs were developed to examine substitutionally inert PPCs binding to DNA. These derivatives of BBR3464, AH44, and TriplatinNC (Figure 2.2), formed unique DNA adducts through noncovalent binding. These noncovalent PPCs had significant differences in cellular accumulation and cytotoxicity profiles for tumor cells compared to each other and BBR3464.[21,22] These studies demonstrated a charge dependence for cellular uptake with the noncovalent compounds having more cellular uptake as their charge increases.[21,22] At the time of this finding, the structure-activity relationship of platinum compounds were thought to have required a neutral charge to be taken up by cells.[22] This observed charge dependence for cellular uptake may be explained by PPC-HSPG interactions on the cell surface in which the higher charged TriplatinNC displayed more cellular accumulation and cytotoxicity for wild type cells than HS-deficient cells comparatively to BBR3464 and AH44[29] –further emphasizing the differences among the three analogs.

In attempt to identify structure-activity relationships among noncovalent PPCs, particularly in regard to their interactions with HS, a small focused library of PPCs was synthesized (Figure 2.2). The PPC library consisted of Pt complexes varying in charge, nuclearity (mono/di/tri/tetra Pt units), and the presence or absence of a dangling amine.

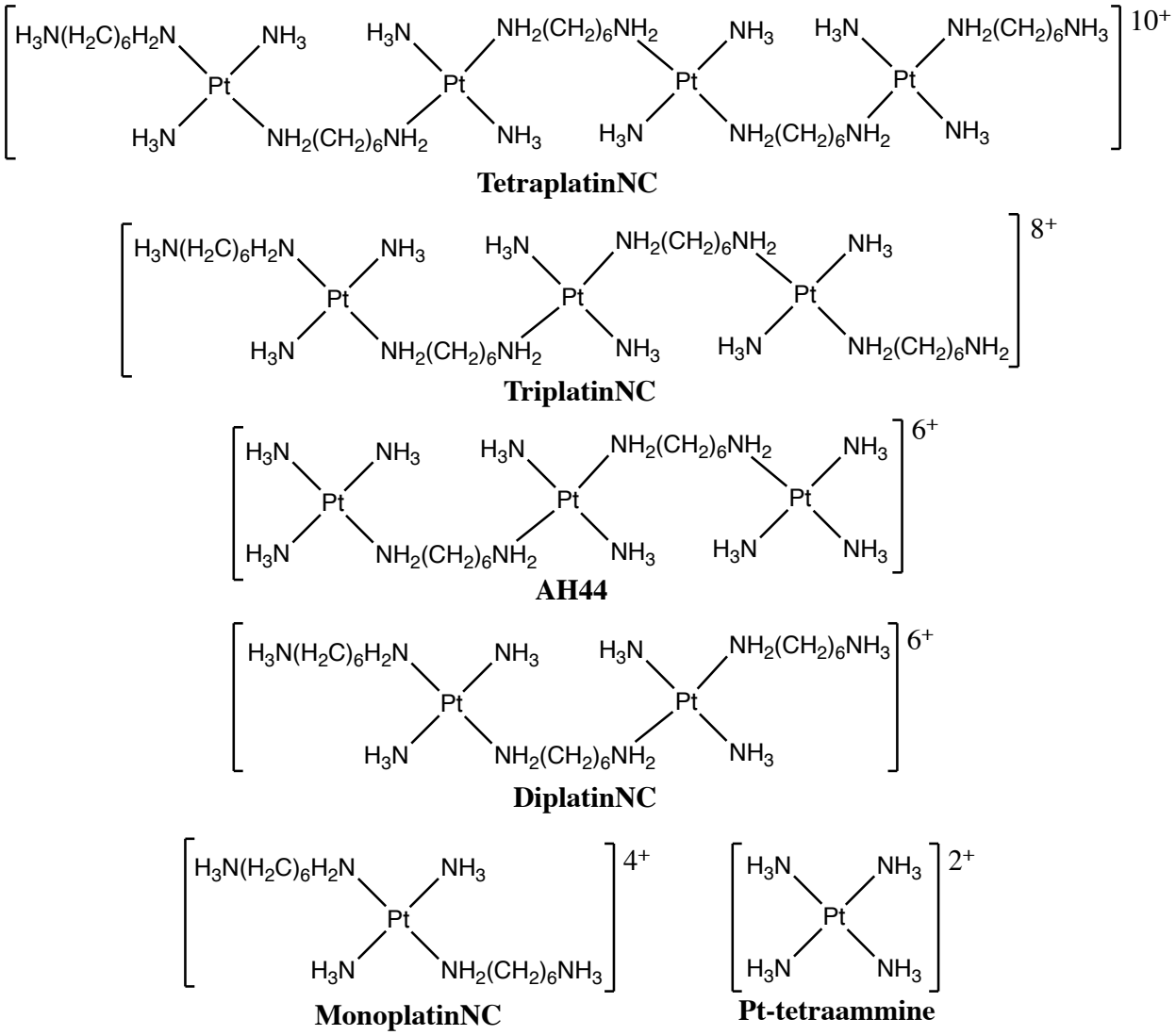

Figure 2.2 Structures of the non-covalent PPC library for structure-activity relationship studies examining PPC-HS interactions. Counter-anions omitted for clarity.

2.2 NC-series interactions with HSPGs in cells.

Polyarginine cellular uptake is mediated by cell surface HSPGs.[26,27] The conceptualization of PPCs as "polyarginine mimics" led to the inhibition of the HSPG-mediated cellular internalization and nucleolar localization of TAMRA-R_9 (nonaarginine peptide (R_9) coupled to the TAMRA

fluorescent label 5-(6)-carboxytetramethylrhodamine) and identification of HSPGs as receptors for PPC cellular internalization.[29,33] In contrast to the mononuclear clinical platinum agents such as cisplatin and oxaliplatin, PPCs uniquely utilize this internalization mechanism, which could provide an approach for selective uptake into tumors with high levels of HSPGs.[29,52]

The PPC library in Figure 2.2 was used to determine how the structure-activity relationships of PPCs influence their interactions with HSPGs on cells. TAMRA-R_9 interacts with HS on the cell surface and then becomes internalized by endocytosis.[26,27] Competition assays have been developed that exploits the TAMRA-R_9 affinity for HS or HS-like molecules (e.g. heparin, fondaparinux) by tracking its fluorescence in cells through confocal microscopy or flow cytometry,[29] and in biophysical assays.[27,45] Using flow cytometry, the TAMRA-R_9 entry into human colorectal carcinoma (HCT116) cells was examined in the presence of different PPCs, which prevented cell entry of the peptide in a charge-dependent manner (Figure 2.3a). A complete inhibition of TAMRA-R_9 fluorescence was observed in the cells containing TetraplatinNC (10+) and TriplatinNC (8+), while the lesser-charged analogs AH44 (6+) and DiplatinNC (6+) reduced the fluorescence somewhat. MonoplatinNC (4+) failed to reduce any fluorescence.

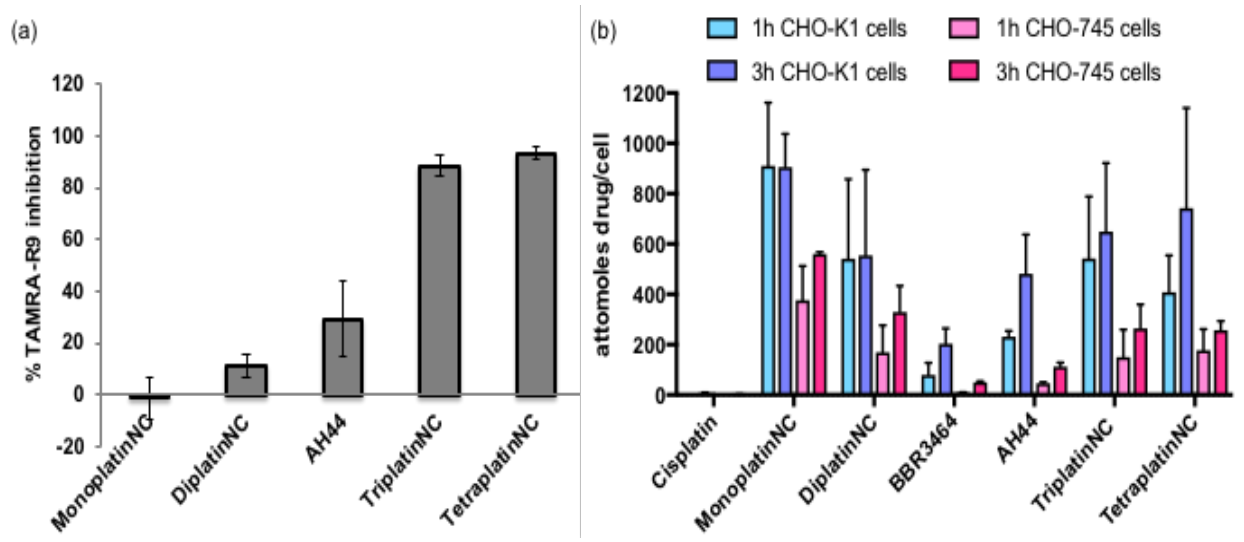

Figure 2.3. (a) PPCs (10 μM) competition with TAMRA-R_9 (1 μM) uptake in human colorectal carcinoma (HCT116) cells was compared by the presence of fluorescence dye using flow cytometry. (b) PPCs (10 μM) cellular accumulation in CHO-K1 and CHO-psgA-745 (lacking HS/CS) cells at 3 and 6 h prior to collection was analysed using ICP-MS for Pt content. Pt readings were normalized to cell number and number of Pt-centers for each compound (attomoles of drug / cell). Error bars represent the mean ± SD of at least 2 independent experiments (each with 2 replicates).

To further assess PPC-HSPG interactions, we examined the HSPG influence on PPC cellular accumulation by using Chinese hamster ovary (CHO) cell mutants. There are several CHO cell mutants that have mutations in different stages of glycosaminoglycan biosynthesis.[53,54] The CHO-psgA-745 mutant has a defect in the xylosyltransferase responsible for the initiation of glycosaminoglycan formation by transferring a xylose (the first sugar attachment) to a serine residue of the core protein in the proteoglycan.[54] Differential accumulation of PPCs into wild type CHO-K1 and mutant CHO-pgsA-745 (lacking HS/CS) cells confirmed the proteoglycan mediation

(Figure 2.3b). Cisplatin low cellular accumulation for 1 and 3-hour incubations was indeed detectable on the inductively coupled plasma mass spectrometry (ICP-MS) and had no variation in accumulation between the cell types.

The relative cellular accumulation of the PPC library in HCT 116 cells suggest the involvement of dangling amine-dependent and size-dependent mechanisms (Figure 2.4a). TriplatinNC's higher cellular accumulation compared to AH44 is consistent with previous results.[21,29] DiplatinNC, TriplatinNC, and TetraplatinNC showed similar cellular accumulation, even though their overall charges ranged from 6+ to 10+, suggesting an influence of the dangling amine. There is no strict correlation between TAMRA-R_9 inhibition and cellular accumulation – as evidenced in the comparison between DiplatinNC and AH44 (Figure 2.3a and 2.4a). Likewise, although MonoplatinNC failed to inhibit TAMRA-R_9 internalization, it showed the highest cellular accumulation compared to the other PPCs and showed higher accumulation into wild type compared to mutant CHO cells (Figure 2.3b). The smaller size may allow it to use multiple entry pathways including a size-dependent one.[55,56] Small mononuclear platinum drugs like cisplatin, carboplatin, and oxaliplatin reportedly use the hCTR1 copper influx transporter for cell entry.[57] Further, the cellular accumulation and cytotoxicity of the covalently binding BBR3464 is also affected by copper status.[58] The relative cytotoxicity of the PPC library in HCT116 cells was investigated using MTT viability assays (Figure 2.4b). The PPC cytotoxicity was not related to their cellular uptake (Table 2.1).

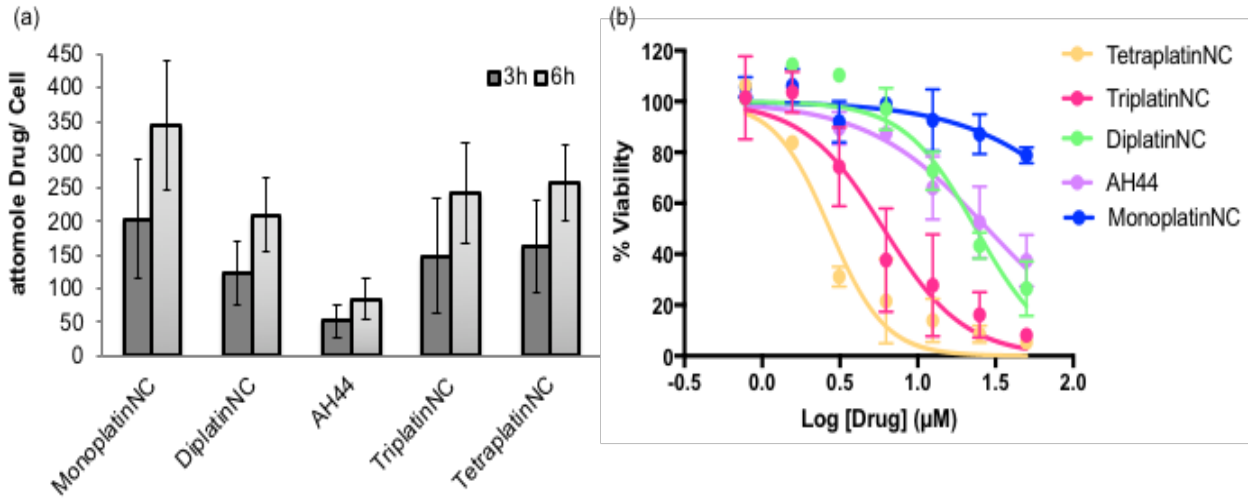

Figure 2.4. An evaluation of PPCs cellular accumulation, and overall cytotoxicity in colorectal carcinomas cells (HCT 116). (a) Cellular accumulation of PPCs (10 μM) at 3 and 6 h prior to collection was analysed using ICP-MS for Pt content. Pt readings were normalized to cell number and number of Pt-centers for each compound. (b) MTT assays were employed to determine overall cytotoxicity of PPCs for a 72 h compound incubation. Error bars represent the mean ± SD of at least 2 independent experiments (each with 2-4 replicates).

Compound	IC_{50} (μM)	Charge
MonoplatinNC	> 50	4+
DiplatinNC	24 ± 5	6+
AH44	30 ± 13	6+
TriplatinNC	7 ± 4	8+
TetraplatinNC	3.0 ± 0.7	10+

Table 2.1. Cytotoxicity of non-covalent PPCs in HCT116 cells. IC_{50} values ± SD of at least 2 independent experiments (each with 4 replicates) were calculated in Graphpad Prism 7.

2.3 Comparing NC-series interaction with DNA to FPX.

Heparan sulfate (HS) in HSPGs is very heterogeneous with variations in its repeating disaccharide motif and sulfation patterns. HS heterogeneous nature raises challenges for understanding direct HS interactions with compounds.[45,59] Consequently, Fondaparinux (FPX) has been used as a HS substitute in previous studies[32] and was used here to compare the noncovalent PPCs interactions with HS. FPX is a homogeneous, highly sulfated synthetic glycosaminoglycan-based fragment with a low molecular weight capable of the same protein interactions (i.e. heparanase cleavage) as HS making it an ideal candidate to determine relative binding interactions.

To compare the PPC-FPX interactions with the well-studied PPC-DNA interactions[31,60,61] an ethidium bromide (EtBr) competition assay was developed applying EtBr as the reporter.[30] This assay exploits the decrease in fluorescent properties when the intercalator is removed from DNA under the influence of DNA-PPC binding (Figure 2.5a,b). The concentration of PPC required to reduce fluorescent >50% by displacing EtBr from DNA to was determined for each compound (Appendix I Figure 1). Upon FPX addition to the EtBr-PPC-DNA system, the intercalator binds back to DNA as FPX sequesters the PPC (Figure 2.5c).[30]

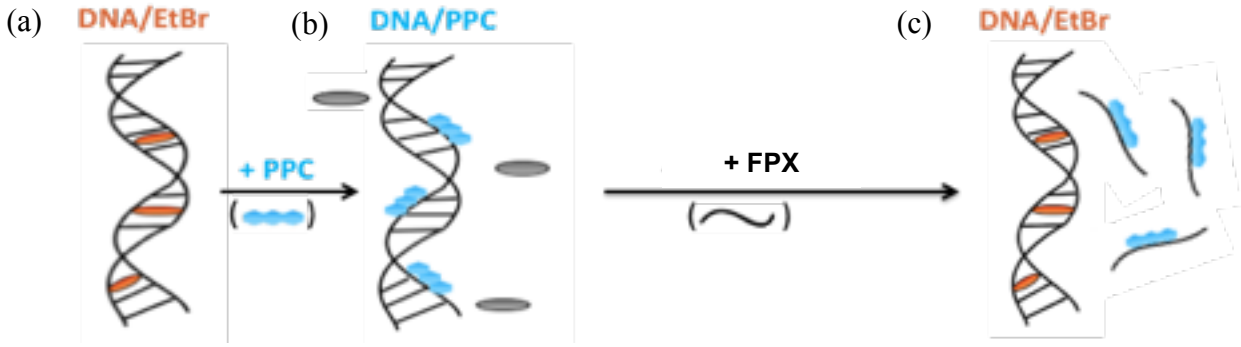

Figure 2.5. PPC-HS binding interaction as measured by novel EtBr reporter assay. Schematic representation of PPC sequestering of DNA bound PPC by FPX.

The comparative binding of different PPCs for DNA and FPX was estimated based on the FPX concentrations required to sequester the PPC from DNA, thus allowing EtBr to intercalate, with a concomitant increase in its fluorescence. Since the ability to displace EtBr from DNA differs amongst the complexes themselves, the concentration for any individual PPC required to produce an initial >50% decrease in fluorescence was normalized as the modified EtBr-PPC-DNA fluorescence ($[PPC_d]$) and 100% fluorescence was control EtBr-DNA. The data are presented in the form of an EC_{50} value which reflects the concentration of FPX, $[FPX_r]$, required to restore EtBr fluorescence to 50% of the control EtBr-DNA sample in absence of either PPC or FPX. (Figure 2.6 and Table 2.2). Note that FPX has no effect on EtBr-DNA fluorescence. This allows a discussion of the EC_{50} as a ratio index of $[PPC_d]/[FPX_r]$ (Table 2.2). The ratio index suggests that above 1, PPCs have more affinity for FPX than DNA, whereas below 1 PPCs have more affinity for DNA than FPX. Thus, AH44 has similar affinities for DNA as FPX with ratio index of 0.97, while MonoplatinNC, DiplatinNC, and TriplatinNC all had slightly higher affinities for FPX than DNA. $[Pt(NH_3)_4]^{2+}$ has a very high ratio index but this reflects its very weak binding to DNA[62] and thus was eliminated from the comparison of strongly binding DNA compounds (Table 2.2).

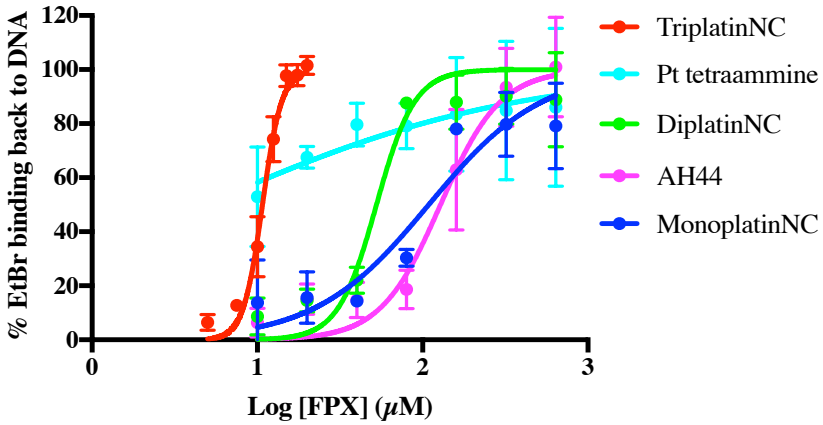

Figure 2.6. Curve graph for the EC_{50} values measured by EtBr reporter assay showing the preference of PPCs for FPX, samples were normalized to the controls (no FPX as 0% and EtBr-DNA as 100%). Error bars represent the mean ± SD of at least 2 independent experiments (each with 4 replicates).

Compound	EtBr assay	
	EC_{50} (μM) [a]	Ratio index [b]
$[Pt(NH_3)_4]^{2+}$	NA	NA
MonoplatinNC	108.90	1.15
DiplatinNC	52.60	1.19
AH44	128.30	0.97
TriplatinNC	10.74	1.17

Table 2.2. Relative FPX-PPC interactions using the EtBr reporter assay. [a] EC_{50} is the concentration of FPX required to restore EtBr-DNA fluorescence and was calculated from the normalization of 0 μM FPX as 0% and DNA-EtBr only as 100%. [b] Ratio index calculated from the $[PPC_d] / [FPX_r]$ where $[PPC_d]$ is the concentration required to produce an initial < 50% decrease

in fluorescence and [FPX_r] is the concentration required to restore EtBr fluorescence to 50% of the control EtBr-DNA sample in absence of either PPC or FPX.

Further examination of DiplatinNC, TriplatinNC, and AH44 interaction with FPX in the EtBr reporter assay of which there is similar EtBr displacement (fluorescence) at 0 µM FPX (Figure 2.7) clearly corresponds to the EC_{50} (Table 2.2) TriplatinNC > DiplatinNC > AH44 trend for relative FPX affinities. TriplatinNC and DiplatinNC higher relative preference for FPX may be attributed to their dangling amine ligands and overall higher charge in the case of TriplatinNC.

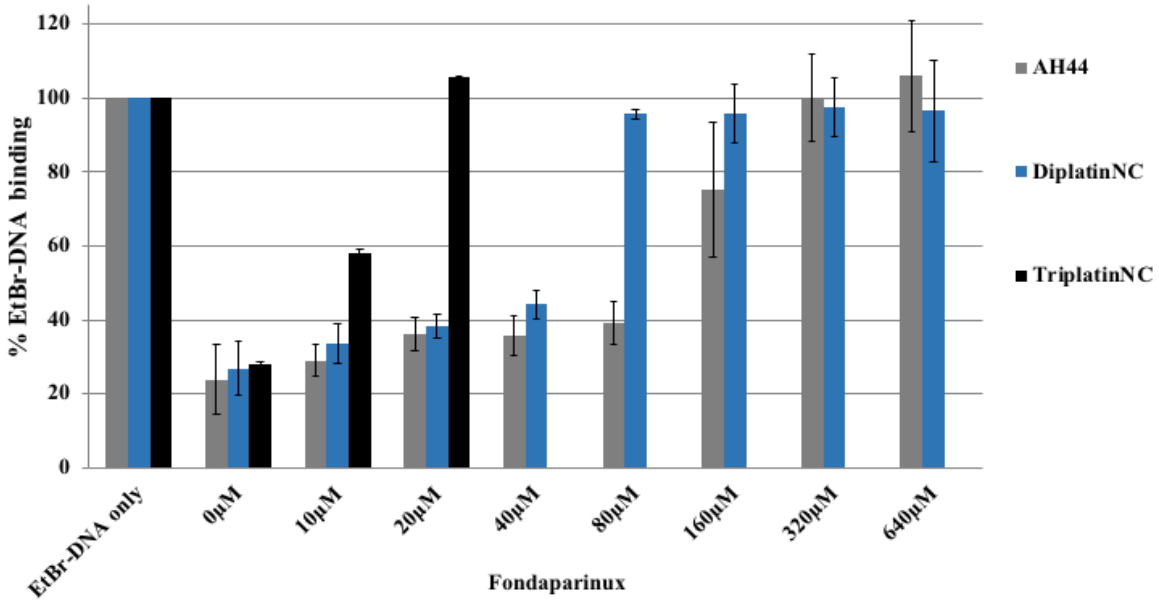

Figure 2.7. The EtBr reporter assay comparing the preference of AH44, DiplatinNC, and TriplatinNC for FPX, samples were normalized to the controls (EtBr only as 0% and EtBr-DNA as 100%). Error bars represent the mean ± SD of at least 2 independent experiments (each with 3 replicates).

Other PPCs were evaluated for interactions with heparin, a heterogenetic HS-like glycosaminoglycan through comparing interactions with DNA with the EtBr reporter assay (Appendix I Figure 2). SpermidineNC (7+) exhibited some affinity for heparin but was less than TriplatinNC (8+) affinity for heparin in the same assay (Appendix I Figure 2). These results further emphasised possible charge-based affinities for HS-like models especially for noncovalent compounds. Further examination of metal complexes affinities for heparin was done in Chapter 3.

2.4 Summary.

The noncovalent PPC library studied here further elucidated structure-activity relationships for PPC interaction with HS. The wt CHO and mutant CHO-pgsA-745 (lacking HS/CS) cells were used to confirm that HSPG-mediated interactions play an important role in the cellular accumulation for this class of molecules. These results followed earlier studies done with only TriplatinNC, BBR3464, and AH44.[29] However, the cellular accumulation for PPCs did not appear to have any clear correlation with structure-activity relationships. Overall, while the HSPG status clearly influenced cell uptake for these compounds, multiple complementary pathways do exist and these results emphasized the reality that platinum complexes use multiple pathways for cellular internalization.[21,55,56]

The HCT116 cells cytotoxicity and TAMRA-R_9 inhibition assays noticeably had a charge-dependent trend with TetraplatinNC +10 > TriplatinNC +8 > DiplatinNC ~ AH44 +6 > MonoplatinNC +4. Interestingly, the cytotoxicity is not related to the cellular accumulation and may be related to their ability to condense DNA and inhibit transcriptional activity.[33,63] The HS

interaction is unique to the PPC class and coupled with the overexpression of HSPGs on many tumor cell surfaces,[28,52] indicate a potential for tumor selectivity of PPC agents. Considering FPX as a well-defined HS model, the HSPG-mediated PPC cellular accumulation and TAMRA-R_9 inhibition assays correlated with the biophysical studies of the FPX-PPC interaction.

As an indirect assay, the EtBr reporter assay gave an estimate of relative FPX(HS)/DNA affinities. The contrast between TriplatinNC and AH44 slight preference for FPX interactions compared to DNA in the EtBr reporter assay emphasizes the importance of dangling amine moieties as well as increased charge dispersion. These structure-active relationships for PPC-FPX interactions were echoed in the PPC-HSPGs cell study results. The inherent nature of the EtBr reporter assay as a four-species system is a caveat for this assay. Still, the trends were consistent with cell studies here and within other assays (ITC and methylene blue inhibition assay[44]) that strongly reflect a charge dependence for PPC-HS interactions. Overall the results demonstrate unique dual-function nature of the PPC series compared to the mononuclear clinical agents and further emphasize developing agents to target glycans.

Data was published in:

- Gorle, A. K., Katner, S.J., *et al.* Substitution-inert Polynuclear Platinum Complexes as Metalloshielding Agents for Heparan Sulfate. *Chem. Eur. J.* in press (2018).
- Peterson, E. J., Daniel, A. G., Katner, S.J., *et al.* Antiangiogenic platinum through glycan targeting. *Chem. Sci.* **8,** 241–252 (2017).

2.5 Experimental.

Cell lines and cell culture

HCT116, CHO-K1, and CHO-pgsA-745 cell lines were obtained from the American Type Tissue Collection. HCT116 cells were cultured in RPMI 1640 media (Invitrogen) with 10% fetal bovine serum (FBS) and 1% penicillin/streptomycin (P/S, Gibco). CHO cell lines were cultured in DMEM/F12 media (Invitrogen) with 10% FBS and 1% P/S. Cells were grown in a humidified atmosphere at 37°C with 5% CO_2.

MTT cell viability assay

HCT116 cells were seeded in 96-well plates (5×10^3 cells/well) in supplemented media (100 μL). After incubation overnight, the cells were treated with varying concentrations of the indicated Pt compound, in sets containing 4 replicates for each concentration. After drug exposure for 72 h, 1 mM MTT (3-(4,5-dimethylthiazol-2-yl)-2,5-diphenyltetrazolim bromide) (Sigma) was added to each well and incubated for 4 h. The MTT reagent was removed, and 100 μL of DMSO was added to each well to lyse the cells and dissolve the purple formazan. All incubations were performed at 37°C with 5% CO_2. Spectrophotometric readings were determined at 570 nm using a microplate reader (Bio-Tek instruments). Percentage cell survival was determined as treated/untreated controls × 100. Data are reported as the average of 2 independent experiments ± SD.

Cellular accumulation

HCT116 cells were seeded in 100 mm dishes (1×10^6 cells/dish) in supplemented media (20 mL). After incubation for 24 h, cells were treated with 10 μM of the indicated Pt compounds for 3 and 6 h incubations (37°C with 5% CO_2). The cells were then washed twice with PBS, harvested with

0.25% trypsin (Gibco), and washed with 10 mL of PBS. The cell pellets were digested in 1 mL of nitric acid for 72 h and diluted with H_2O (2 mL). The solutions were filtered through a 0.45 GHP filter. Platinum analysis was performed on Varian 820 inductively coupled plasma mass spectrometer (ICP-MS). The standards were prepared with K_2PtCl_4 in concentrations of 10, 50, 100, 150, and 250 ppb. The blank was 7% nitric acid. Data was normalized to number of platinum centers per drug.

Cellular internalization

HCT116 cells were seeded in 6-well plates (5×10^5cells/well) in supplemented media (3 mL). After incubation for 24 h, cells were treated with 10 μM of the indicated Pt compounds and incubated for 5 min before the addition of TAMRA-R_9 (1.0 μM) and further incubation for 1 h at 37°C with 5% CO_2. Cells were washed three times with PBS, harvested with 0.25% trypsin (Gibco), and washed twice with cold PBS. The cells were passed through a cell strainer (40 μM Flowmi) and then analyzed at 488 nm (excitation) and 585 ± 42 nm bandwidth emission using a Becton Dickinson FACSCanto II Analyzer flow cytometer (BD Biosciences).

Ethidium Bromide (EtBr) reporter assay

All samples were read in a 96 well plate at 530/590 nm using a microplate reader (BioTek instruments). Ethidium bromide (EtBr) at 5 mM in water was diluted in HEPES buffer (80 mM HEPES, 7.2 pH) and incubated with calf thymus (ct) DNA for 5 min at 25°C to a final control concentration of 12.5 μM EtBr and 10 μM DNA in a final volume of 100 μL. In separate wells, the concentration of each individual PPC (dissolved in water and diluted in HEPES buffer) needed

to *decrease* EtBr fluorescence by at least or greater than 50% after 1h incubation was calculated to be the following: TriplatinNC 12.5 μM, DiplatinNC 62.5 μM, AH44 125 μM, MonoplatinNC 125 μM, and $[Pt(NH_3)_4]^{2+}$ 500 μM and denominated as $[PPC_d]$. This concentration was normalized as the modified (0 %) EtBr-PPC-DNA fluorescence and 100% fluorescence was the control EtBr-DNA. Next, 10 μL of varying concentrations of FPX (0-640 μM) in HEPES buffer were added to 90μL of a combined solution of platinum complex, DNA and EtBr such that the final concentrations were $[PPC_d]$, 12.5 μM (EtBr) and 10 μM (DNA). After 1h, the fluorescence was read allowing the calculation of $[FPX_r]$, the concentration of FPX required to *restore* EtBr fluorescence to 50% of the control EtBr-DNA sample. Samples were normalized to the controls ($[PPC_d]$ and no FPX as 0% and EtBr–DNA only as 100%) to calculate EC_{50} values using Prism software as *per* Table 2.2. The ratio index was calculated from the drug concentration divided by the EC_{50} value.

EtBr Displacement Assay with Heparin

Calf-thymus DNA (ct-DNA) was dissolved and dialyzed in HEPES buffer (80 mM HEPES, pH 7.2). Buffer exchanges occurred three times every 12 h. The DNA concentration was determined by UV–vis with absorbance at 260 nm and the average molecular weight of a nucleotide (333 g/mol). EtBr at 5 mM in water was diluted in HEPES buffer and incubated with ct-DNA in HEPES buffer for 5 min at room temperature. An aliquot of 1 mM PPCs in water was diluted in HEPES buffer and incubated for 1 h to reduce fluorescence to approximately 30% (20–25% for other compounds). Finally, increasing concentrations of heparin MW 18000 in buffer from 20.5 to 82 μM final (100–1000 μM final for other compounds) were incubated for an additional 1 h. Final concentrations were the following: EtBr, 12.5 μM; ct-DNA, 10 μM; TriplatinNC, 12.5 μM or

SpermidineNC, 62.5 μM. All samples were read (after a total of 2 h 5 min) in a 96-well plate at 530/590 nm using a microplate reader (Bio-Tek instruments). Samples were normalized to the controls (EtBr only as 0% and EtBr–DNA as 100%). All incubations were done at 37 °C.

Chapter 3. HS-Model Interactions with Metal-Ammine Compounds

3.1 Rationale.

Glycosaminoglycans (GAGs) such as heparan sulfate (HS) are linear polysaccharides composed of repeating disaccharide units of alternating uronic acid and hexosamine residues. When conjugated with proteins, heparan sulfate proteoglycans (HSPGs) are found on the cell surface and extracellular matrix with critical functions in cellular adhesion and migration.[64,65] HS is structurally related to heparin, a free GAG chain produced by mast cells that may be deployed as an immune defense mechanism.[59,66] Heparin usually remains highly sulfated, whereas HS displays varying degrees of sulfation.[64,65] HS has a multitude of protein partners, mediated through hydrogen-bonding and electrostatic interactions between sulfated regions of the polysaccharide and the basic amino acids of the protein.[28,34,67] Specifically, HSPGs interact with pro-angiogenic growth factors such as fibroblast growth factor (FGF) to induce dimerization for subsequent activation of its receptor.[67,68] FGF-2 directly stimulates tumor and endothelial cell proliferation, migration, and survival.[28] In addition to protein interactions, heparin and HSPGs are cleaved at glycosidic bonds by bacterial and mammalian enzymes (heparinase and heparanase, respectively). This HS cleavage leads to degradation of the extracellular matrix and release of growth factors for tumor angiogenesis.[36] Heparanase has a high abundance in many tumors, correlating with increased metastatic potential and poor clinical prognosis.[37,41] HSPGs and their associated proteins and enzymes are thus attractive drug targets because of their promotion of tumor progression at multiple levels: proliferation, invasion, angiogenesis, and metastasis.[28,34,59,66,67]

The highly anionic nature of heparin and HS means they are associated in vivo with physiologically relevant cations, similar to nucleic acids.[69–71] Cation association affects the biomolecule conformation and, in some cases, facilitates heparin−protein interactions such as Cu^{2+} -dependent heparin−annexin A2 binding.[72] More broadly, Cu^{2+} promotes angiogenesis, although the detailed mechanism is not defined.[73,74] Growth factors are also copper-dependent, with a slightly higher affinity for FGF-1 compared to FGF-2.[75,76] Aquated Cu^{2+}, Mg^{2+}, Fe^{3+}, and Zn^{2+} ions, at higher than physiological concentrations, reduce FGF-1 interactions with HS−heparin.[69] For heparin and HS, there are no strong donor atoms such as the heterocycle nitrogen atoms of purines and pyrimidines or even sulfur and nitrogen donors of amino acids such as cysteine and histidine available for binding to metal centers, suggesting that harder acids may preferentially bind and/or the oligosaccharides can enter into “noncovalent” electrostatic or hydrogen-bonding interactions (Figure 3.1). In recent papers, we have suggested that metalloglycomics, defined as the study of metal ion−oligosaccharide interactions, can be expanded beyond the study of physiologically relevant aquated metal cations to use defined coordination compounds.[29–32]

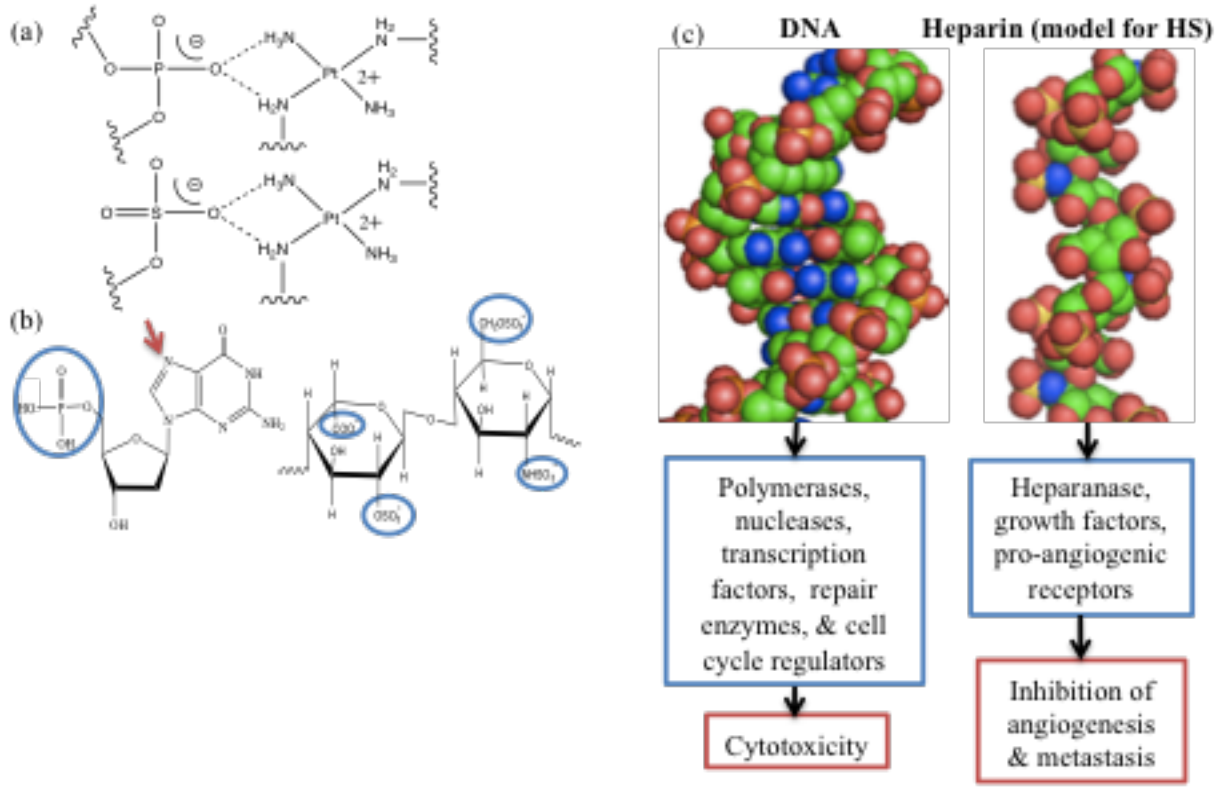

Figure 3.1. (a) Proposed structural analogy of the phosphate clamp to DNA (top) and sulfate clamp to heparan sulfate (bottom) formed by polynuclear platinum complexes (PPCs). (b) Blue circles on the repeating IdoA(2S)-GlcNS(6S) dimer in heparin/HS (right) and 2'-deoxyguanosine 5'-monophosphate (left) in DNA indicate possible electrostatic interaction sites while a red arrow shows the favored GuanineN7 site of covalent binding. (c) DNA (PDB: 309D) and heparin/HS (PDB: 1HPN) have high negative charge densities, and glycans such as HS having different protein recognition and signaling pathways (blue box). Inhibition of these pathways results in different biological consequences (red box).

Using coordination compounds, alteration of the oxidation state, coordination number, and geometry and substitution lability of ligands allows for the study of a wide variety of structural types to examine the structure and function of sulfated oligosaccharides, extending bioinorganic

chemistry to this third major class of biomolecules after DNA/RNA and proteins. Specifically, HSPGs act as receptors for cellular accumulation of the highly cationic polynuclear platinum complexes (PPCs).[29] Molecular recognition of a compound such as TriplatinNC (Figure 3.2) is effected through electrostatic and hydrogen-bonding interactions with the sulfate groups on the HS chains, analogous to the phosphate clamp formed by the same complex on DNA (Figure 3.1 a,b).[30–32] This high-affinity sulfate binding, or metalloshielding, has functional consequences including stabilization of the sulfate moieties, in a defined sequence octasaccharide, from dissociation in the gas phase.[32] In biophysical studies, PPC metalloshielding inhibits oligosaccharide backbone cleavage by both bacterial (heparinase I) and mammalian (heparanase) enzymes.[30,32] Growth factor binding to HS is inhibited in the presence of TriplatinNC with consequent effects on downstream kinase signaling.[30] Overall, these interactions lead to the inhibition of cellular angiogenesis and eventually the inhibition of *in vivo* metastasis (Figure 3.1 c).[46,48]

The molecular-level explanation of these events requires a detailed understanding of PPC−glycan interactions. The identity and conformation of the sugar and the number and positions of sulfation make GAGs highly complex systems, with significantly more variability than DNA, also with respect to non-bond-forming interactions. As polyelectrolytes, heparin and DNA have strong electrostatic interactions that, for heparin and other glycans such as HS, are influenced by the positions and amount of sulfation. Heparin is often used as a model for a highly sulfated HS and is considered to have the highest negative charge density of any biomolecule at an average of 2.7 sulfate groups per disaccharide.[59]

Here, we evaluated spectroscopic and biophysical approaches to examine metal ion−heparin interactions, especially in the case of substitution-inert PPCs such as TriplatinNC. The fundamental unit of TriplatinNC is the mononuclear tetraam(m)ineplatinum(II), and charge-related effects may be examined by a comparison of mononuclear and poly(tri)nuclear species. The generality of these approaches is exemplified by extension to other mononuclear metal−ammine complexes based on cobalt and ruthenium. The fluorescent properties of $[Ru(bpy)_3]^{2+}$ and its analogues have been used as analytical probes to examine the heparin concentration and even content in cells.[77–79] We therefore compared the relative reactivities of the chosen set of compounds toward both biomolecules (DNA and heparin) and in a novel competition assay showed that heparin is a competitor for metal complex−DNA binding. The overall results emphasize the relevance of glycan interactions for understanding the biological properties of coordination compounds and the potential for extending bioinorganic chemistry to this important class of biomolecules.

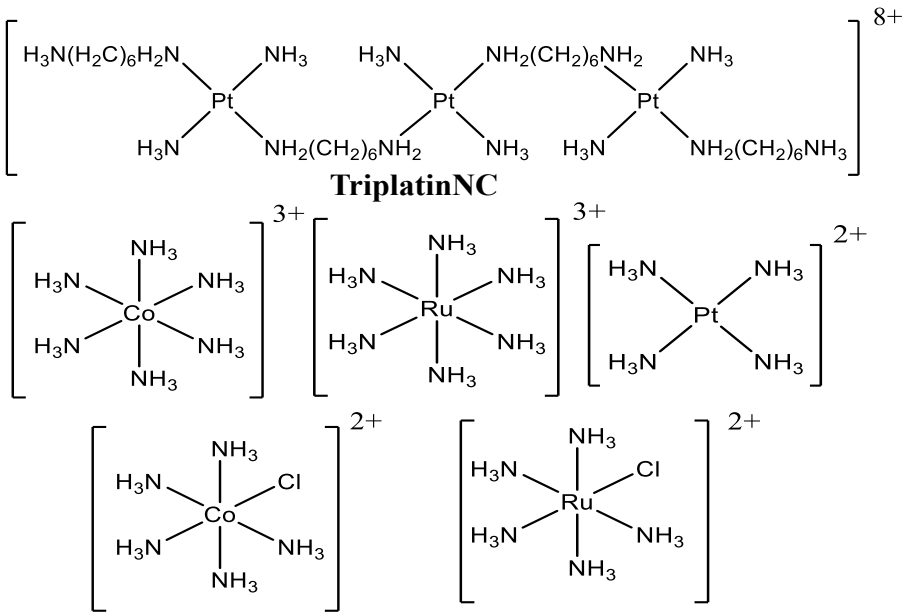

Figure 3.2. Structures of TriplatinNC and metal-ammine compounds used in this study. Counter ions omitted for clarity.

3.2 Direct binding of PPC-heparin using SPR.

For direct analysis, surface plasmon resonance (SPR) was used to estimate the TriplatinNC−heparin affinity. SPR is a label-free, real-time quantification of the interaction between the immobilized ligand on the sensor chip and the analyte being injected into a continuous flow over the ligand.[80] When the ligand and the analyte interact, the refractive index changes and the response is reported as RU (refractive units). Specifically, when polarized light hits the sensor chip metal surface causing surface plasmons (oscillations of free electrons from the metal layer) to excite, and inducing surface plasmon resonance, the reflected light intensity is reduced at the SPR angle.[81] The SPR angle is sensitive to changes in the refractive index at the sensor chip metal surface such as analyte binding to immobilized ligand and the resulting shift in the SPR angle provides the kinetics of the event by monitoring the change in real time.[81]

SPR has been used for determining the heparin concentration, metal−heparin binding, and metal−heparin binding effects on the growth factor and growth factor receptor recognition.[69,82] A mixture of metal ions reduced the affinity of FGF-1 binding to heparin from K_d = 22 to 350 nM.[69] In the study of heparin−protein interactions by SPR, heparin is preferentially immobilized onto the sensor chip rather than the protein because this more closely mimics natural biological systems, where HS is found at the cell surface as a proteoglycan and binds to target proteins.[83,84] A common method for heparin immobilization is to use a biotinylated heparin and a streptavidin coded sensor chip.[83]

First, we used a biotinylated heparin and tried to attach it to a streptavidin-coated carboxymethyl dextran (CMD) chip, but immobilization did not occur. Perhaps charge repulsion between the

highly negative charge heparin and CMD chip caused adequate heparin immobilization. Hence, we switched the heparin for a biotinylated heparin with a 12-atom spacer, which resulted in 120 RU of immobilized heparin (Appendix II Figure 1 a). Also, we were able to obtain a binding response for TriplatinNC at several concentrations, but unfortunately, TriplatinNC had high background noise from TriplatinNC non-specific binding (Appendix II Figure 1 b). The high charge of TriplatinNC may aided in the significant non-specific binding to possibly both the dextran sensor chip surface and the streptavidin coating. Therefore, to help reduce the non-specific binding, Reichert Technologies blocked the sensor chip surface with ethylene diamine instead of ethanol amine to introduce a positive charge but to no avail. Then we tried another custom chip with low density CMD and thus lower overall negative charge on the sensor chip, but again to no avail. Although, these new modified chips had immobilized heparin, TriplatinNC still had significant non-specific binding (Appendix II Figure 2).

Finally, in collaboration with Reichert Technologies, a Neutravidin-coated mixed self-assembled monolayer (mSAM) sensor chip (Reichert part # 13306065) was used to minimize the background noise and resulted in significantly lower nonspecific binding of TriplatinNC to the sensor surface. Although there was still some binding to the reference, causing some distortion in the binding curves (Figure 3.3). At the lowest 111 nM concentration, there was a large (repeatable) decrease in the signal, which may be due to random adsorption of the highly charged molecule in the system. An analysis of the binding curves for the interaction between heparin and TriplatinNC was generated using the TraceDrawer program. Although a global fit was not possible, a one-site model and 1:1 TriplatinNC−heparin stoichiometry, gave a K_d value of 340 ± 30 nM (Figure 3.3). The repeated assay under the one-site binding model had 440 ± 40 nM (Appendix II Figure 3).

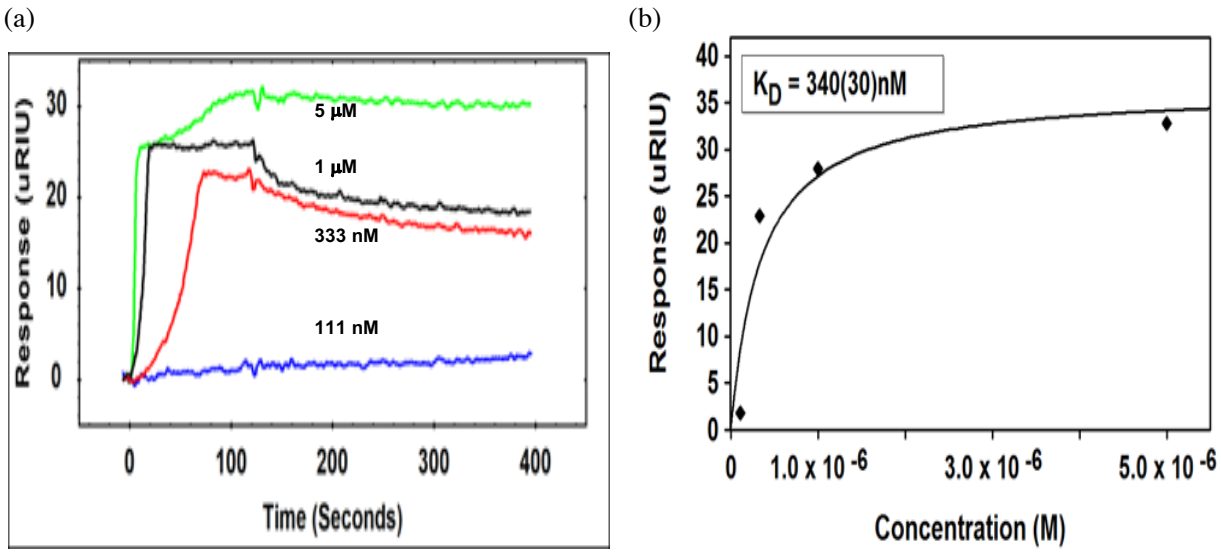

Figure 3.3. *SPR trial 4.* Determination of the TriplatinNC−heparin binding affinity by SPR using a biotinylated heparin (MW ∼15000) immobilized to Neutravidin on a planar mSAM chip. (a) After injection of 5, 1, 0.333, and 0.111 µM of TriplatinNC, the solution was allowed to flow over the chip for 5 min to allow binding; a buffer was then injected, and after flowing for 5 min, dissociation was assessed. (b) The amount of TriplatinNC bound at equilibrium was corrected for background and plotted versus input TriplatinNC concentration. Analysis by equilibrium parameters using a 1:1 binding model yielded a K_d value of 340±30nM.

A two-site binding model was applied to the 1µM TriplatinNC curve and the equilibrium dissociation constant for the first site was 2.98 nM, while the second site was 341 µM (Figure 3.4). The repeated assay under the two-site binding model had K_{d1} = 2.8 nM and K_{d2} = 4.96 µM (Appendix II Figure 4). These results may reflect the microheterogeneity of heparin and it is possible that a two-site model reflects first a site-specific binding and secondly a random binding

due to electrostatics. Because the immobilized heparin had MW 15000, it is plausible that there could be multiple binding sites, which may affect the estimated K_d values.

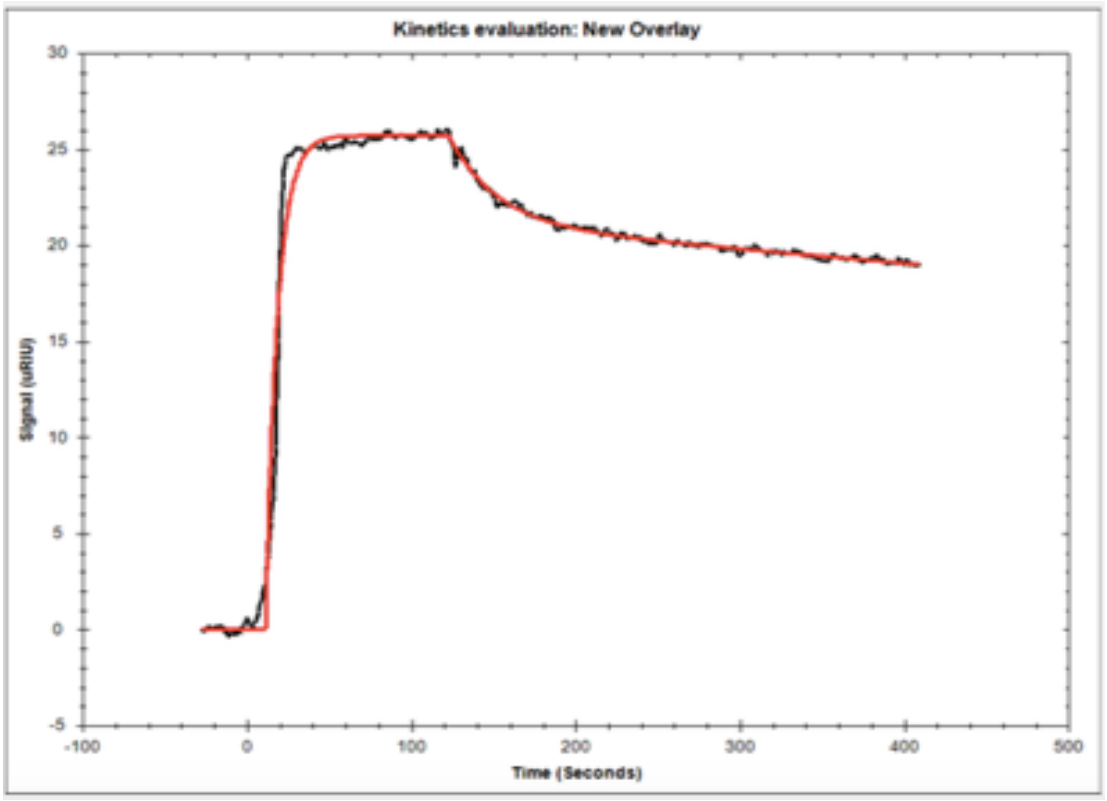

Figure 3.4. *SPR trial 4.* A two-site model for TriplatinNC-heparin binding by SPR. The 1µM TriplatinNC injection gave the best curve and fit to a two-site model with immobilized heparin.

SPR confirmed strong TriplatinNC−heparin interactions. Because the SPR system measured TriplatinNC interacting with heparin immobilized to the surface of the sensor chip, this immobilization may reduce the degrees of freedom of the heparin molecule to interact and thus affect the kinetics and affinity of the TriplatinNC−heparin interaction.[85] However, the heparin immobilization more closely mimics natural biological systems where the HS chains are

covalently attached to core proteins as HSPGs. There are few small molecule−heparin binding data for comparison by SPR because the majority of studies have been on protein−heparin interactions.

3.3 Comparing TriplatinNC binding to DNA and heparin.

The K_d values with heparin from the direct SPR and other techniques[45] raise questions about the relative affinity of TriplatinNC for DNA or heparin. TriplatinNC and substitution-inert complexes in general bind with high affinity to DNA with a measured $K_{d(app)}$ value of 17.7 nM (reported as $K_{a(app)}$).[60] Given the highly anionic nature of both biomolecules, what are the relative affinities of a molecule such as TriplatinNC for DNA or heparin? As mentioned, heparin is considered to have an average of 2.7 sulfate groups per disaccharide compared to that of two phosphate groups per base pair for DNA. We therefore developed a number of competitive binding assays to answer this question and to complement the indirect and direct HS−PPC assays.[45] EtBr, and circular dichroism (CD) competition assays compared the ability of heparin to compete with DNA for the binding of charged metal complexes.

As metal complex-HS interactions are part of an emerging field, the development of novel assays is required to probe such interactions while complementing current binding assays. We used an adaptation of the well-known EtBr fluorescence assay to measure the binding affinities of metal complexes.[30,60] The fluorescence from intercalator binding to DNA is quenched when the intercalator is displaced upon TriplatinNC−DNA binding. Upon the addition of increasing concentrations of heparin, TriplatinNC is sequestered and the nucleic acid now becomes available to bind the intercalator, with a resultant increase in fluorescence (Table 3.1). From Figure 3.5, we can see that a concentration of 12.5 μM TriplatinNC reduced EtBr fluorescence to approximately

25% of the control value. A concentration of 20.5 μM heparin increases fluorescence to approximately 50%, while full fluorescence is restored in the 35−40 μM range. The experiment allows us to define EC_{50} as the sequestration concentration of heparin required to restore 50% EtBr binding (Table 3.1). This experiment again confirms the similar affinities of the two biomolecules for TriplatinNC.

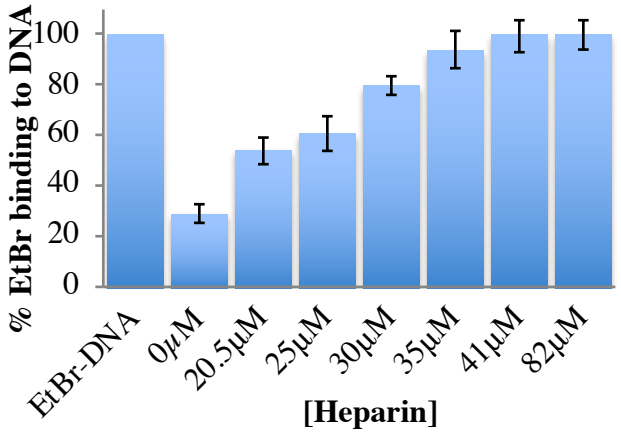

Figure 3.5. Heparin, a competitive inhibitor of TriplatinNC−DNA binding. EtBr bound to ct-DNA was displaced upon the addition of TriplatinNC, while increasing the concentration of heparin MW ~18000 sequestered TriplatinNC from DNA, allowing EtBr−DNA binding to occur. EtBr bound to DNA was normalized to 100% with EtBr only as 0%. Error bars represent the mean ± SD of at least 3 independent experiments (each with 3 replicates).

Metal Complex	EC_{50} (μM)
TriplatinNC^{8+}	24.60±1.38
$[Pt(NH_3)_4]^{2+}$	<100
$[Co(NH_3)_6]^{3+}$	689.35±17.04
$[Ru(NH_3)_6]^{3+}$	852.60±185.5
$[RuCl(NH_3)_5]^{2+}$	>1000
$[CoCl(NH_3)_5]^{2+}$	>1000

Table 3.1. EC_{50} was defined as the sequestration concentration of heparin MW ∼18000 required to return 50% EtBr binding to DNA from the bound metal−ammine compound. EtBr bound to DNA was normalized to 100%, with EtBr only as 0%. EC_{50} values ± SD of at least 2 independent experiments (each with 4 replicates) were calculated in Graphpad Prism 7.

The competitive binding of heparin and DNA can also be easily envisaged by CD spectroscopy monitoring of the conformational changes during each event. The CD spectrum of the DNA structure influenced by its environment and changes such as TriplatinNC binding can be monitored without the need for labels. Circular dichroism is the result of the interaction of polarized light with chiral molecules like DNA. The positive CD band of DNA centered at approximately 270 nm is decreased in the presence of TriplatinNC (Figure 3.6). Upon the addition of heparin to the DNA−TriplatinNC mixture, the positive band is restored in a heparin concentration-dependent manner through sequestration of TriplatinNC and restoration of DNA to its original conformation. Neither heparin nor heparin−TriplatinNC mixtures show any CD absorbance in the 250−280 nm range, and thus the changes observed are direct visualizations of competitive binding.

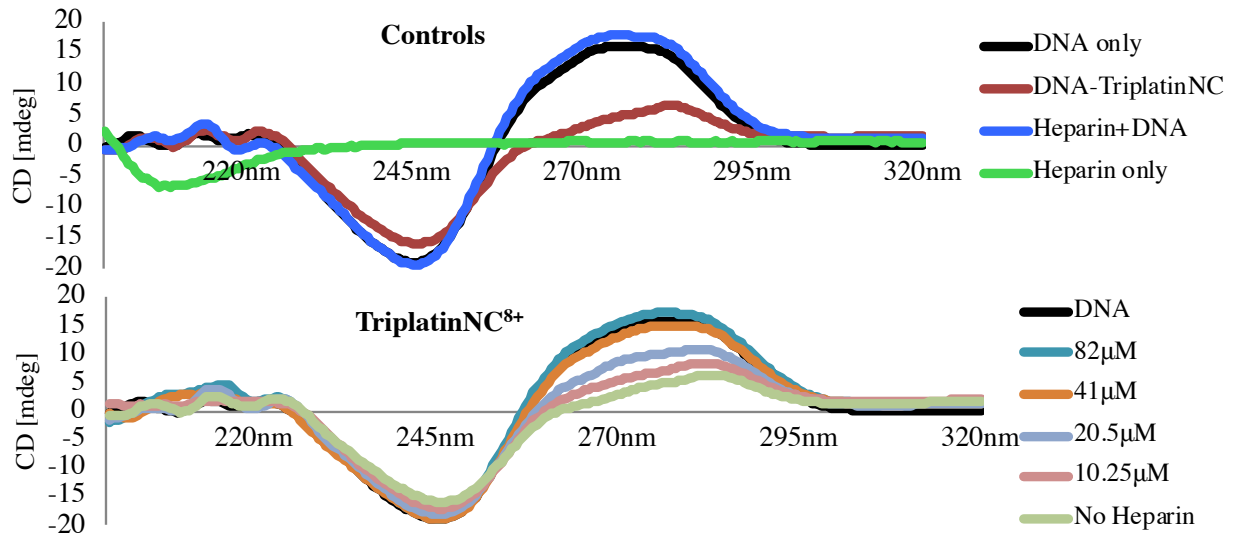

Figure 3.6. CD spectra of ct-DNA in presence and absence of heparin (18000 MW) and TriplatinNC (0-82µM). DNA conformation (measured by the 280nm absorbance specific for ct-DNA) is restored upon increasing heparin concentrations. HEPES buffer effects were observed below 230nm for DNA. Representatives of at least 2 independent experiments (each with 2 replicates).

Electrostatic and hydrogen-bonding interactions with noncovalent metal complexes observed on DNA translate to heparin−HS interactions. To determine the relative affinity of TriplatinNC for heparin and/or DNA, competition assays were used with reporters for the TriplatinNC−DNA interaction. The EtBr competition assay showed that TriplatinNC has a broadly similar affinity for both heparin and DNA.

3.4 Comparing metal-ammine compounds binding to DNA and heparin.

Trinuclear complexes are modular in nature, and the strong interactions of TriplatinNC with heparin led us to explore the individual contributions of the mononuclear tetraam(m)-

ineplatinum(II) units and further compare charge-related effects based on cobalt and ruthenium analogues (Figure 1). While, in principle, the chloropentaammine complexes of cobalt(III) and ruthenium(III) can enter into covalent interactions through Co−Cl or Ru−Cl substitution, the nature of the assays developed and the kinetic inertness of substitution on the cobalt(III) and ruthenium(III) centers suggests that any trends observed across the series of compounds will be most likely due to simple differences in charge.

Metal-ion interactions with nucleic acids have been widely studied;[86] more specifically, the chosen cobalt and ruthenium complexes bind tightly to DNA.[87–90] Thus, we compared the affinities of metal−ammine compounds for DNA and heparin. Because previous studies demonstrated $[Pt(NH_3)_4]^{2+}$- and $[Co(NH_3)_6]^{3+}$-induced DNA conformational change using CD,[89,90] we employed this method to observe metal−ammine compound binding to DNA and then the effects of the addition of heparin observed by the return of the DNA conformation. The potential covalent metal−ammine compounds (up to a concentration of 500μM) did not change the DNA conformation at 280 nm, indicating little interaction, even in comparison to the square-planar $[Pt(NH_3)_4]^{2+}$ (Figure 3.7).

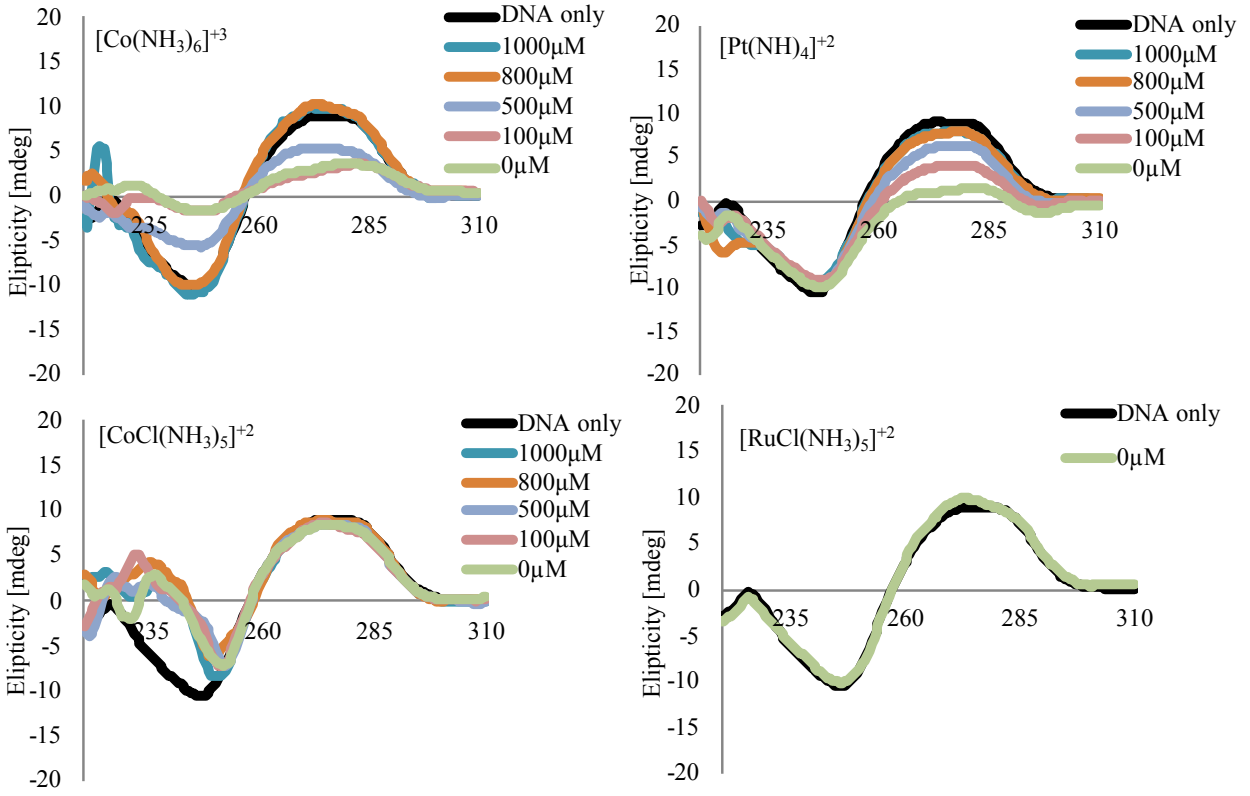

Figure 3.7. CD spectra of ct-DNA in presence and absence of heparin (18000 MW) and metal-ammines (0-1000µM). DNA conformation (measured by the 280nm absorbance specific for ct-DNA) is restored upon increasing heparin concentrations. HEPES buffer effects were observed below 230nm for DNA. Representatives of at least 2 independent experiments (each with 2 replicates).

For EtBr competition assay, at a concentration identical with that of the intercalator, a much larger concentration of 500 µM was needed for the mononuclear metal−ammine compounds to displace the EtBr compared to TriplatinNC (12.5 µM; Table 3.1 and Figure 3.8). Care must be taken in analyzing these trends across a range of compounds because the inherent affinities of the compounds themselves for DNA as a starting point differ widely. Further, the different assays themselves represent different phenomena. The dangers in extrapolating across a series such as the

one studied here is demonstrated for $[Pt(NH_3)_4]^{2+}$, which has demonstrably low affinity for DNA.[62] In principle, charge effects (2+) should be the same as those for the $[CoCl(NH_3)_5]^{2+}$ and $[RuCl(NH_3)_5]^{2+}$ compounds, as seen in fluorescence polarization assay.[45] An apparently higher affinity for heparin in EtBr assay compared to fluorescence polarization assay[45] may reflect its reduced ability to displace the intercalator, perhaps because of its smaller square-planar geometry versus the octahedral geometry of the cobalt and ruthenium systems, giving an apparently (but false) higher heparin affinity. This anomaly emphasizes the need to employ more than one approach to assess accurately the questions of relative affinity of heparin and DNA for coordination compounds.

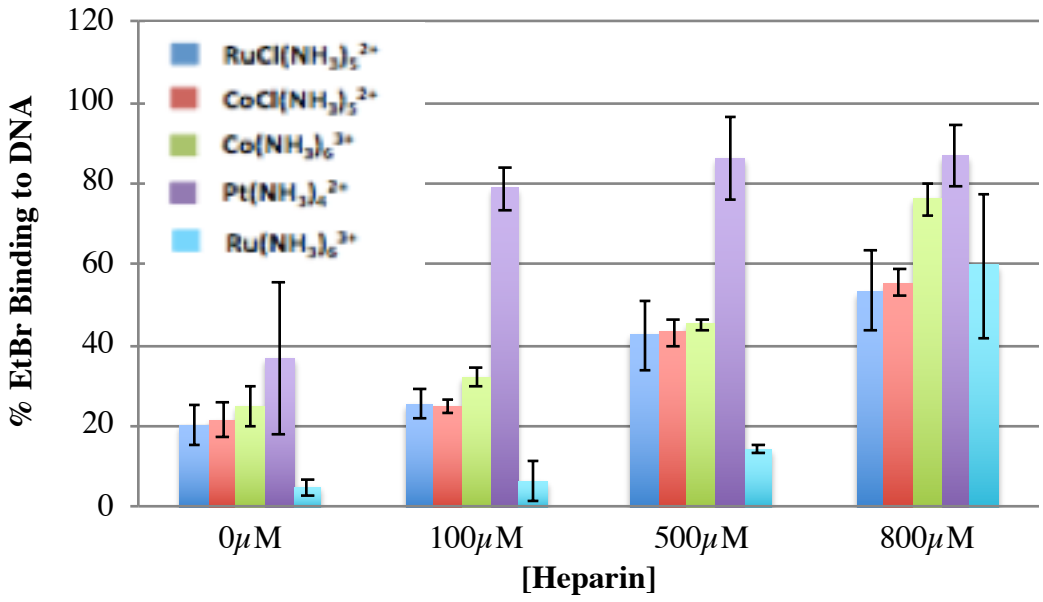

Figure 3.8. Ethidium bromide competition assay for comparison of metal-ammine compounds binding to ct-DNA and heparin (MW ~18000). EtBr displaced by metal-ammine compound-DNA binding rebinds to DNA upon the concentration-dependent sequestration of the metal-ammine compound (500 μM) by heparin. EtBr bound to DNA was normalized to 100% with EtBr only as

0%. Error bars represent the mean ± SD of at least 2 independent experiments (each with 3 replicates).

3.5 Summary.

We observed broadly similar trends for metal−ammine compound interaction with heparin across the dye reporter techniques[45] and DNA comparison assays reported here. Slight discrepancies can be accounted for by the nature of the technique. Another caveat is the complexity across the experiments where the SPR system is a simple two-species system, DNA comparison with CD assay is a three-species system, and DNA comparison with EtBr assay is four-species system. Given these caveats, these results are a testament to the relative accuracy of these methods for determining trends of coordination compound interaction with heparin.

Future SPR experiments could be used to determine relative PPC affinities for heparin or other GAGs. It would be interesting to compare TriplatinNC to other noncovalent PPCs like DiplatinNC or covalent PPCs like Triplatin and BBR3571. Smaller heparins (3000 MW) may prove more useful in providing true one-one interactions but such heparins are not biotinylated. Therefore, mSAM sensor chips (Reichert 13206061) that has carboxy-terminated alkanthiol without avidin could be linked to heparin (or reducing end of a glycan) by a 2-aminobenzamide acid (AB) linker.[91] Effectively, forming heparin-AB linker-alkane-thiol-Au-chip where the heparin is bound to the AB linker through reductive amination,[92] while the AB linker amine couples (using EDC crosslinking agent) to the carboxy-terminated alkanethiol attached to the gold chip (Au-S coordination).[91]

Data was published in:

- Katner, S.J., Johnson, W.E., Peterson, E.J., Page, P., Farrell, N.P. Comparison of metal-ammine compounds binding to DNA and heparin. Glycans as ligands in bioinorganic chemistry. *Inorg. Chem.* **57,** 3116-3125 (2018).
- Katner, S.J., *et al. Proc. AACR Washington, DC.* Abstract **#17** (2017)

3.6 Experimental.

The concentrations of heparin were calculated using the dimer IdoA(2S)–GlcNS(6S) with a molecular weight of 609.46 g/mol unless otherwise noted.

SPR 1 – 4 trials

Binding experiments were carried out at 25 °C on a Reichert Technologies (Depew, NY) SR7500DC two-channel system equipped with a Streptavidin-coated carboxymethyl dextran (CMD) sensor chip (Reichert Technologies – modifications were explained in the text) using 20 mM 4-(2-hydroxyethyl)-1-piperazineethane- sulfonic acid (HEPES), and 150 mM NaCl at pH 7 (HBS) as the running buffer. Prior to heparin capture, the Streptavidin-coated CMD sensor chip was preconditioned with three consecutive injections of 50 mM NaOH for 1 min, respectively. Biotinylated heparin (MW ~15000, Sigma with 12-atom spacer) at a concentration of 20 μg/mL was subsequently injected onto the avidin surface on the left channel and captured to a level of 120 μRIU (~120 RU), whereas the right channel was left as the bare avidin surface to serve as a reference for nonspecific binding of TriplatinNC. Under a flow rate of 25 μL/ min, TriplatinNC was injected over both channels at concentrations of 50, 5, and 0.5 μM, respectively, for 2 min followed by a 5 min dissociation in a HBS running buffer. The kinetic data were analyzed using

TraceDrawer (Ridgeview Instruments) with a 1:1 model, while the equilibrium data were fit using Scrubber (Biologic Software) to a 1:1 binding model.

SPR 5 – 6 trials

Binding experiments were carried out at 25 °C on a Reichert Technologies (Depew, NY) SR7500DC two-channel system equipped with a Neutravidin-coated mSAM sensor chip (Reichert Technologies, part 13306065) using 10 mM HEPES, 150 mM NaCl, and 0.005% Tween-20 (HBST) as the running buffer. Prior to heparin capture, the Neutravidin-coated mSAM sensor chip was preconditioned with three consecutive injections of 50 mM NaOH for 1 min, respectively. Biotinylated heparin (MW ~15000, Sigma) at a concentration of 100 μg/mL was subsequently injected onto the avidin surface on the left channel and captured to a level of 110 μRIU (~110 RU), whereas the right channel was left as the bare avidin surface to serve as a reference for nonspecific binding of TriplatinNC. Under a flow rate of 25 μL/ min, TriplatinNC was injected over both channels at concentrations of 5, 1, 0.33, and 0.11 μM, respectively, for 2 min followed by a 5 min dissociation in a HBST running buffer. The kinetic data were analyzed using TraceDrawer (Ridgeview Instruments) with a 1:1 model, while the equilibrium data were fit using Scrubber (Biologic Software) to a 1:1 binding model.

Ethidium Bromide (EtBr) Displacement Assay with Heparin

Calf-thymus DNA (ct-DNA) was dissolved and dialyzed in HEPES buffer (80 mM HEPES, pH 7.2). Buffer exchanges occurred three times every 12 h. The DNA concentration was determined by UV−vis with absorbance at 260 nm and the average molecular weight of a nucleotide (333 g/mol). EtBr at 5 mM in water was diluted in HEPES buffer and incubated with ct-DNA in HEPES

buffer for 5 min at room temperature. An aliquot of 1 mM TriplatinNC (4 mM for other compounds) in water was diluted in HEPES buffer and incubated for 1 h to reduce fluorescence to approximately 30% (20–25% for other compounds). Finally, increasing concentrations of heparin MW 18000 in buffer from 20.5 to 82 μM final (100–1000 μM final for other compounds) were incubated for an additional 1 h. Final concentrations were the following: EtBr, 12.5 μM; ct-DNA, 10 μM; TriplatinNC, 12.5 μM (500 μM for other compounds). All samples were read (after a total of 2 h 5 min) in a 96-well plate at 530/590 nm using a microplate reader (Bio-Tek instruments). Samples were normalized to the controls (EtBr only as 0% and EtBr–DNA as 100%). All incubations were done at 37 °C.

CD Studies

TriplatinNC (r_i = 0.075 compound/DNA ratio) or metal–ammine compounds (r_i = 5) were incubated with 100 μM ct-DNA for 1 h at 37 °C in HEPES buffer (80 mM HEPES, pH 7.2). Then heparin MW ~18000 was added with 10.25–230 μM final concentrations (only 10.25–82 μM are shown) and incubated for an additional 1 h at 37 °C. Final concentrations after heparin addition were the following: 100 μM ct-DNA and 7.5 μM TriplatinNC (r_i = 0.075) or 500 μM (r_i = 5). After the incubations, samples were placed in a 10 mm submicro cuvette to record the CD spectra at room temperature using a Jasco J600 spectropolarimeter.

Chapter 4. Biological Consequences of PPC-HS interactions

4.1 Rationale.

Heparan sulfate proteoglycans (HSPGs), composed of the linear polysaccharide heparan sulfate (HS) conjugated to a protein core, are located on the cell surface and extracellular matrix. The HS chains display varying degrees of sulfation, which constitutes the molecular recognition motif for many HS-protein interactions. HSPGs, associated growth factors, and heparanase promote tumor progression by facilitating invasion, angiogenesis, and metastasis.[28] Sulfate clusters on the glycan backbone also mediate the interaction of polynuclear platinum complexes (PPCs) with HSPG through a "sulfate clamp." Such PPC-HS interactions can be conceptualized as "polyarginine" mimics. Strong HS-PPC binding protects the oligosaccharide against sulfate loss through metalloshielding.[32] The biological consequences of metalloshielding will in principle affect HS interactions with relevant enzymes and proteins such as heparanase and growth factors, similar in concept to the inhibition of DNA-protein binding through modification of DNA structure and conformation. In this chapter, we examine these biological consequences of HS-PPC interactions (from previous chapters).

4.2 PPCs tumor selectivity with modified syndecan expression.

Syndecans are transmembrane heparan sulfate proteoglycans (HSPGs) with core proteins having extracellular (HS attachment sites) and cytoplasmic domains. Since PPCs interact with heparan sulfate (HS), which we have demonstrated in chapters 2[44] and 3[45] as well as previous studies,[29–32] PPCs may interact with HS chains on syndecans. Therefore, we hypothesized that modified syndecan expression may affect PPC available binding sites that influence mechanisms such as

cytotoxicity, and cell uptake. Moreover, syndecans are overexpressed in aggressive breast carcinomas,[93] suggesting a possible tumor selectivity role for PPCs targeting syndecans.

NS1-NS2, NS1, or NS2 MDA-MB-231 cells are breast carcinoma cells that have been transfected with a non-silencing vector (NS) to use as a control for the stable knockdown (KD) of syndecan (Sdc) 1, 4, 1&2, or 1&4 cells. Flow cytometry and qPCR data from Dr. Koblinski's lab (where the cells were generated) verified no change in other syndecan expression when one or more syndecans were knockdown. Therefore, modified syndecan expressing cells do not have an increase in other syndecans compared to their respective empty vector (NS) cells.

DiplatinNC, BBR3464, AH44, TriplatinNC, and cisplatin were examined for their cellular accumulation in the KD Sdc 4 cells and their respective empty vector NS2 cells. After 1 and 3-hour treatments, cells were analysed on the ICP-MS for Pt content. PPCs had overall similar cell accumulation between the cells lines (Figure 4.1 a) indicating that a loss of Syndecan 4 may not have an overall dramatic impact on PPC cell uptake. However, since the knockdown cells are only reducing syndecans 1 & 4 expression, there are still other syndecans and glypicans to allow cell uptake whereas the modified GAG expression in the CHO-psgA-745 (lacking HS/CS) cells mutant cells had complete GAG loss across all proteoglycans, which was previously shown to considerably influence PPC cell uptake (Chapter 2).[44] Therefore, we next examined the double knockdown of syndecans 1 & 4 cellular accumulation of TriplatinNC and cisplatin. Our reasoning was that the double knockdown would probably have more of an impact on available PPC binding sites on the cell surface compared to a single knockdown. With 1, 3, and 6-hour treatments, TriplatinNC had reduced cellular accumulation in the double KD Sdc 1 & 4 cells compared to the

empty vector cells (Figure 4.1 b, Table 4.1). The results suggest syndecans may aid in PPC cell uptake and thus demonstrate TriplatinNC interacting with syndecans.

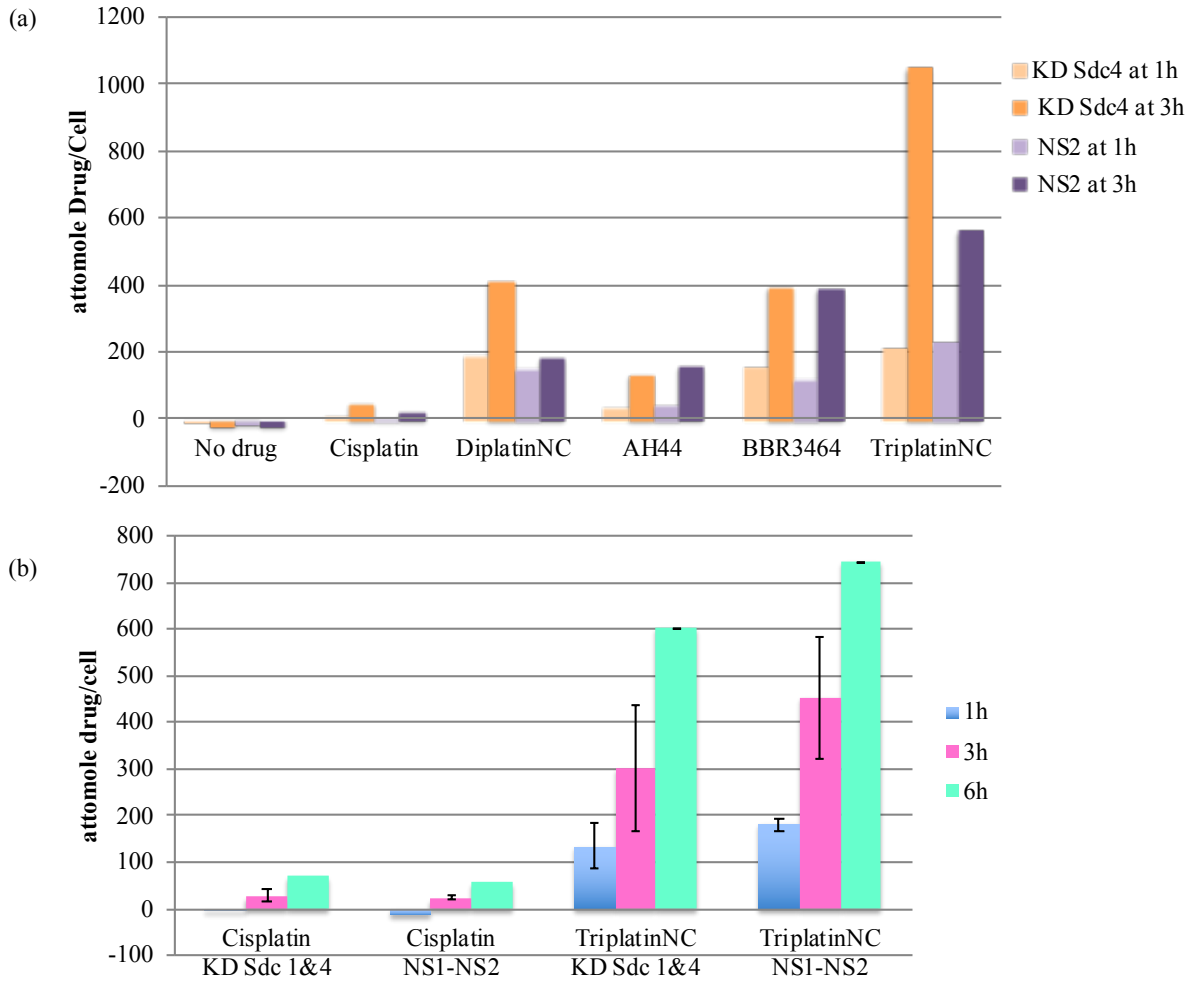

Figure 4.1. PPC cellular accumulation with modified syndecan expression. (a) PPC and cisplatin (10 μM) were incubated for 1 and 3-hours in control empty vector NS2 MDA-MB-231 cells vs. KD Sdc4 MDA-MB-231 cells. (b) Cisplatin and TriplatinNC (10 μM) were incubated at 1, 3, and 6-hours in control empty vector NS1-NS2 MDA-MB-231 cells and double KD Sdc 1& 4 MDA-MB-231 cells. Cells were collected and analysed using ICP-MS for Pt content. Pt readings were normalized to cell number and number of Pt-centers for each compound. Error bars represent the mean ± SD of at least 2 independent experiments (each with 2 replicates).

	1 H	3H	6H
TRIPLATINNC	180.4 ±13.9	451.73 ±130.6	743.1
TRIPLATINNC *(KD)*	133.5 ±49.0	300.3 ±134.7	602.1
CISPLATIN	ND	24.0 ±3.6	58.2
CISPLATIN *(KD)*	ND	28.7 ±12.9	68.8

Table 4.1. Cell uptake of TriplatinNC and cisplatin in NS1-NS2 MDA-MB-231 cells and KD Sdc 1 &4 MDA-MB-231 cells (*KD*) after 1, 3, and 6h drug treatments. Cells were collected and analysed using ICP-MS for Pt content. Pt readings were normalized to cell number and number of Pt-centers for each compound. ND denotes "could not be determined" since it was too low for standards. The mean ± SD was calculated from least 2 independent experiments (each with 2 replicates).

Cells with single knockdown of syndecans were first examined for influence on PPC cytotoxicity. Cisplatin, AH44, BBR3464, TriplatinNC, and DiplatinNC were evaluated for cytotoxicity in KD Sdc 4 cells and NS2 vector control cells. Overall, PPCs were slightly more cytotoxic in the control empty vector cells than the KD Sdc 4 cells (Table 4.2, Appendix II Figure 1). This trend was observed at both 72 and 24-hour treatments. Intriguingly, cisplatin cytotoxicity was more cytotoxic in the NS2 cells than the KD Sdc 4 cells indicating that differences in cytotoxicity between these two cell lines may be influenced by other factors such as proliferation rate particularly since

cisplatin does not interact with syndecans. Another cell line with a single knockdown of syndecan 1 was examined that had similar previous trends of cisplatin and DiplatinNC being more cytotoxic in the NS 1 cells than the KD Sdc 1 cells (Figure 4.2).

IC50 (μM)						
		Cisplatin	AH44	BBR3464	TriplatinNC	DiplatinNC
72h	NS2 MDA-231 cells	1.87	4.23	>50	3.15	41.54
72h	KD Sdc 4 MDA-231 cells	8.54	17.93	>50	4.07	>50
24h	NS2 MDA-231 cells	25.06	>50	-	37.88	>50
24h	KD Sdc 4 MDA-231 cells	45.84	>50	-	48.08	>50

Table 4.2. PPC cytotoxicity with modified syndecan expression. IC_{50} values were calculated in GraphPad Prism 7 from 2 independent experiments (each with 2 replicates). Error bars are in plots see Appendix III Figure 1.

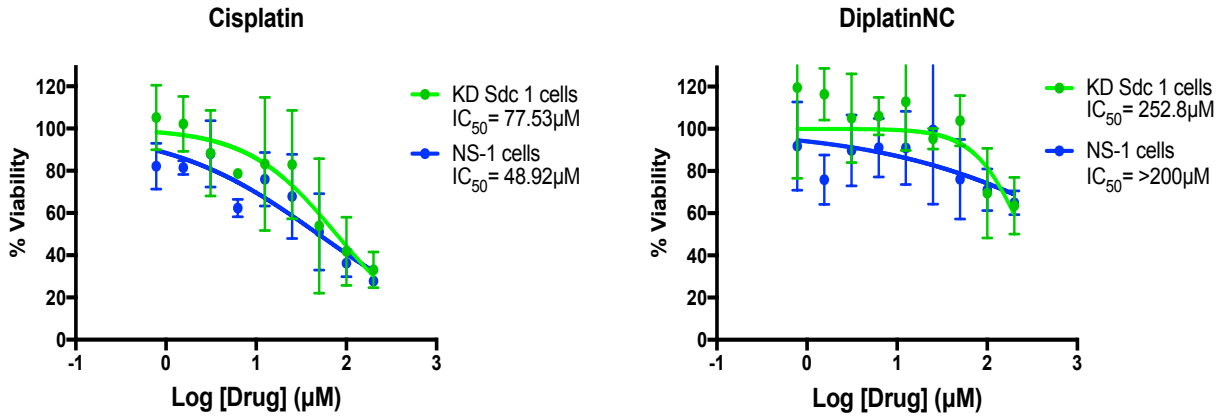

Figure 4.2. Cisplatin and DiplatinNC cytotoxicity in KD Sdc 1 and non-silencing vector control cells after 24-hour treatment. IC_{50} values ± SD of at least 2 independent experiments (each with 4 replicates) were calculated in Graphpad Prism 7.

Further, cytotoxicity of PPCs and cisplatin were evaluated in cells with double knockdowns of syndecans. However, the cytotoxic profiles were different than the ones observed in the single knockdown syndecan cells. The treatments exhibited increased cytotoxicity in the double knockdown cells than the non-silencing vector cells (Figure 4.3). Since the treatments were long 72-hour or even 24-hour incubations, a knockdown of one or two of the many HSPG receptors for PPCs many have little influence on the overall cytotoxicity. Therefore, 1-hour treatments of PPCs followed by a 72-hour drug free incubation were examined in the double knockdown cells. However, the 1-hour treatment of PPCs had similar cytotoxicity values in the knockdown and non-silencing cells (Figure 4.4).

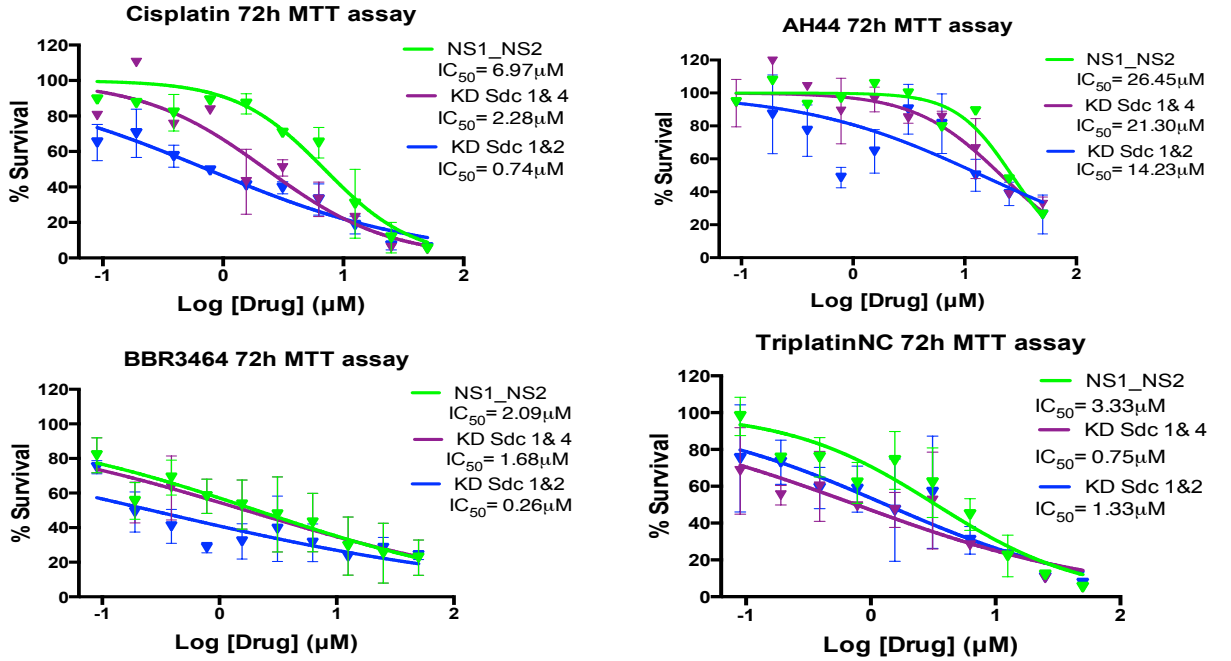

IC50 (µM)				
	Cisplatin	AH44	BBR3464	TriplatinNC
NS1-NS2 MDA-231 cells	6.97	26.45	2.09	3.33
KD Sdc 1&4 MDA-231 cells	2.28	21.3	1.68	0.76
KD Sdc 1&2 MDA-231 cells	0.74	14.23	0.26	1.33

Figure 4.3. PPC cytotoxicity in KD Sdc 1 & 2, KD Sdc 1 & 4, and non-silencing vector control cells after 72-hour treatment. IC_{50} values ± SD of at least 2 independent experiments (each with 4 replicates) were calculated in Graphpad Prism 7.

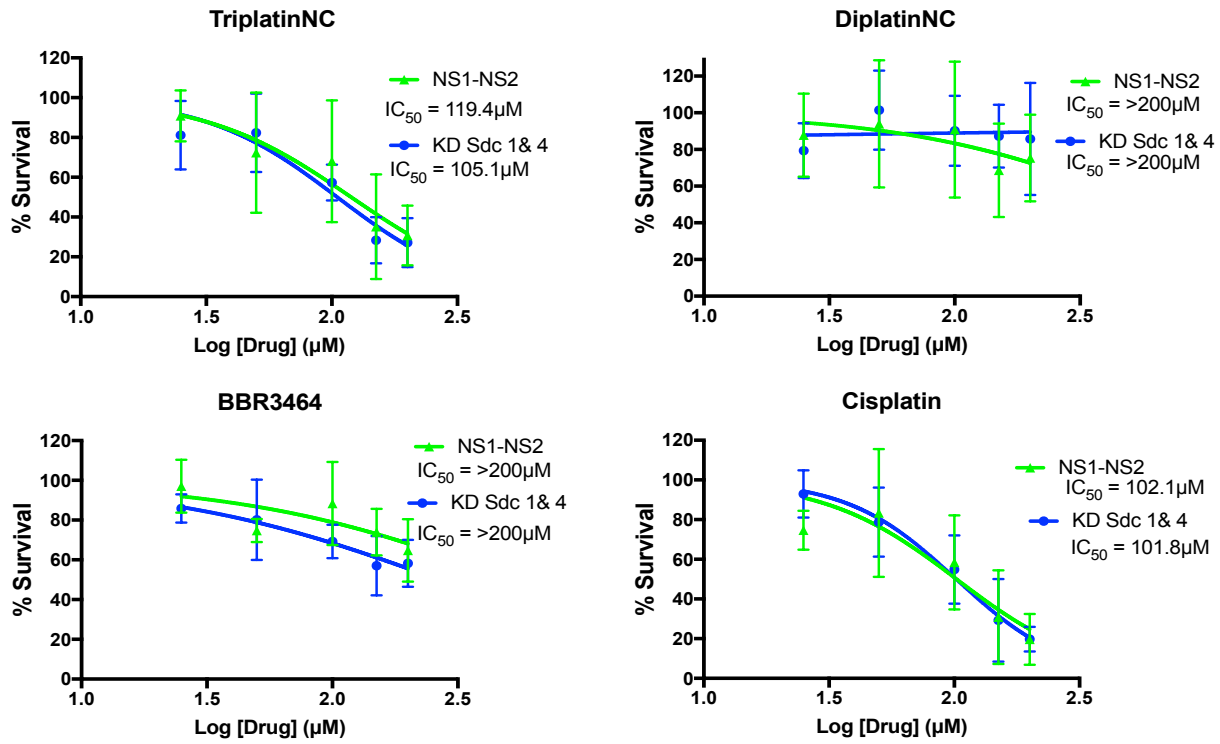

Figure 4.4. PPC cytotoxicity in KD Sdc 1 & 4, and non-silencing vector control cells after a 1-hour treatment followed by a 72-hour drug free incubation. IC_{50} values ± SD of at least 2 independent experiments (each with 4 replicates) were calculated in Graphpad Prism 7.

4.3 PPCs block VEGF-A-mediated processes on endothelial cells.

Tumor cells produce angiogenic growth factors that are captured by pro-angiogenic receptors on nearby endothelial cells of a pre-existing blood vessel.[94] This process activates the "angiogenic phenotype" for the endothelial cells and thus initiates tumor angiogenesis.[28] Critical angiogenic growth factors: VEGF-A[95] and FGF2[96] require HSPGs and other molecule interactions concurrently with their receptors, VEGFR2 and FGFR1 respectively, for a full angiogenic effect.[28] Compounds that affect HSPG expression on endothelial cells have prevented FGF2 and VEGF-A induced angiogenesis *in vivo*.[97] Given that multiple signaling pathways influence angiogenesis,

using inhibitors selectively directed against a single angiogenic growth factor is likely to have little therapeutic value.[98] PPCs compete with FGF2 for direct HS binding and inhibit FGF2-induced endothelial cell migration and signaling.[30] Therefore, we proposed that PPCs can also block VEGF-A-HSPG interactions on endothelial cells resulting in a multi-targeted, anti-angiogenic effect.

The vascular endothelial growth factor (VEGF) family is composed of five related factors with VEGF-A being the most essential for angiogenesis.[28] VEGFs signal through their tyrosine kinase receptors VEGFR1, VEGFR2, and VEGFR3 with VEGFR2 highly expressed in vascular endothelial cells.[99] VEGF-A induces angiogenesis by dimerizing VEGFR2 receptors for autophosphorylation on their intracellular tyrosines that lead to specific phosphotyrosine-protein interactions causing downstream signaling.[100]

Endothelial cell migration and tube formation is necessary for blood vessel formation in angiogenesis and ultimately tumor angiogenesis. To assess the anti-angiogenic action of PPCs in cell-based models, human umbilical vein endothelial cells (HUVECs) were stimulated with rhVEGF-A to induce migration and tube formation in monolayer wound healing and Matrigel tube formation assays respectively. Drug concentrations that do not cause cytotoxic effects in HUVECs for a 24h treatment determined in Figure 4.5 were used for both assays. MTT cell viability assays were used to determine the non-cytotoxic dose of 2 μM for PPCs, cisplatin, and suramin in HUVECs.

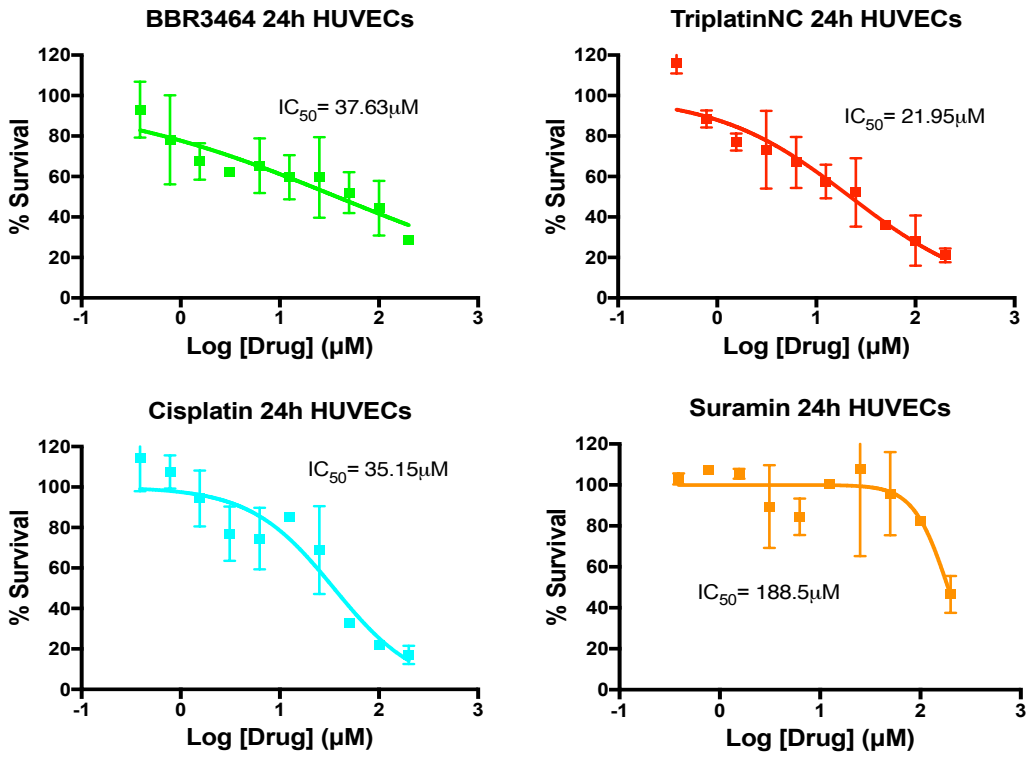

Figure 4.5. PPC, cisplatin, and suramin cytotoxicity were determined in HUVECs after a 24-hour treatment incubation. IC_{50} values ± SD of at least 2 independent experiments (each with 4 replicates) were calculated in Graphpad Prism 7.

The wound-healing assay is a widely established assay for observing *in vivo*-like endothelial cell migration with the cell-cell interactions.[101] Upon creating a "scratch" on a confluent HUVEC monolayer in a 12-well plate, cells migrate across this artificial gap until closure.[101] The addition of a chemoattractant like VEGF-A to serum-starved endothelial cells increases the rate of migration for a complete wound closure monitored by phase-contrast microscopy.[102] The VEGF stimulus mimics the tumor secreting pro-angiogenic growth factors to endothelial cells. Before the treatments, the assay format was determined with multiple VEGF concentrations (5, 10, 20, 25, 50 ng/mL) and multiple time points for wound closure, as well as serum starvation procedures

resulting in the following optimized procedure. PPC treatments at non-cytotoxic doses (2 μM) inhibited VEGF-A (25 ng/mL) induced cell migration and had the artificial gap present as in the vehicle control (Figure 4.6). Cisplatin did not have an effect on VEGF induced cell migration. The results suggested that PPCs inhibited VEGF growth factor response, which PPCs were also observed to inhibit FGF-2 growth factor responses.[30]

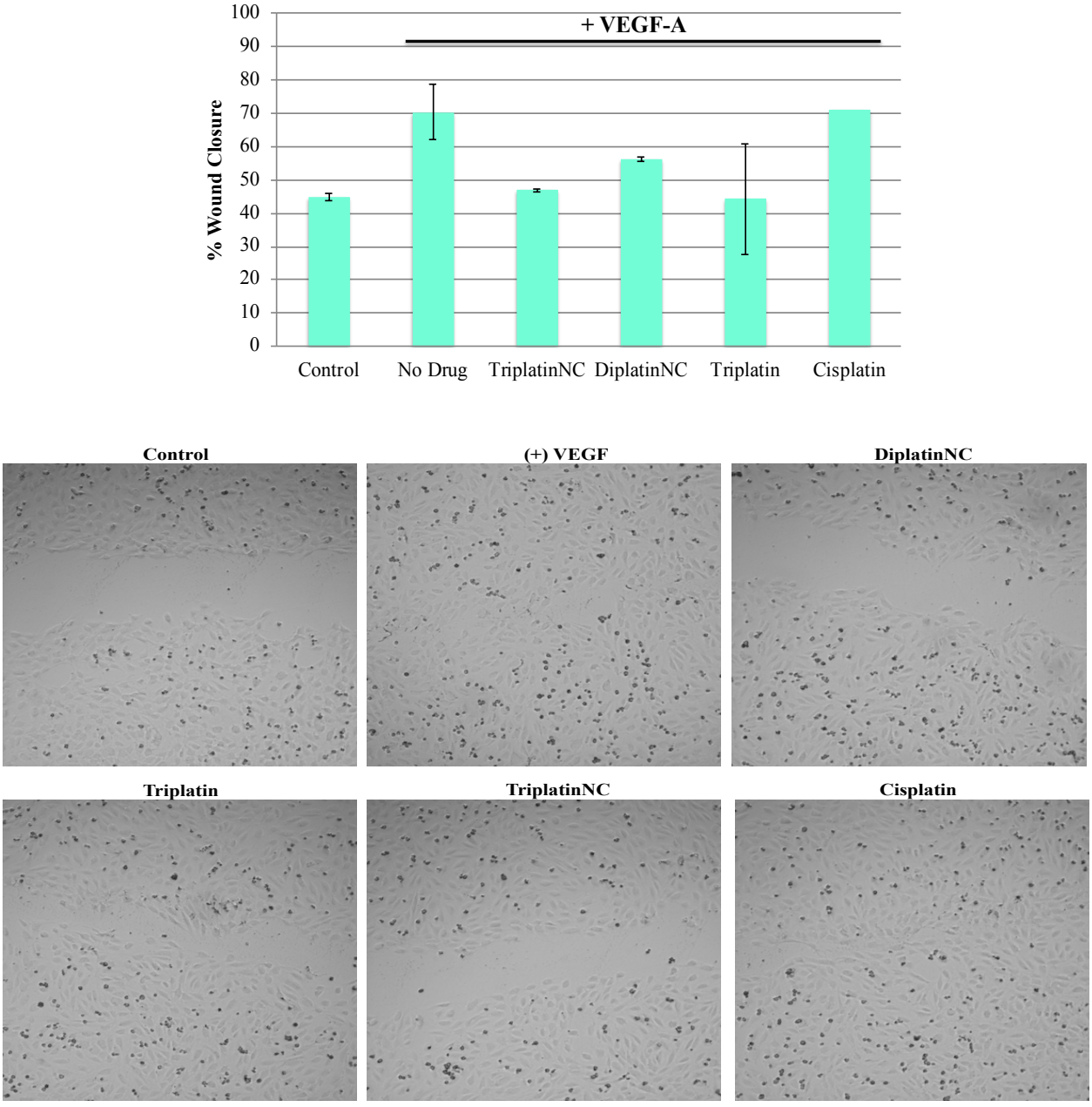

Figure 4.6. PPC inhibited VEGF-A inducted wound healing. Non-cytotoxic concentration of

cisplatin, or PPCs (2 μM) and VEGF (25 ng/mL) were added to the scratched cell monolayer. Cell migration was photographed at 7 h and compared to the 0 h control. Images are representative of 2 repeated experiments each with 4 replicates and quantified using ImageJ with error bars representative as the mean ± SD.

To further mimic angiogenesis, a tube formation assay on HUVECs encompasses endothelial cell: adhesion, migration, protease activity, and tube formation.[103] When HUVECs were seeded onto the reduced-growth factor Matrigel (extracellular matrix derived from a murine tumor[104])-coated 96-well plate, they formed capillary-like structures within 24h. Exposure to VEGF-A (50 ng/mL) significantly improves the formation of the tube network.[102] PPC treatments inhibited VEGF-A induced tube formation with less formation of and shorter tubes visualized by phase-contrast microscopy (Figure 4.7), which is a common indicator of anti-angiogenic activity.[103] Cisplatin did not inhibit the VEGF induced tube formation. Data was expressed as percentage from the "no drug" control containing VEGF (100%) for number of nodes total branching length and total tube length using the Angiogenesis Analyzer in ImageJ. PPCs have previously been reported to inhibit other growth factor (FGF-2 and HB-EGF) induced tube formation.[48] Therefore, VEGF-A can be added to the ever-growing list of growth factors that PPCs can influence.

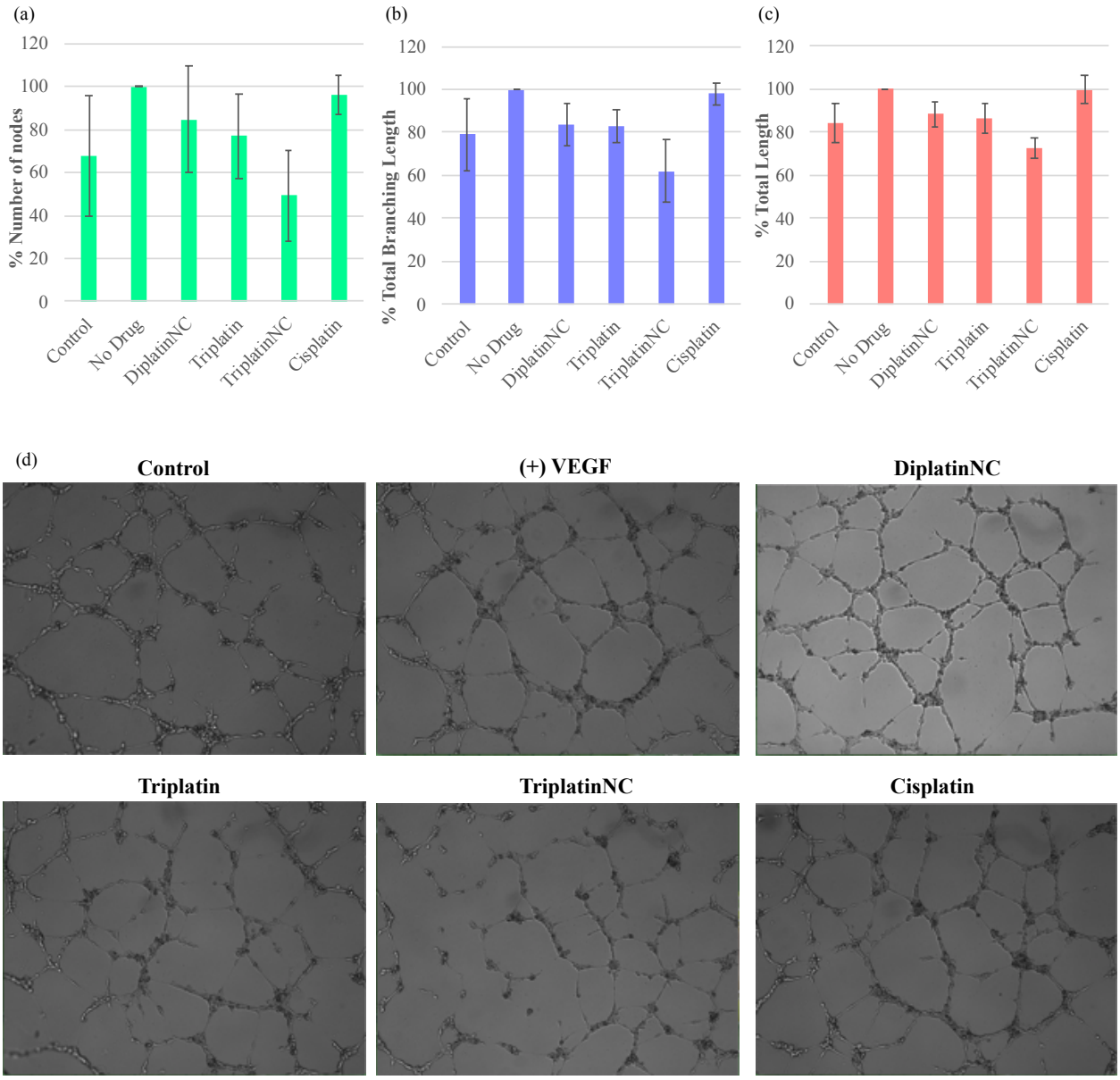

Figure 4.7. PPC inhibited VEGF-A inducted tube formation. Non-cytotoxic concentration of cisplatin, or PPCs (2 μM) and VEGF (50 ng/mL) were added to the cells with matrigel. Tube formation was photographed at 10 h and compared to the (+) VEGF control (100%) by using ImageJ Angiogenesis Analyzer analysis for (a) number of nobes, (b) total branch length, and (c) total tube length. (d) Images are representative of 2 repeated experiments each with 4 replicates and error bars represent the mean ± SD.

4.4 PPCs inhibit heparinase cleavage in a cell-based model.

Heparanase is over-expressed in tumors and there is significant correlation between metastatic potential and HPSE activity.[41] Heparanase cleaves HS chains from the HSPGs resulting in the release of growth factors and HS fragments that affect the proliferation, invasion, and survival of tumor cells and other cells in the tumor microenvironment.[28,39] Also heparanase facilitates the degradation of the base membrane and remolding of the ECM thereby encouraging tumor cell invasion.[28,39] Overexpression of HSPGs is associated with the increased growth in breast cancer.[93] Previously, PPCs have been shown to block bacterial heparinase I[32] and human heparanase[30] cleavage of fondaparinux using *in vitro* inhibition assays. PPCs were compared against cisplatin for determining heparanase inhibition in breast cancer cells.

A common method to detect heparanase activity in cells is the heparin-degrading enzyme assay (GenWay) using a modified FGF-2 as a detection system for intact HS after heparanase exposure[105–107] however, this assay was inappropriate for PPCs since PPC-HS interactions block FGF2-HS binding.[30] Therefore, we had to develop an assay to observe PPC inhibiting heparanase degradation of HS in a cell-based model. Previous studies used flow cytometry with anti-heparan sulfate antibody (amsbio) 10E4 epitopes to measure heparanase activity in cells.[108–110]

Since heparanase activity is optimal at pH 6.3 and tumors generate an acidic extracellular pH[105], cells were incubated at pH 6.3 in HEPES 10mM buffer during treatments of drug (10 minutes) and recombinant HSPE (an additional 45 minutes). Flow cytometry was used to detect the fluorescence intensity corresponding to the amount of intact HS for each sample displayed as median fluorescence. The unstained control (without treatments and secondary antibody) had the lowest

median fluorescence, while the untreated (without HPSE) had highest among the samples. We expected that the heparanase only sample would have the lowest fluorescence, while increasing PPC concentrations would prevent heparanase degradation showing an increase in fluorescence (intact HS). However, we observed the opposite trend with PPCs having lower median fluorescence (Figure 4.8). Upon further investigation, we found that the antibody is partially inaccessible to the 10E4 epitope in cells which is unmasked by heparanase.[108] So the 10E4 antibody recognizes most heparanase-degraded HS chains – making a decrease in fluorescence by PPCs actually indicative of more intact HS and less HPSE activity. Since we used human breast cancer MDA-MB-231 cells where the heparanase expression is abundant[40], the PPCs may have inhibited the endogenous HPSE, and thus reduced the 10E4 epitope resulting in decrease in fluorescence. However, the drug could also be blocking the 10E4 antibody from binding to HS which further complicates this experiment.

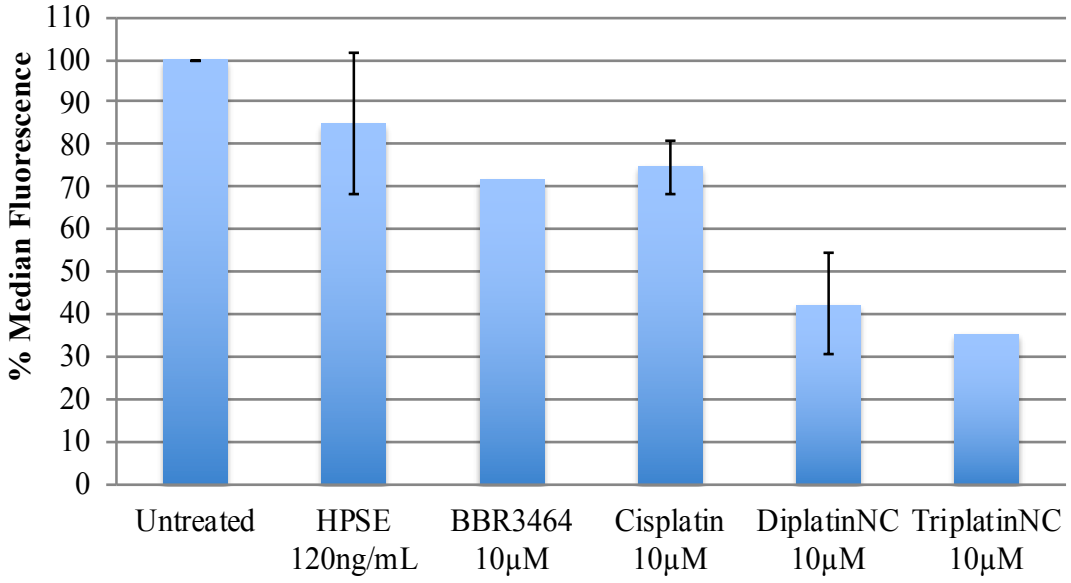

Figure 4.8. HPSE activity assay in a cell-based model using MDA-MB-231 cells. Cells were incubated with PPCs for 10 minutes prior to rhHPSE addition (120 ng/mL). 10E4 HS antibody was used to detect intact HS. HPSE activity was quantified by median fluorescence gathered from

flow cytometry. Error bars represent the mean ± SD of at least 2 independent experiments (each with 2 replicates).

To confirm the PPCs inhibition of HPSE activity, we used CHO-K1 cells that have been previously used in other similar assays.[110] We also switched to bacterial heparinase I, which (unlike mammalian heparanase) is well-known for its degraded HS fragments being undetectable by the 10E4 antibody. We first determined that 0.25U/mL of bacterial heparinase was an appropriate concentration to degrade HS for 10E4 antibody detection in MDA-MB-231 cells and CHO-K1 cells (Figure 4.9). Also, the 10E4 HS antibody was not binding to HS fragments since the fluorescence was minimal and therefore, fluorescence correlated with the amount of intact HS. Furthermore, the drug concentrations were reduced at least 2-fold to ensure non-cytotoxic treatments (1-4 µM) that possibly may have influenced reduced HS antibody recognition. As we initially suspected, PPCs inhibited the bacterial heparinase degradation of HS in a dose-response increase in % intact HS (binding of 10E4 HS antibody), whereas cisplatin failed to influence heparinase activity (Figure 4.10 and Appendix III Figure 2).

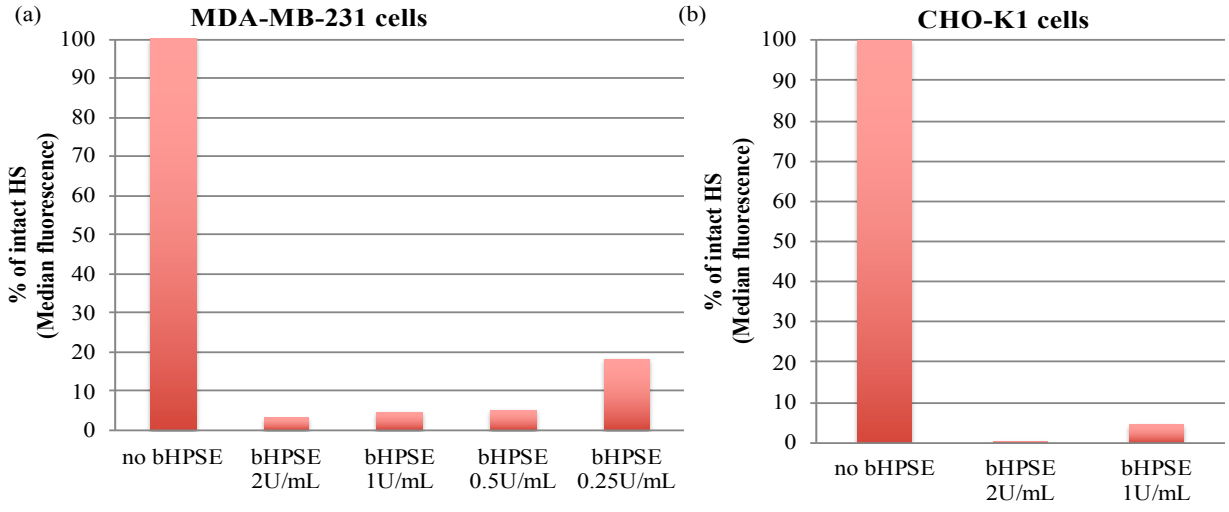

Figure 4.9. Treatment with bacterial heparinase at 2-0.25 U/mL concentrations to determine

enzyme concentration for HS digestion in (a) MDA-MB-231 cells and (b) CHO-K1 cells. Intact HS were detected by a labeled-HS specific antibody using flow cytometry. Error bars represent the mean ± SD of at least 2 independent experiments (each with 2 replicates).

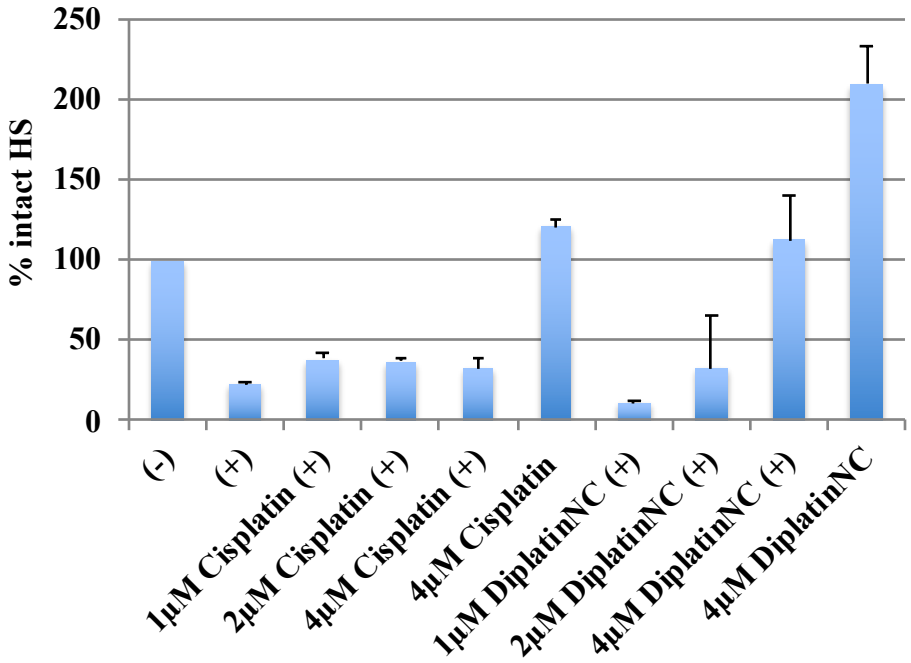

Figure 4.10. Treatment with bacterial heparinase (+) at 0.25 U/mL had low % intact HS, while increasing PPC concentrations interacted with HS and prevented the heparinase degradation in CHO-K1 cells. Cisplatin did not appear to protect the HS from heparinase cleavage. Intact HS were detected by a labeled-HS specific antibody using flow cytometry. Error bars represent the mean ± SD of at least 2 independent experiments (each with 2 replicates).

4.5 Summary.

Overall our results from the modified syndecan studies suggested a lack of tumor selectivity between the knockdown syndecan and non-silencing cells. Although we observed a slight increase in overall PPC cellular accumulation for non-silencing cells compared to double knockdown

syndecan cells (Figure 4.1), the PPC cytotoxicity profiles remained unchanged. Also single knockdown syndecan cells did not have a decrease in cellular accumulation which may emphasize abundant PPC binding sites available and thus require more dramatic knockdowns like observed for the CHO mutants (lacking HS and CS).[29,44] Assays that measure overall cell surface sulfation (Methylene Blue, Blyscan Assay) or HS-specific antibodies could help determine the level of available binding sites for PPCs in these syndecan modified cells.

Currently, 66cl4 cells with and without overexpression of syndecan-1 will be injected into the mammary fat pad of BALB/c mice following Rautela *et al.* 2015 protocol.[111] After tumors have noticeably developed around 9 days,[111] Triplatin treatment regimen (0.3 mg/kg every 4 days for 3 treatments) will begin. Tumors burden will be analyzed by bioluminescent image and caliper measurements. We hypothesize that Triplatin-treated mice would have more reduction in tumor size for overexpressing syndecan-1 tumors than empty vector tumors displaying a tumor selectively for PPC.

PPCs demonstrated inhibition of VEGF-induced migration and tube formation, whereas cisplatin was not effective. Assays that would further confirm PPCs influence on VEGF-induced pathways include: VEGF-induced proliferation of HUVECs assay measured by a colorimetric MTT assay, and VEGF-induced signal transduction measured by western blots of anti-VEGFR2, anti-phospho-VEGFR2 (Y1175) anti-PLCγ, anti-p-PLCγ anti-ERK, and anti-p-ERK1/2 antibodies. VEGF induces angiogenesis by dimerizing VEGFR2 receptors for autophosphorylation on their intracellular tyrosines that lead to specific phosphotyrosine-protein interactions causing downstream signaling.[100]

The heparanase activity assays appeared to be plagued by endogenous heparanase levels (in both CHO and MDA-MB-231 cells) and the drugs ability to block 10E4 antibody from binding to HS. To circumvent these issues, the 3G10 antibody could be used in place of the 10E4 antibody for HS detection. The 3G10 antibody only detects heparinase III digested HS thereby eliminated the endogenous heparanase and the PPC-HS influences.

In the next chapter, 5, we reported proof-of-principle of strong *in vivo* anti-metastatic activity of PPCs in triple negative breast cancer (TNBC) models. Therefore, we examine in Chapter 4 the origin of these anti-metastatic and anti-angiogenic effects in these *in vivo* models through consequences of PPC-HS metalloshielding on tumor selectivity, multiple growth factor signaling pathways, and heparanase activity in breast cancer and endothelial cells.

Data was published in:

- Katner, S.J., *et al. Proc. AACR Chicago, IL.* Abstract **#3941** (2018)
- Peterson, E. J., Daniel, A. G., Katner, S.J., *et al.* Antiangiogenic platinum through glycan targeting. *Chem. Sci.* **8,** 241–252 (2017).

4.6 Experimental.

Cell lines and cell culture

The NS1-NS2 MDA-MD-231 cells, NS1 MDA-MD-231 cells, NS2 MDA-MD-231 cells, KD Sdc 1 MDA-MD-231 cells, KD Sdc 4 MDA-MD-231 cells, KD Sdc 1 & 2 MDA-MD-231 cells, and KD Sdc 1 & 4 MDA-MD-231 cells were provided by Dr. Koblinski and were cultured in DMEM/F12 media (Invitrogen) with 5% FBS (Serum Source International), 1% L-glutamine, 2%

non-essential amino acids, 1% sodium pyruvate, and 1% penicillin/streptomycin (Gibco). Human umbilical vein endothelial cells (HUVECs) were purchased from ATCC and maintained in Vasculife Endothelial Medium containing 10% FBS. MDA-MD-231 cells were cultured in Leibovitz's media, 10% FBS, and 1% penicillin/streptomycin. Chinese hamster ovary cells (CHO)-K1 cells were maintained in DMEM/F12 media with 10% FBS, and 1% penicillin/streptomycin. All cells were grown in a humidified atmosphere at 37°C with 5% CO_2.

Cellular Accumulation assay.

NS1-NS2 MDA-MD-231 cells, NS2 MDA-MD-231 cells, KD Sdc 4 MDA-MD-231 cells, and KD Sdc 1 & 4 MDA-MD-231 cells were each seeded in 100mm dishes at $1x10^6$ cells/dish in 20 mL of supplemented media. Cells were incubated for 24 hours to adhere, and then the cells were treated with 10uM of platinum drug for 1, 3, and 6-hour incubations. All incubations were done at 37°C with 5% CO_2. After their respective incubation, cells were washed twice with PBS, harvested with 0.25% trypsin (Gibco), and washed with 10 mL of PBS. The cell pellets were digested in 1 mL of nitric acid for 72 hours and diluted with 2 mL of diH_2O. The solutions were filtered through a 0.45 GHP filter and ran on the Varian 820 ICP-MS to determine the concentration of platinum in each sample. The standards were prepared with K_2PtCl_4 in concentration of 10, 50, 100, 150, and 250 ppb. Blank was 7% nitric acid.

MTT cell viability assay - MDA-MD-231 cells

NS1-NS2 MDA-MD-231 cells, NS1 MDA-MD-231 cells, NS2 MDA-MD-231 cells, KD Sdc 1 MDA-MD-231 cells, KD Sdc 4 MDA-MD-231 cells, KD Sdc 1 & 2 MDA-MD-231 cells, and KD Sdc 1 & 4 MDA-MD-231 cells were seeded in 96-well plates (5×10^3 cells/well for 72 h, or 1×

10^4 cells/well for 24 h) in supplemented media (100 µL). After incubation overnight, the cells were treated with varying concentrations of the indicated Pt compound, in sets containing 4 replicates for each concentration. After drug exposure for 72 h or 24 h, 1 mM MTT (3-(4,5-dimethylthiazol-2-yl)-2,5-diphenyltetrazolim bromide) (Sigma) was added to each well and incubated for 4 h. The MTT reagent was removed, and 100 µL of DMSO was added to each well to lyse the cells and dissolve the purple formazan. All incubations were performed at 37°C with 5% CO_2. Spectrophotometric readings were determined at 570 nm using a microplate reader (Bio-Tek instruments). Percentage cell survival was determined as treated/untreated controls × 100. Data are reported as the average of 2 independent experiments ± SD.

MTT cell viability assay - MDA-MD-231 cells 1h drug incubation

NS1-NS2 MDA-MD-231 cells, and KD Sdc 1 & 4 MDA-MD-231 cells were seeded in 96-well plates at 5 x 10^3 cells/well in 100 µL of supplemented media. Cells were incubated overnight to adhere, and the media was replaced with 100 µL of media containing various concentrations of platinum drugs in sets containing 3 replicates. After 1-hour drug incubations, media was replaced with 100 µL of media. After an additional 72 hours, media was replaced with 1mM MTT and incubated for 4 hours. All incubations were done at 37°C with 5% CO_2. The MTT reagent was replaced with 100 µL of DMSO in each well and read at 570 nm using a microplate reader. Percentage cell survival was determined as treated/untreated controls × 100. Data are reported as the average of 2 independent experiments ± SD.

MTT cell viability assay – HUVEC 24h drug incubation

HUVECs were seeded in 96-well plates at 1.1 x 10^3 cells/well in 100 µL of supplemented media. Cells were incubated overnight to adhere, and the media was replaced with 100 µL of media containing various concentrations of platinum drugs in sets containing 3 replicates. After an additional 24 hours, media was replaced with 1mM MTT and incubated for 4 hours. All incubations were done at 37°C with 5% CO_2. The MTT reagent was replaced with 100 µL of DMSO in each well and read at 570 nm using a microplate reader. Percentage cell survival was determined as treated/untreated controls × 100. Data are reported as the average of 2 independent experiments ± SD.

Wound healing assay with VEGF induction

5 x 10^4 HUVECs/well below passage 6 were seeded in 1 mL supplemented media (VascuLife Endothelial Cell Media, Lifeline Cell Technologies) in a 24-well plate. The cells were grown to confluence (24 hours). Cell were washed 3 times with warm unsupplemented media. A scratch was made on the monolayer using p10 pipette tips, removing the cells to expose the growth surface. The wells were washed once with warm unsupplemented media. The media was replaced with unsupplemented media for the control and sample wells containing 2 µM of treatments. For VEGF-A- induction, 25 ng/mL recombinant VEGF-A (R&D Systems) was added with or without drug to unsupplemented media. The extent of closure of the scratch at 7 h was compared to the control by light microscopy, digital imaging, and analysis by ImageJ software.

Tube formation assay with VEGF induction

Reduced growth factor matrigel gel was thawed overnight at 4°C, plated in 50 µL volumes into a 96-well plate, and incubated for 30 minutes at 37°C to solidify. HUVECs were washed twice with unsupplemented, and then once with 1xPBS before harvested with trypsin. HUVECs were collected in unsupplemented media were added to the top of the plated matrigel 1.1 x 10^4 cells/well in 50 µL volumes. 50 µL unsupplement media containing treatment or no treatment were added to the cells followed by a 50 µL addition of VEGF-A (50 ng/mL). After 10-hour incubation, images were taken using a light microscope and analyzed through ImageJ Angiogenesis Analyzer for number of nobes, total branch length, and total tube length.

Heparanase activity assay

MDA-MB-231 cells or CHO-K1 cells were collected with trypsin and aliquoted into 15 mL centrifuge tubes at $5x10^5$ cells in 1 mL supplemented media. Cells were centrifuged to remove media and replaced with cold 1 mL of HEPES 10 mM, pH 6.3 buffer. Cells were pretreated with and without PPCs for 10 minutes to protect HS and then active recombinant human heparanase (rhHPSE, R&D systems, 120 ng/mL) or bacterial heparinase I (Sigma, 0.25 U/mL) was added for another 45 minutes at 37ºC. Afterwards, cells were washed with 5 mL of cold 1xPBS and centrifuged to remove PBS. Samples were fixed with 1 mL of 4% formaldehyde solution (methanol free) diluted in 1xPBS for 10 minutes at 37ºC. Samples were immediately chilled on ice for 1 minute and the 2 mL of cold PBS was added for a centrifuge wash. Samples were resuspended in 1 mL of 1xPBS and stored at 4ºC. The next day, the samples were centrifuged to pellet and resuspended in 900 µL of incubation buffer (0.5% BSA in 1x PBS) and passed through a 40 µm cell strainer (Flowmi) into new 15 mL centrifuge tubes. Samples were centrifuged,

resuspended in 100 μL of primary antibody 10E4 (USBiological, 1:250 diluted in incubation buffer), and incubated for 1 hour at room temperature. Samples were washed by centrifugation in 2 mL of incubation buffer. Samples were resuspended in 100 μL of fluorochrom-conjugated secondary antibody: Goat anti-mouse IgM AlexaFluor647(1:400 incubation buffer) and incubated for 30 minutes in dark at room temperature. Samples were then washed by centrifugation in 2 mL of incubation buffer and then repeated in 1 mL of incubation buffer. Cells were resuspended in 0.5 mL of 1xPBS into flow cytometry tubes and analyzed at 635 nm laser using a Becton Dickinson FACSCanto II Analyzer flow cytometer (BD Biosciences).

Chapter 5. PPCs as Anti-Metastatic Agents for Breast Cancer

5.1 Rationale.

Although advances and awareness have been made in early detection and treatment options, mortality remains relatively high and is dependent on the development of metastases.[112] Breast cancer commonly metastasizes to the bone, lung, liver, and brain with triple negative breast cancer (TNBC) patents having the worst survival.[113,114] Each location of the metastases in breast cancer patients is an independent prognostic factor such as the median survival rates of breast cancer patients with bone, lung, liver, or brain metastases were the following: 10.3-22.9 months, 11.7 to 20.8 months, 3.5 to 14.4 months, and 0.6 to 8 months respectively.[115] Patients with liver or brain metastases had the poorest survival,[115] and furthermore, patients with metastases to both sites had significantly shorter survival than patients presenting with only brain metastases.[116] This decrease in survival was only observed for brain metastatic patients with additional liver metastases and not for additional lung or bones.[116] Overall, this indicates that the lack of systemic therapy and liver involvement are associated with increased risk of death.[116]

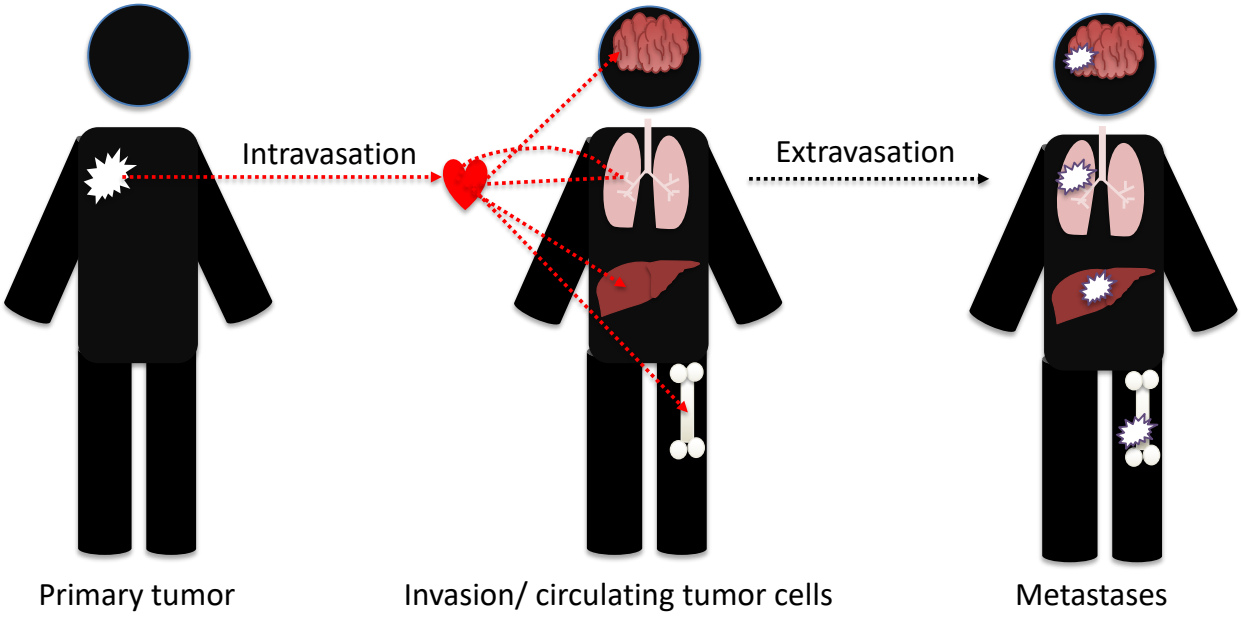

Figure 5.1. The metastatic process and breast cancer cells propensity for lung, bone, liver, and brain metastases.

Briefly, the metastatic process requires tumor cells to: form primary tumors, undergo epithelial mesenchymal transition (EMT), invade basement membrane and stroma, intravasate into the blood vessel, travel through the circulation, extravasate into a secondary tissue, undergo mesenchymal epithelial transition (MET), and establish secondary tumors (Figure 5.1).[117,118] When tumor cells are transported through the circulation, the cells tendency to disseminate metastases in another tissue is reflected in the cell's phenotypic propensity to extravasate and colonize in that secondary tissue (metastatic niche) as well as the layout of the circulation may strong influence the site of metastases.[118] Therefore, *in vivo* assays that replicate these metastatic steps are necessary to evaluate drugs for anti-metastatic activity.

The use of luciferase-expressing cells (denoted by *luc*) facilitates imaging of tumor cell survival and proliferation *in vivo* for assessing tumor burden as a non-invasive technique.[119] In the presence of oxygen and ATP (adenosine triphosphate), the luciferase enzyme catalyzes light production from the luciferin substrate that was subcutaneously injected. Generally, the oxidative decarboxylation of the luciferin by luciferase with oxygen yields photon emission. This bioluminescence imaging technique is dependent on metabolically active transformed tumor cells generating photons and thus may not represent necrotic regions of the tumor.[119] Furthermore, other techniques (caliper, and magnetic resonance imaging: MRI) directly measure tumor volume that may encompass live/dead tumor cells, fibroblasts, immune cells, endothelial cells, and calcified parts that all may overestimate the actual size of the tumor. The bioluminescence images generated from firefly-luciferase reaction with luciferin emit long wavelengths of light (>600 nm) that facilitates efficient transmission through mammalian tissues for great sensitivity.[120] Photon scattering within tissue can be easily overcome by combining the ventral and dorsal images to determine overall tumor burden.

In an effort to reevaluate Triplatin under the new HSPG-targeting and thus anti-metastatic role (further investigated in Chapter 4), Triplatin and its analogs were considered here in preclinical mouse studies (Figure 5.2). TriplatinNC is a noncovalent derivative of Triplatin with a higher charge where the Pt-Cl bonds are replaced by a substitution-inert "dangling" amine $H_2N(CH_2)_6NH_3^+$. DiplatinNC is an anolog of TriplatinNC without the presence of the central platinum unit (platinum-tetraam(m)ine coordination sphere) and thus has a reduced charge of 6+. Furthermore, substitution of the central platinum unit in Triplatin with a polyamine nitrogen yields BBR3571 of which has demonstrated activity in human glioblastoma mouse models.[121] These

PPCs have demonstrated activity in *in vitro* systems. Typically cytoxicity for these compounds is as follows: Triplatin = BBR3751 nanomolar,[121] TriplatinNC single digit micromolar, and DiplatinNC double digit micromolar range.[44] Here, these PPCs were evaluated for anti-metastatic activity in these syngeneic and xenografts metastases models. The PPC dose schedule of every 4 days totaling 3 treatments was determined from previous xenograft studies done in nude mice.[122]

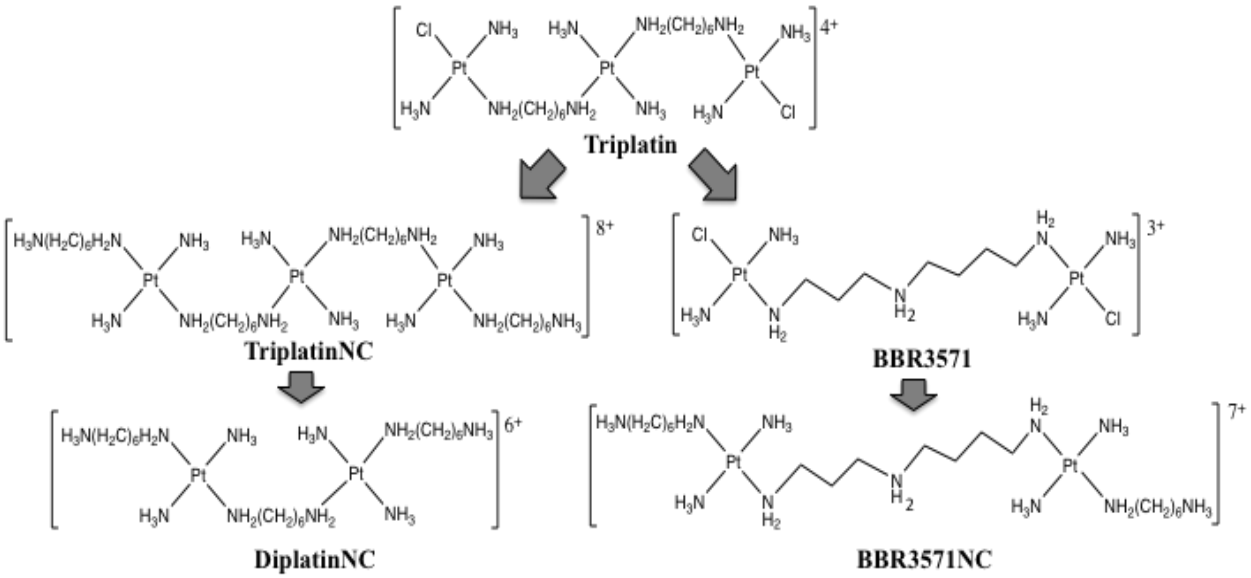

Figure 5.2. Structures of PPCs used in Chapter 5 for *in vivo* studies. Counter ions were omitted for clarity.

5.2 PPCs activity in orthotopic TNBC immunocompetent mouse models.

Through collaborations with Dr. Takabe's lab, the *in vivo* activity of DiplatinNC, TriplatinNC, and BBR3464 (Triplatin) was evaluated in syngeneic orthotopic mouse models for their ability to reduce the primary tumor and the surrounding metastases. An orthotopic implantation in the mouse mammary fat pad allows for replication of the entire metastatic process with tumor cells.[117] Female BALB/c mice (immune-intact) received 4T1-*luc2* murine breast cancer cells (an aggressive triple-

negative model) through an implantation into the mammary fat pad. The orthotopic injection places the tumor cells into a biologically relevant environment and with the immune-intact interplay from the Balb/c mice allows for this model to mimic human cancer progression and metastases more efficiently than conventional human xenografts.[123] After cell-implantation on day 1, mice were treated by intraperitoneal (i.p.) injections with cisplatin, DiplatinNC, Triplatin, or saline with the dosing scheduled for every 4 days (day 9, 13, 17). On day 20, mice were injected with luciferin for detection and quantification of luciferase-expressing 4T1-*luc2* tumors by bioluminescence using the *in vivo* imaging system (IVIS). Primary tumor growth and metastases were suppressed in PPC treated mice (Figure 5.3 a) while only Triplatin significantly reduced primary tumor volume (Figure 5.3 b) indicating that PPCs have an effect on the primary tumor and local metastases.

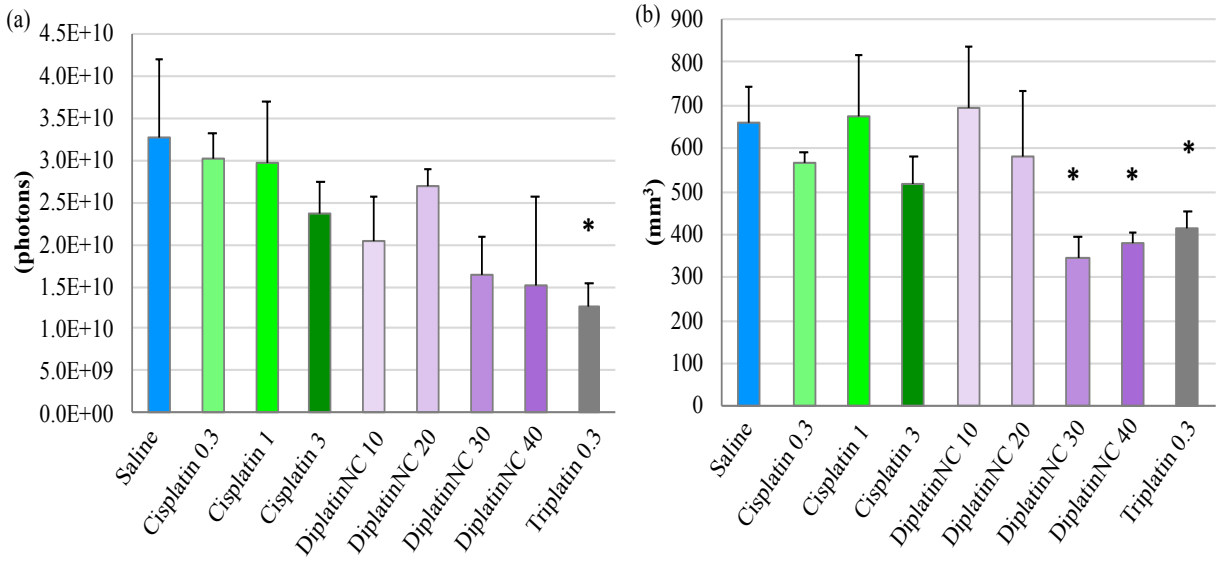

Figure 5.3. PPC reduction of murine TNBC primary tumor. Female BALB/c mice were injected with 1x10^4 4T1-*luc2* cells (murine TNBC) into the mammary fat pad on day 0. Mice were then treated with saline control, cisplatin (0.3, 1, 3 mg/kg), DiplatinNC (10, 20, 30, 40 mg/kg), or Triplatin (0.3 mg/kg) on days 9, 13, and 17 by i.p. injections. (a) On day 20, mice were imaged

with IVIS to quantify primary tumor and metastases. (b) Primary tumors were then removed, and the tumor volume was measured using a caliper. Asterisks denote significance with $p < 5$. Error bars represent the mean ± SD of 5 mice for each group. Data was generated in Dr. Takabe lab.

PPC activity was then analyzed in a metastatic breast cancer and survival mouse model after mastectomy to confirm anti-metastatic action. The primary tumor resection method closely representations the surgical treatment (mastectomy) in humans while determining the effects of compounds directly on metastases by eliminating the primary tumor.[124,125] Female BALB/c mice (immune-intact) with 4T1-*luc2* murine breast cancer cells were orthotopic-implanted into the mammary fat pad on day 0 and primary tumor resections occurred on day 8. Mice were then treated via i.p. injections of Triplatin (0.3mg/kg), TriplatinNC (25mg/kg), or saline with the dosing scheduled on days 10, 14, and 18 (Figure 5.4 a). After day 21, PPCs reduced developing metastases (Figure 5.4 b,c,d) with Triplatin significantly reducing tumor load ($p = 0.038$), TriplatinNC markedly reduced the tumor load ($p = 0.055$). Both PPCs had prolonged survival with 1 mouse (out of 7) from each PPC treatment surviving over 100 days indicating a cure (Figure 5.4 e). Tumors were quantified by bioluminescence using the IVIS.

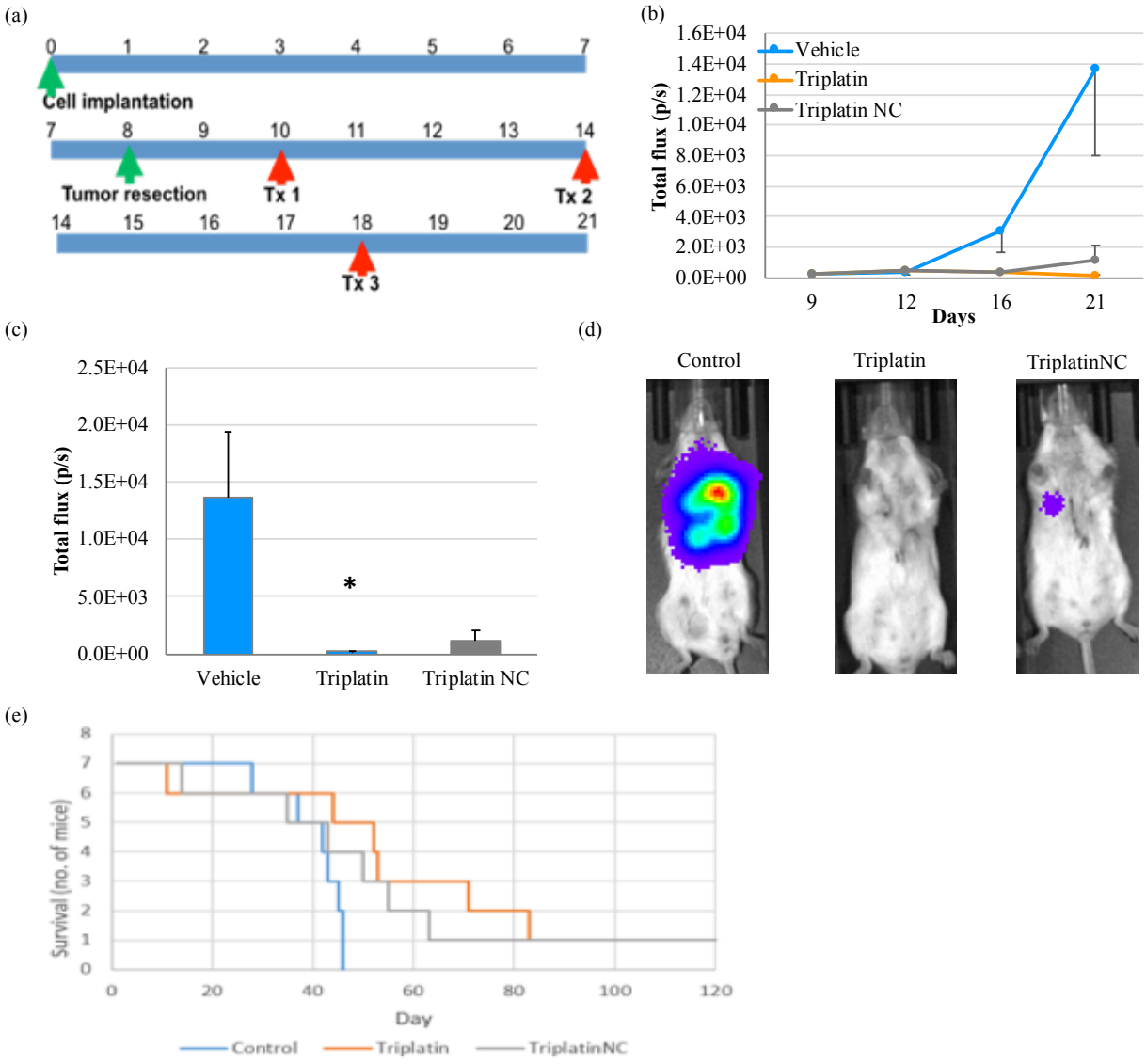

Figure 5.4. PPC reduction of developing lung metastases and prolong survival after primary tumor resection in murine TNBC mouse model. Female BALB/c mice were injected with 1x10^4 4T1-*luc2* cells (murine TNBC) into the mammary fat pad on day 0. (a) Primary tumor was surgically removed on day 8, and mice were then treated with saline control, TriplatinNC (25 mg/kg), or Triplatin (0.3 mg/kg) on days 10, 14, and 18 by i.p. injections. (b) Mice were imaged with IVIS to track metastases. (c, d) On day 21, PPCs suppressed developing metastases. (e) Also, PPCs had

prolonged survival compared to saline control. Asterisks denote significance with $p < 5$. Error bars represent the mean ± SD of 7 mice for each group. Data was generated in Dr. Takabe lab.

In the orthotopic model as done here, secondary tumors are usually confined to the surrounding organs (lung, lymph node).[117] Also, tumors of murine origin (4T1 cells) are problematic for development of species-specific biological agents and the tumors tend to exhibit very rapid growth. Therefore, the next *in vivo* experiments have further explored PPCs anti-metastatic role using human derived TNBC cells and their efficacy in targeting metastases in locations beyond just lung and lymph nodes.

5.3 Evaluation of PPCs treating human TNBC metastases in mouse models.

NOD (Non-obese diabetic mouse strain)-SCID (severe combined immunodeficiency)-IL2Rγ (null mutation of interleukin 2 receptor γ) (NSG) mice have essentially no innate or adaptive immunity making NSG one of the most immunodeficient mouse strains.[126] The NOD background results in defective macrophages and dendritic cells effectively reducing the mouse innate immunity.[127] The SCID context contains a mutated *Prkdc* gene[128] that influences the V(D)J recombination necessary to generate variation in the antigen-binding pockets of antigen-recognition receptors for both B cells and T cells (BCR and TCR respectively).[129] Therefore, T and B cells (collectively lymphocytes) cannot mature and ultimately restricts the mouse adaptive immunity. To further obliterate the mouse innate immunity, the natural killer (NK) cells were severely depleted through a null mutation of IL2Rγ[126] which the NK cell survival and development is dependent upon.[130] Such immunodeficiency allows for efficient engraftment of xenografts and for metastases to easily arise in the mice.[117,131] PPCs were compared against cisplatin and carboplatin for determining anti-

metastatic activity using human TNBC NSG mouse models.

Under Dr. Koblinski's and Dr. Hu's supervision, I was trained throughout these experiments to handle mice, observe overall health of mice, administrate treatments, run IVIS for imaging proposes, euthanize mice, and dissect mice for harvesting organs (brain, lung, liver, kidneys, ovary, heart, and skeleton), and analyze all of the data.

NSG mice are particularly sensitive to DNA damaging agents due to their SCID background carrying the mutated *Prkdc* gene, which its encoded protein is also involved in DNA double strain break repair in most tissues. Therefore, chemotherapies that cause DNA damage can have a higher toxicity in SCID mice compared to other mice strains. Hence, maximum tolerated dose (MTD) studies were conducted on understudied *in vivo* PPCs. MTD was defined as the dose at which all of the mice developed acceptable dose limiting toxicities (body weight loss <20% at any point during the treatments) after the last treatment. Intravenous (i.v.) injection route administrations were tested for the relatively new PPC, DiplatinNC since previous covalent PPCs (i.e. Triplatin and BBR3571) have been given i.v. for *in vivo* studies. However, mice died within minutes of injection at the higher 40 and 20 mg/kg doses whereas in the BALB/c strain (Figure 5.3) mice tolerated 40 mg/kg using intraperitoneal (i.p.) injections. The low 10 mg/kg dose given i.v. in the NSG mice seemed to be well tolerated with similar weight as control (Figure 5.5).

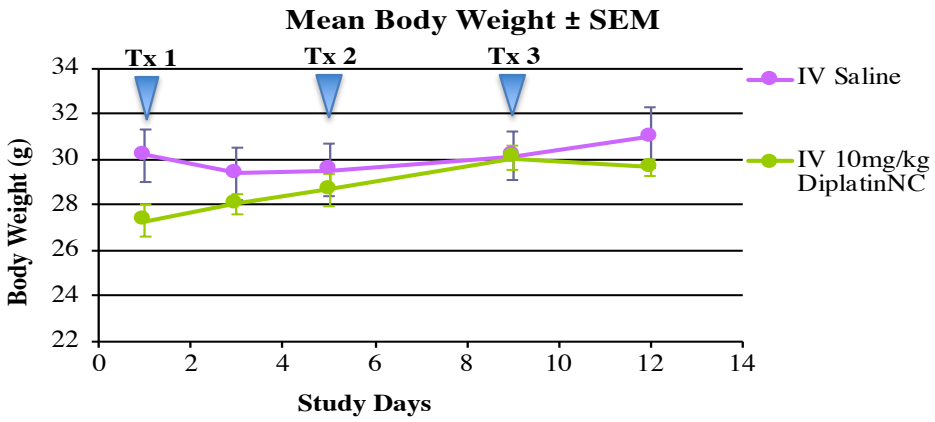

Figure 5.5. Maximum tolerated dose of DiplatinNC *in vivo* through i.v. route administration. NSG mice were treated on days 1, 5, and 9 with saline control, or DiplatinNC (40, 20, and 10 mg/kg). The mean body weight was observed until day 12 when the mice were euthanized. Error bars represent the mean ± SD of 5 mice for each group.

In an attempt to increase the dosage, PPCs were switched to i.p. injections as in the previous BALB/c studies (Figures 5.3 and 5.4). The NSG mice seemed to tolerate 40 mg/kg as the maximum dose for DiplatinNC with a beginning 5% body weight loss from its initial weight and then a slight increase to a steady acceptable 2% loss (Figure 5.6). Note that in the protocol, a body weight loss of more than 20% results in euthanasia. The highest tested dose for DiplatinNC (60 mg/kg) had 2 deaths (5 mice per group) after the second treatment and thus the dose was not considered as the MTD. Higher doses (50 and 75 mg/kg) were evaluated for BBR3571NC than DiplatinNC because of a miscommunication of BBR3571NC structure and thus was thought to have a lower charge of 5+ than DiplatinNC 6+. During a clarification, BBR3571NC structure correctly has a charge of 7+, but all 5 mice died immediately in both BBR3571NC treatment groups highlighting how slight variations in PPC structure (Figure 5.2) have profound effects *in vivo*.

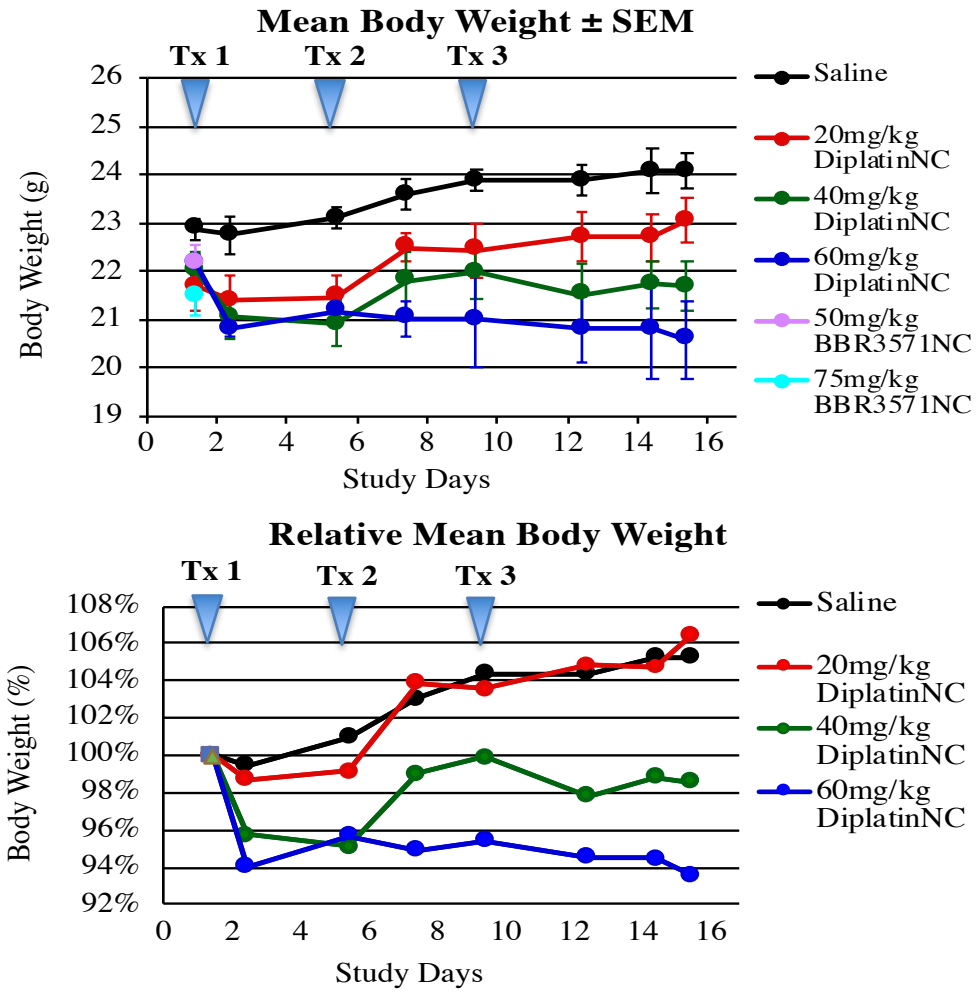

Figure 5.6. Maximum tolerated dose of DiplatinNC and BBR3571NC *in vivo* through i.p. route administration. NSG mice were treated on days 1, 5, and 9 with saline control, DiplatinNC (20, 40, and 60 mg/kg), or BBR3571NC (50 and 70 mg/kg). (top) The mean body weight and (bottom) % body weight from day 1 were observed until day 15 when the mice were euthanized. Error bars represent the mean ± SD of 3 mice for each group.

Continuing with the i.p. route injection method, the NSG mice seemed to tolerate the all of the doses of TriplatinNC with mice gaining weight similar to control (Figure 5.7). The mice in the BBR3571 treatment groups all lost some body weight compared to their initial weight with the highest dose having most loss 9% at one time, but still in the acceptable body lost range (Figure

5.7). Therefore, MTD for TriplatinNC and BBR3571 were 20 mg/kg and 0.3mg/kg respectively in NSG mice.

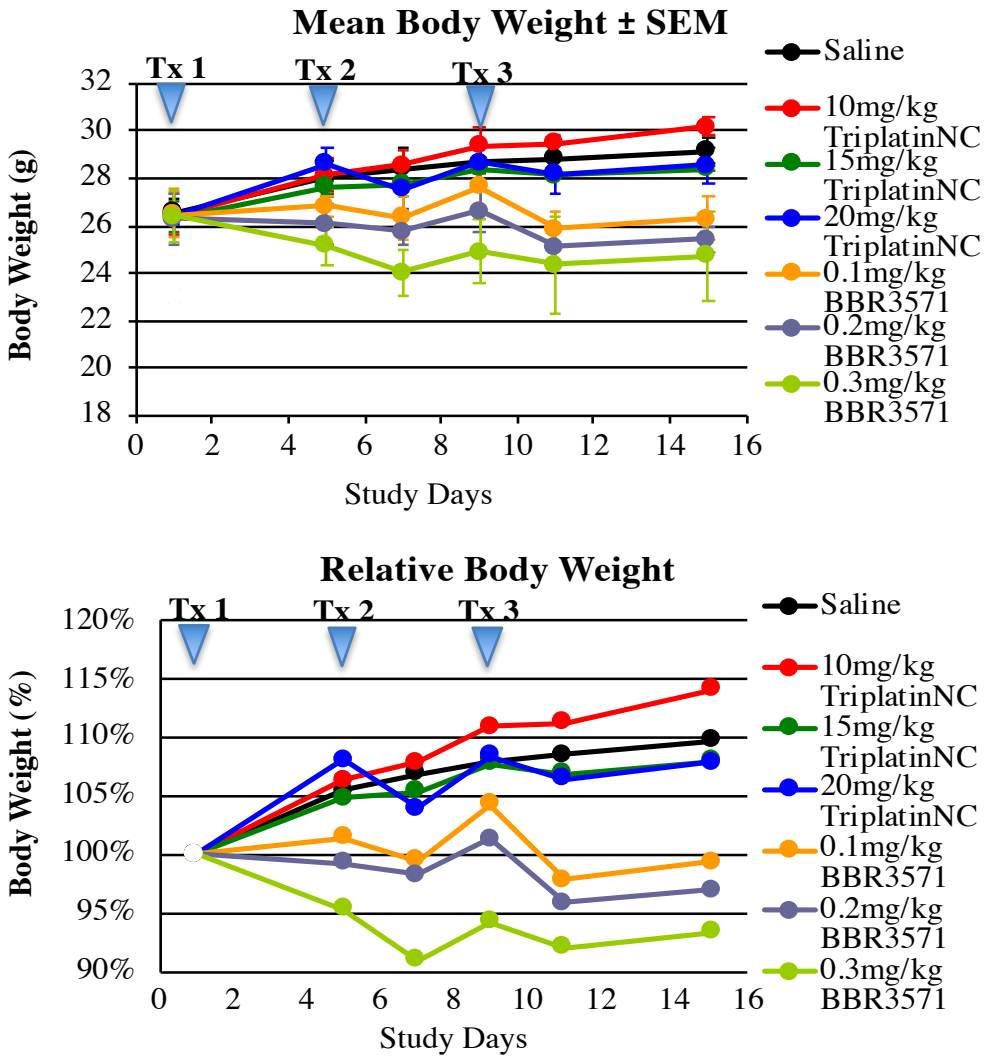

Figure 5.7. Maximum tolerated dose of TriplatinNC and BBR3571 *in vivo* through i.p. route administration. NSG mice were treated on days 1, 5, and 9 with saline control, TriplatinNC (20, 15, and 10 mg/kg), or BBR3571NC (0.1, 0.2, and 0.3 mg/kg). (top) The mean body weight and (bottom) % body weight from day 1 were observed until day 15 when the mice were euthanized. euthanized. Error bars represent the mean ± SD of 3 mice for each group.

After MTD studies, PPCs were evaluated for anti-metastatic potential in breast cancer using *in vivo* TNBC mouse models. To study PPCs effect on widespread metastases, we used the human TNBC MDA-MB-231-*luc* brain trophic (-BrM2) cells that allowed for consistent metastases in the brain.[132] The MDA-MB-231-BrM2-*luc* cells exhibit higher expression levels of heparanase and HB-EGF than the parental MDA-MB-231 cells,[132] which fits with PPCs ability to inhibit heparanase cleavage and block growth factor binding to HSPGs.[30] Therefore, PPCs should influence the tumors microenvironment as well as induced cytotoxicity.

A cell viability assay was conducted using MTT colorimetric assay to examine PPC in vitro cytotoxicity of the MDA-MB-231-BrM2-*luc* cells. Metabolically active cells reduce the yellow tetrazolium 3-(4,5-dimethylthiazol-2yl)-2,5-diphenyltetrazolium bromide (MTT) reagent to purple formazan with the number of proliferating cells positively corresponding to the increase in absorbance at 570nm using a plate-reader spectrophotometer. This absorbance data was normalized to vehicle control as 100% proliferation. The act of blocking growth factor stimulation can cause cells to become quiescent (non-proliferating) and thus have low metabolism[133] resulting in a lower MTT assay response. Also, dead cells from drug treatments that were cytotoxic for the dosage and or incubation period would have a low MTT assay response as well. Therefore, IC_{50} values from the MTT assay were unexpectedly high compared to cisplatin (Table 5.1) since both growth factor blocking and cytotoxicity actions of the PPCs should have reduced the IC_{50} values. A similar trend of reduced cytotoxicity was observed for the PPCs in a parental MDA-MB-231 cell line with longer treatment incubation (Appendix IV Figure 1).

	24H IC_{50} (μM)
TRIPLATIN	186.1 ± 26.7
TRIPLATINNC	233.9 ± 97.5
DIPLATINNC	Not toxic
CISPLATIN	21.4 ± 12.6

Table 5.1. Cytotoxicity of PPCs in MDA-MB-231-BrM2-*luc* cells after 24h drug treatment. IC_{50} values ± SD of at least 2 independent experiments (each with 4 replicates) were calculated in GraphPad Prism 7. Plots are in Appendix IV Figure 2.

PPCs were examined in a metastatic TNBC *in vivo* mouse model by intracardiac injection of MDA-MB-231-BrM2-*luc* cells[132] into NSG mice in collaboration with Dr. Koblinski's lab. Intracardiac injection of the tumor cells is a common delivery method to obtain widespread metastases (bone, brain, lung, liver, etc.) and especially consistent brain metastases for brain trophic tumor cells.[134] NSG mice were injected with $1x10^5$ MDA-MB-231-BrM2-*luc* cells into the left cardiac ventricle on day 0.[135] Randomization of mice into 3 groups occurred on day 7 while treatment began on day 10. This early randomization resulted in DiplatinNC treatment group being significantly reduced in overall metastases than control before treatment began and thus influenced subsequently results (Figure 5.8). Therefore, DiplatinNC was unfortunately discarded from the results.

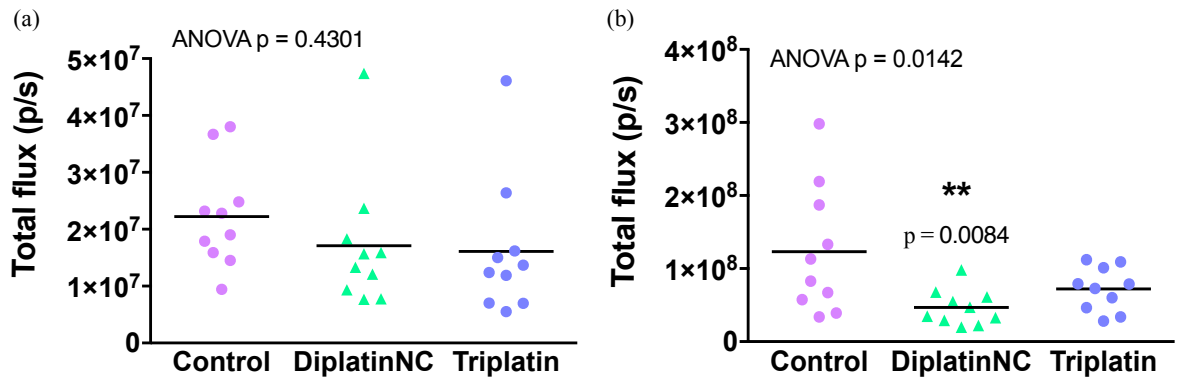

Figure 5.8. Mice randomization occurred on (a) day 7 post-intracardiac injection of MDA-MB-231-BrM2-*luc* cells into NSG mice. (b) On day 10, before the treatment regimens began, and DiplatinNC treatment group had significantly less overall metastases than control. All metastases were quantified by IVIS. Each group had 10 mice.

Mice were treated *via* i.p. injections of Triplatin (0.3 mg/kg), DiplatinNC (40 mg/kg), or saline with the dosing scheduled on days 10, 14, and 18 (Figure 5.9 a). Throughout the *in vivo* studies, we chose an intraperitoneal route for administration of chemotherapy because it allowed for 4-fold higher treatment dose dictated from the previous MTD studies, and the injection route is less demanding to administrate in mice – ensuring proper dosing. Moreover, in clinical practice intraperitoneal delivery is being used more frequently to administrate chemotherapies and some human studies have verified similar response rates as intravenous route.[136–138]

Mice were injected with luciferin throughout the study for live bioluminescent imaging using the IVIS to observe overall tumor burden. It is important to note that the control started to lose weight around day 18, and that the Triplatin dose 0.3 mg/kg was the MTD for this *in vivo* model. Triplatin-treated mice had a continual decrease in body weight with 17% maximum lost on day 21 when

they were euthanized (Appendix IV Figure 3). On day 21, mice were imaged for overall metastases and then sacrificed for *ex vivo* imaging of bone, and brain. Triplatin significantly reduced overall tumor burden and bone metastases (Figure 5.9 b,c) but not for brain metastases (Figure 5.9 d). During mice dissecting, we noticed that the livers were riddled with surface metastases in the control but not in the Triplatin-treated group (Figure 5.10 a). Therefore, we stained the liver sections using HLA-antibody and hematoxylin counter stain (Figure 5.10 b). HLA (human leukocyte antigen) is a cell membrane protein involved in the presentation of foreign antigens to the immune system and is only present on most cells in humans and some monkeys. Therefore, the human breast cancer metastases were easily observed against a mouse liver. The hematoxylin is a basic dye that bind to the phosphate backbones of nucleic acids (DNA/RNA) and stains them violet. Quantification of these metastases in 5 livers from each group revealed that Triplatin-treated mice had a significant reduction in liver metastases cell number identified by the HLA staining and then normalized to liver area using cell counter on ImageJ (Figure 5.10 c,d).

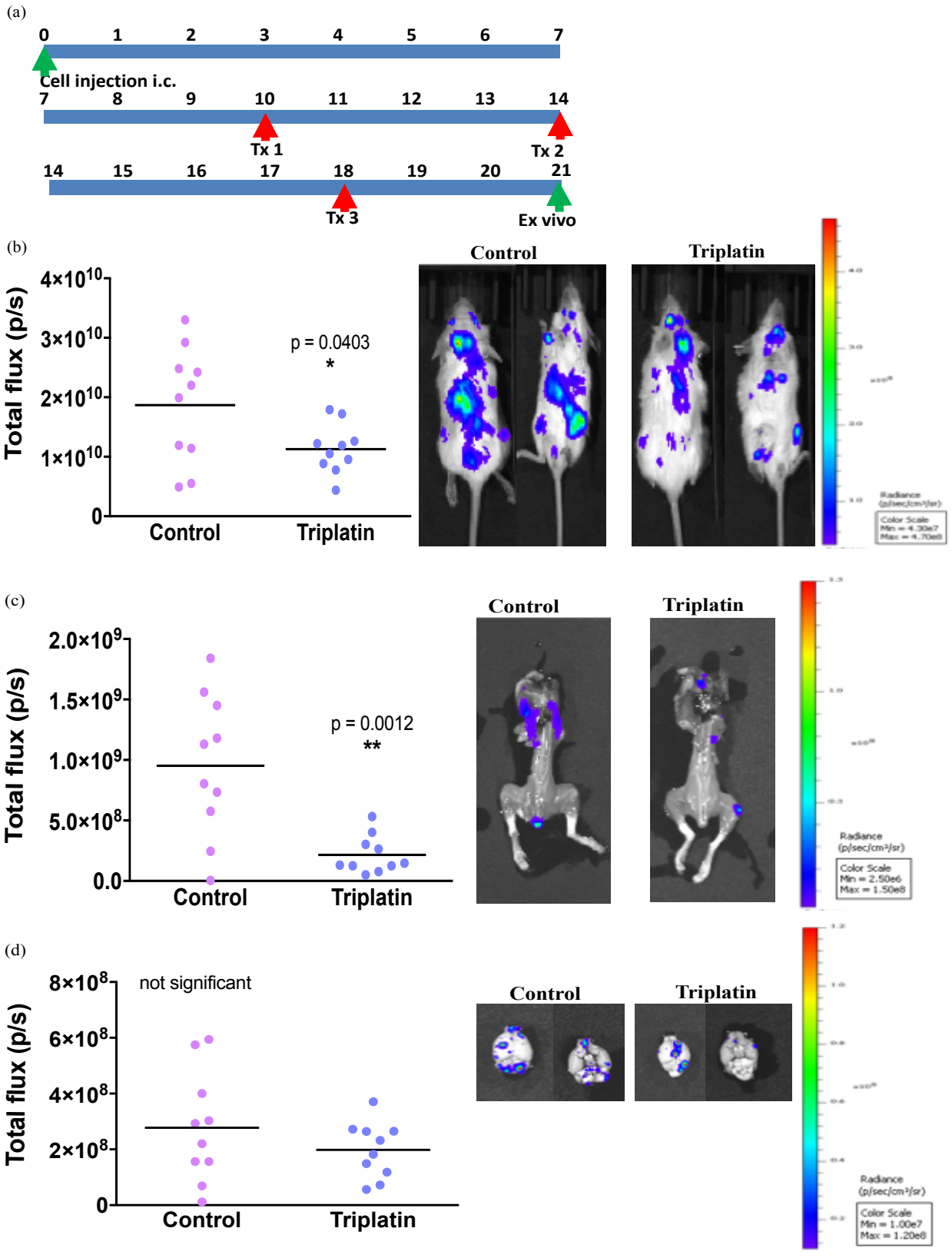

Figure 5.9. *In vivo* experiment 1. Triplatin diminished overall metastases and bone metastases in

female NSG mice that were intracardiac injected with human breast cancer MDA-MB-231-BrM2-*luc* cells (day 0). (a) Mice were treated with Triplatin (0.3 mg/kg) or saline on days 10, 14, and 18 by i.p. injections. (b) On day 21, Triplatin reduced the overall metastases ($p < 0.05$) (dorsal view left, ventral view right). Once skeletons were harvested, (c) *ex vivo* images confirmed that Triplatin reduced bone metastases ($p < 0.01$). Brains were harvested, but (d) *ex vivo* images revealed they were unremarkable (cranial view left, cadual view right). All metastases were quantified by IVIS. Each group had 10 mice.

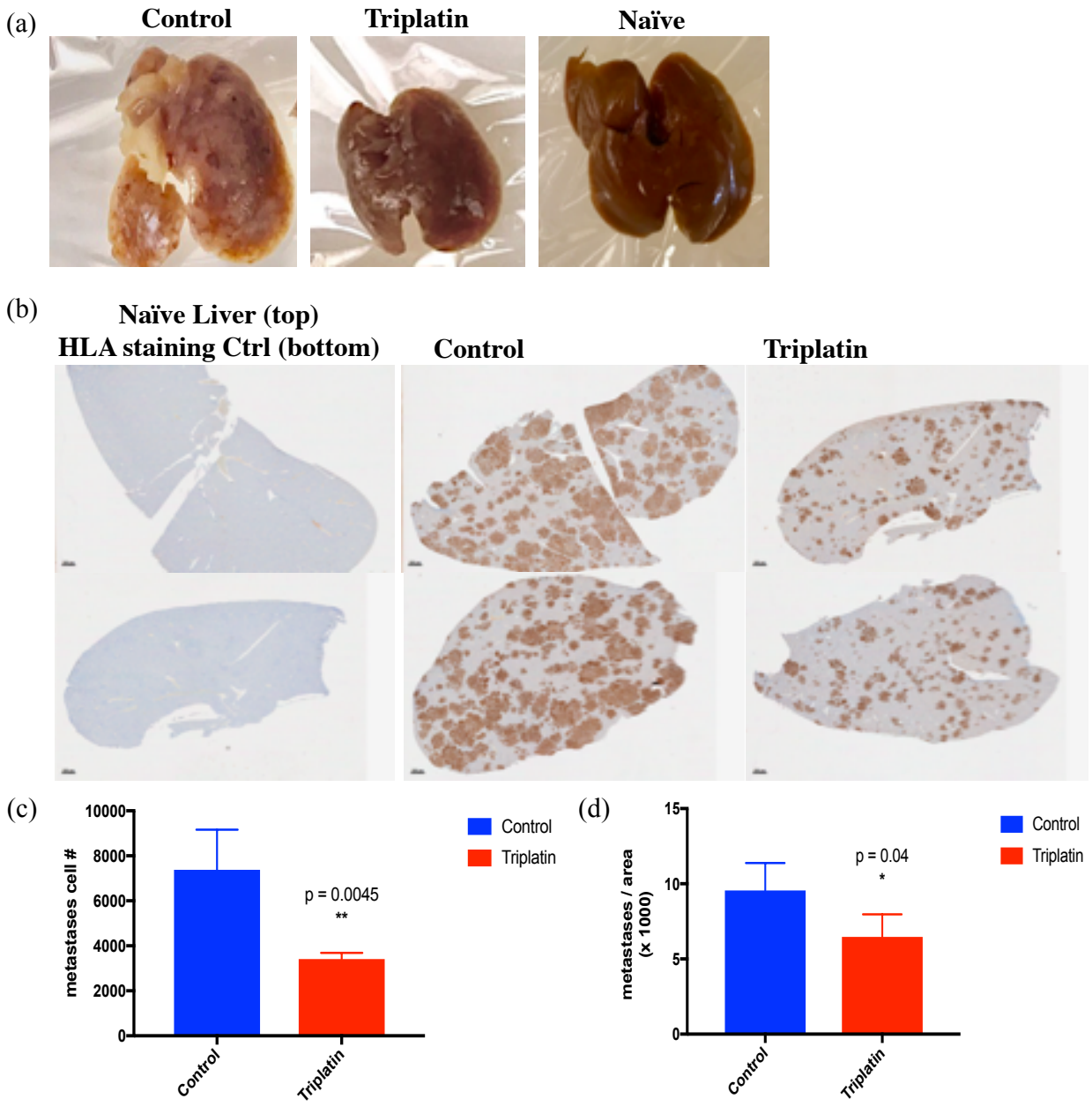

Figure 5.10. *In vivo* experiment 1. Triplatin reduced liver metastases in female NSG mice that were intracardiac injected with human breast cancer MDA-MB-231-BrM2-*luc* cells (day 0). Mice were treated with Triplatin (0.3 mg/kg) or saline on days 10, 14, and 18 *via* i.p. injections. On day 21, livers were harvested in formalin fixation, and (a) imaged using an iPhone S7 camera before sectioning to show surface metastases reduction in Triplatin treated group compared to control and naïve livers. (b) Livers were stained with HLA antibody with hematoxylin counter stain to naïve

liver (top left), HLA staining control (bottom left), control group (center), and Triplatin group (right). (c) Triplatin reduced liver metastases quantified by metastases cell number identified by the HLA staining and (d) then normalized to liver area using cell counter on ImageJ. Error bars represent the mean ± SD of 5 mice.

To understand why Triplatin did not reduce brain metastases, we hypothesized that Triplatin was targeting high tumor burden areas since the metastases bioluminescence signal was the lower in the brain than in the bone (Figure 5.9 c, d). Triplatin accumulation in tissues was evaluated in a patient treated with Triplatin (0.14mg/m^2/day for 5 days) 28 days prior to her death and found Pt levels in mostly in the kidney (32 ng/g), heart (16 ng/g), lung (16 ng/g), liver (10 ng/g) and other tissues (<10 ng/g).[139] Therefore, we examined the mouse model using 10-fold fewer cells to: 1. determine and extend mice survival since mice could not survive beyond 21 days in the previous model with more cells, and 2. determine the highest tumor burden areas. NSG mice were intracardiac injected with 1x10^4 MDA-MB-231-BrM2-*luc* cells (day 0) and were monitored for metastases by IVIS. On days 10, 19, and 35, mice were imaged, and 2 mice were sacrificed for *ex vivo* images of the following organs: brain, bone, kidneys, liver, lung, and ovary (Figure 5.11). We found metastases in all of the examined organs with the liver having the most for all of the time points. The MDA-MB-231-BrM2-*luc* cells were developed in nude mice and were shown to have mostly brain metastases.[132] Although leakiness to other organs was not reported, the change from nude to NSG mice might have exacerbated the metastases to other areas besides the brain.[131] However, consistently every mouse did indeed develop brain metastases, which is unique to the brain trophic cell line from its parental MDA-MB-231 cell line.

After day 19-time point, the remaining 4 mice survived until around day 30 when 2 mice were found dead, and the other 2 mice were euthanized on day 35. Therefore, the average survival for this model with $1x10^4$ cells injected is around 32 days. Since the previous in vivo experiment in Figures 5.8-5.10 all of the mice required euthanasia at 21 days – only 3 days after last treatment, fewer cells needed to be injected to reduce overall tumor burden to a state of clinical intervention. As in a typical clinical trial setting, eligibility criteria for patients (in this case post-injected mice) need to have a life expectancy where therapy would improve survival. Therefore, the mice need to live long enough for: the tumors to develop (10 days post injection), then treatment regimen (9 days), and addition days to see therapy benefits in survival – making the average 32 day-survival observed in the previous experiment (Figure 5.11) acceptable life expectancy criteria.

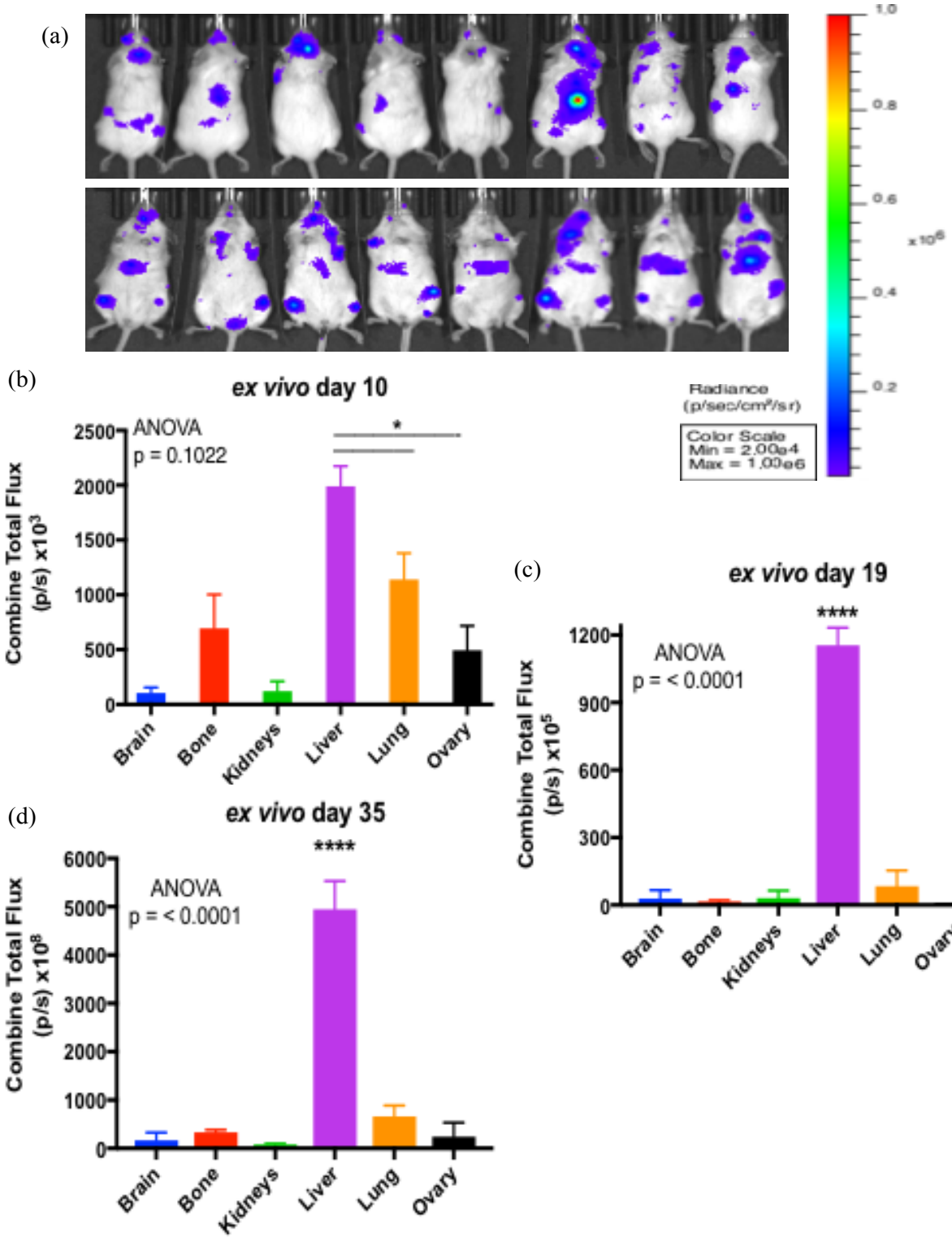

Figure 5.11. ***In vivo*** **experiment 2.** Female NSG mice were intracardiac injected with human breast cancer MDA-MB-231-BrM2-*luc* cells (day 0). (a) All 8 mice were imaged for overall

metastases (dorsal view top and ventral view bottom) on day 10. Mice were sacrificed and organs (brain, bone, kidneys, liver, lung, ovary) were harvested for ex vivo imaging of metastases on days (b) 10, (c) 19, and (d) 25. All metastases were quantified by IVIS and analyzed in GraphPad Prism7. Each time point had 2 mice.

Triplatin, cisplatin, and DiplatinNC were compared to control to determine their overall benefit on survival in the metastatic TNBC mouse model previously used in Figures 5.8-5.11. Female NSG mice were intracardiac injected with human breast cancer MDA-MB-231-BrM2-*luc* cells on day 0. Mice were randomized on day 10 into 4 groups and then treated with Triplatin (0.3 mg/kg), DiplatinNC (40 mg/kg), cisplatin (3 mg/kg) or saline on days 10, 14, and 18 by i.p. injection. A range of 1-6 mg/kg is commonly used dosage in mice for cisplatin throughout the literature[122] and given the frequency of the treatments and the NSG mice host we chose 3 mg/kg dose. Triplatin had less overall metastases compared to the other groups on day 35 (Figure 5.12 a), which was the last time point measured since mice began to die frequently in the other groups around day 35. Moreover, Triplatin had significantly extended survival compared to DiplatinNC, control, and cisplatin from 37.5 to 60 days resulting in a 60% increase in life span (Figure 5.12 b, Table 5.2).

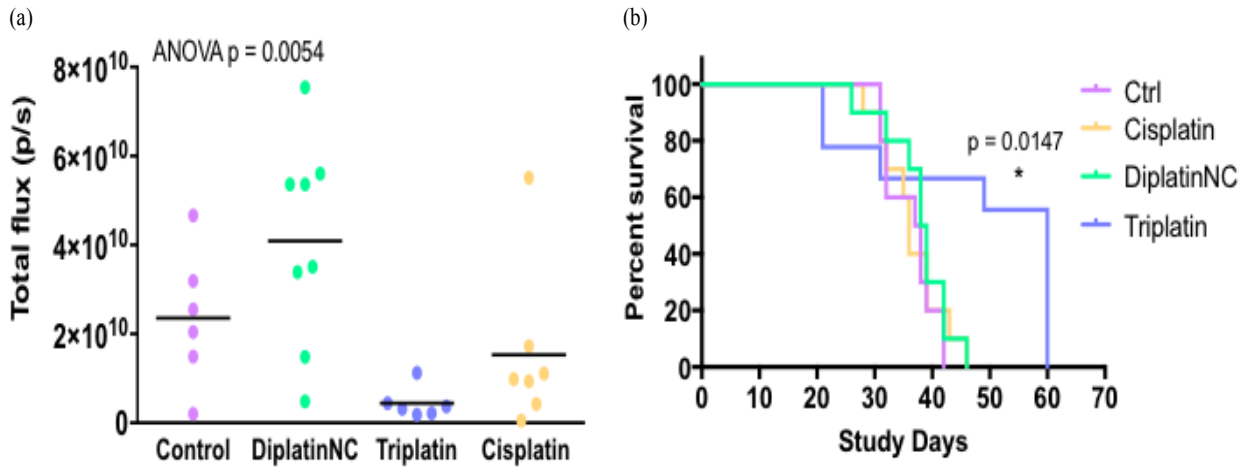

Figure 5.12. *In vivo* experiment 3. Triplatin prolonged survival compared to cisplatin or saline control. Female NSG mice were intracardiac injected with human breast cancer MDA-MB-231-BrM2-*luc* cells on day 0. Mice were treated with Triplatin (0.3 mg/kg), DiplatinNC (40 mg/kg), cisplatin (3 mg/kg) or saline on days 10, 14, and 18 by i.p. injection. (a) On day 35 Triplatin had less overall metastases and (b) extended overall survival compared to DiplatinNC, control, and cisplatin. Metastases were quantified by IVIS and analysis was done in GraphPad Prism7. Each group had 10 mice.

	MEDIAN SURVIVAL (DAYS)	INCREASE IN LIFE SPAN (%)
TRIPLATIN	60	60.0
DIPLATINNC	38.5	2.6
CISPLATIN	36	- 4.0
CONTROL	37.5	

Table 5.2. The median survival and percent increase in life span (treated (T) over control (C) mice (T x 100/C) – 100) were calculated from the *in vivo* studies.

The initial *in vivo* experiment (Figures 5.8-5.10) was repeated to evaluate other PPCs anti-metastatic activity. TriplatinNC and BBR3571 were investigated to compare structure-activity relationships with Triplatin previous data (Figures 5.9 and 5.10). Carboplatin was used as a common platinum therapeutic for metastatic breast cancer for PPC activity to be compared against. The 40 mg/kg dose was chosen based on common *in vivo* doses used throughout the literature, and the frequency of administrations in NSG mice. NSG mice were intracardiac injected with $1x10^5$ MDA-MB-231-BrM2-*luc* cells on day 0. Randomization of mice into 4 groups occurred on day 10 immediately before treatments of TriplatinNC (20 mg/kg), BBR3571 (0.3 mg/kg), carboplatin (40 mg/kg), or saline with the dosing scheduled on days 10, 14, and 18 by i.p. injections. Mice were injected with luciferin throughout the study for live bioluminescent imaging using the IVIS to observe overall tumor burden. BBR3571-treated mice had a continual decrease in body weight with 20% maximum lost on day 21 when they were euthanized, and 3 mice died (out of 11) from drug toxicity and tumor burden (Appendix IV Figure 3). TriplatinNC treatment group lost 5 mice (out of 11) group to drug toxicity and tumor burden. Importantly, carboplatin and saline control also experienced continual body weight lost with 16% maximum lost on day 21 – suggesting this model may have been particularly aggressive since the original model had little body weight lost (Appendix IV Figure 4).

On day 21, mice were imaged for overall metastases and then sacrificed for *ex vivo* imaging of bone, brain, kidneys, liver, lungs, and ovary. BBR3571 significantly reduced overall tumor burden compared to control whereas carboplatin only mildly reduced metastases (Figure 5.12 a). Both BBR3571 and carboplatin significantly reduced liver metastases (Figure 5.12 c). Metastases appeared to be suppressed in the BBR3571-treated mice for all of the organs harvested except for

brain. These results match up well with the covalent analog Triplatin suppression of metastases in Figures 5.9 and 5.10. TriplatinNC slightly reduced overall metastases and lung metastases of which was observed in the previous 4T1 orthotopic model in Figure 5.4.

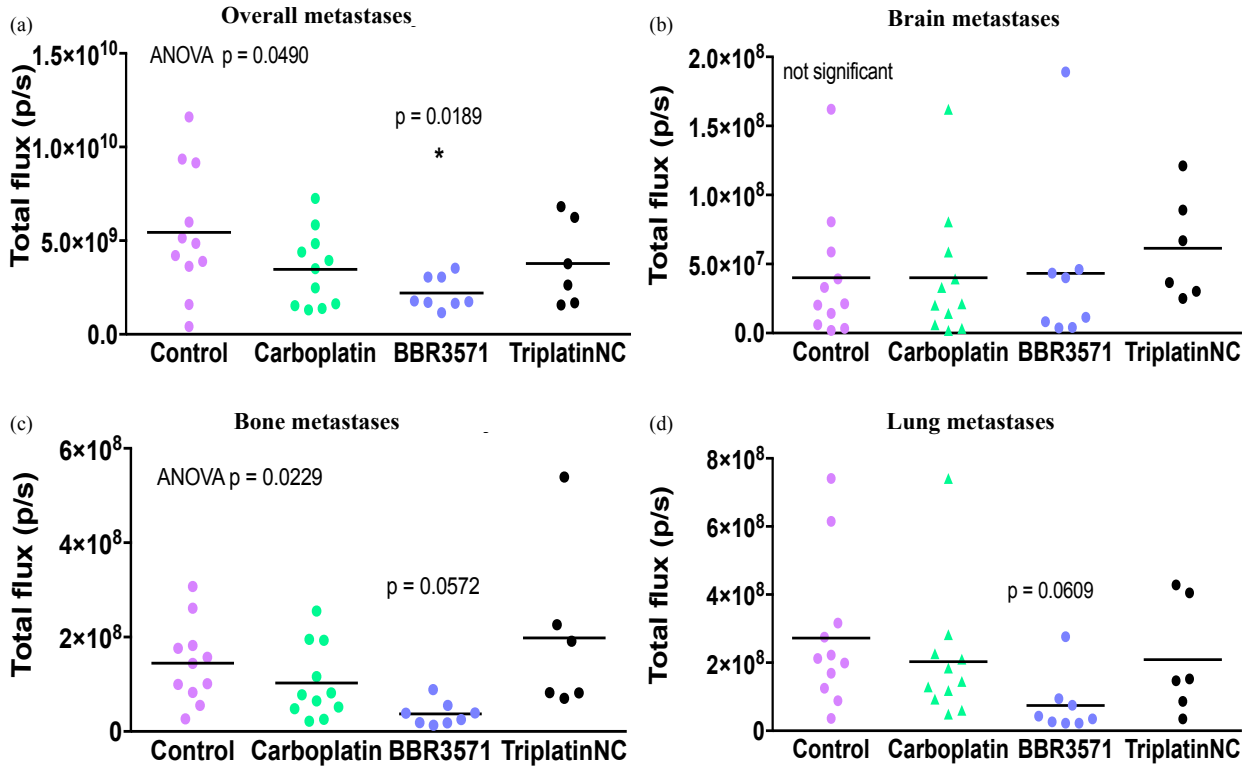

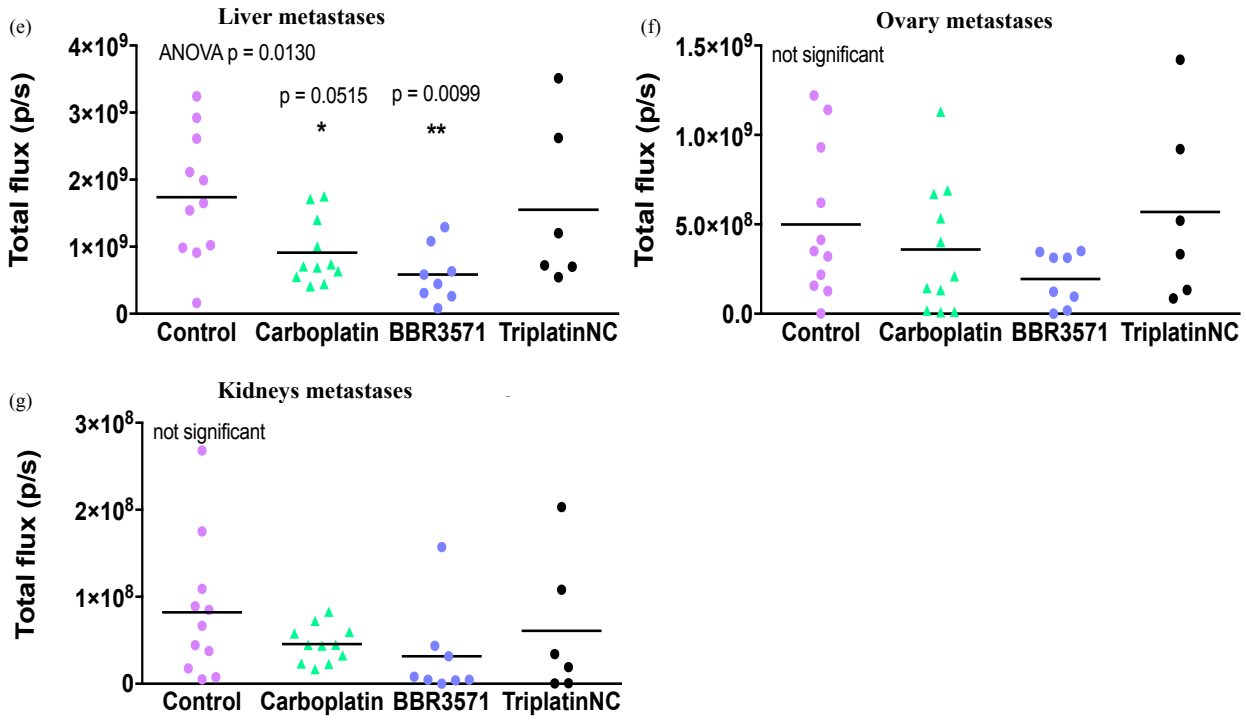

Figure 5.13. *In vivo* experiment 4. BBR3571 significantly diminished overall metastases, and liver metastases in female NSG mice that were intracardiac injected with human breast cancer MDA-MB-231-BrM2-*luc* cells (day 0). Mice were treated with BBR3571 (0.3 mg/kg), TriplatinNC (20 mg/kg), carboplatin (40 mg/kg), or saline on days 10, 14, and 18 by i.p. injections. (a) On day 21, BBR3571 reduced the overall metastases ($p < 0.05$). Once organs were harvested, *ex vivo* images by IVIS were used to quantify metastases in (b) brain, (c) bone, (d) lung, (e) liver, (f) ovary, and (g) kidneys. Each group had 11 mice.

Since xenografts required the use of immunodeficient mice that lacks the immune system interplay in tumor development and treatment, we next used an immunocompetent mouse model intracardiac injected with murine mammary carcinoma cells for modeling anti-metastatic activity with immune system interplay. For the intracardiac injection model, female BALB/c mice were used and purchased from The Jackson Laboratory. As an inbred mouse strain, BALB/c have some

immunosuppression such as mutations in *Mx1* and *Mx2* genes involved in the innate immunity, as well as a deficiency in IL-12 that causes TH2 helper T cell dominance effecting the adaptive immunity.[128] Additionally, BALB/c had intermediate recruitment of macrophages compared to commonly used immunocompetent mouse strains.[140] This slight immunosuppression (especially compared to NSG) results in an increase susceptibility to pathogens.[128]

Female BALB/c mice were intracardiac injected with $4x10^4$ 4T1-*luc* cells (aggressive murine mammary carcinoma) on day 0. Previous studies were done in Dr. Koblinski Lab to determine optimal cell number for wide spread metastases and mouse survival. These results are briefly summarized here: mice injected with $1x10^5$ cells or $5x10^4$ cells developed wide spread metastases but only lived 8 or 10 days post injection respectively, while mice injected with $2.5x10^4$ or $1x10^4$ cells lived >10 days but metastases were not well distributed. Therefore, in order to have the mice live long enough to receive the entire treatment regimen and have widespread metastases, we chose $4x10^4$ cells for injection. After mice were randomized into 4 groups on day 1, treatments of carboplatin (40 mg/kg), BBR3464 (Triplatin, 0.3 mg/kg), DiplatinNC (40 mg/kg), or saline-control were administrated on days 1, 5, and 9 post injection. Unexpectedly, after day 9 of post cell injection, all of the mice experience dramatic body weight loss with the control at 10% loss, DiplatinNC and carboplatin at 13% loss, and Triplatin at 23% on day 13 (Appendix IV Figure 5). Then mice were immediately euthanatized on day 13. Upon mouse dissection, control mice were riddled with tumors in the diaphragm and the heart was a solid tumor mass.

All of the treatments appeared to reduce the overall metastases burden with BBR3464 having the most reduction (Figure 5.14 a). Although metastases in the brain were not reduced in any of the

treatments (Figure 5.14 b), the rest of the analyzed organs had reductions especially in carboplatin and BB3464 treated-groups (Figure 5.14 c,d,e,f,g,h). Metastases in the bone and lung had the most dramatic decrease for carboplatin and BBR3464 treated-groups. Notably, this model did not generate consistent or even high tumor burden in the liver (had the lowest bioluminescent signal along the analyzed organs). The low occurrence of liver metastases in this model may have been due to the high tumor burden in other areas especially the heart, which decreased the mouse survival before liver metastases could develop prominently suggesting that a portal vein delivery of 4T1 cells may be the best way to evaluate liver metastases for this particular model.

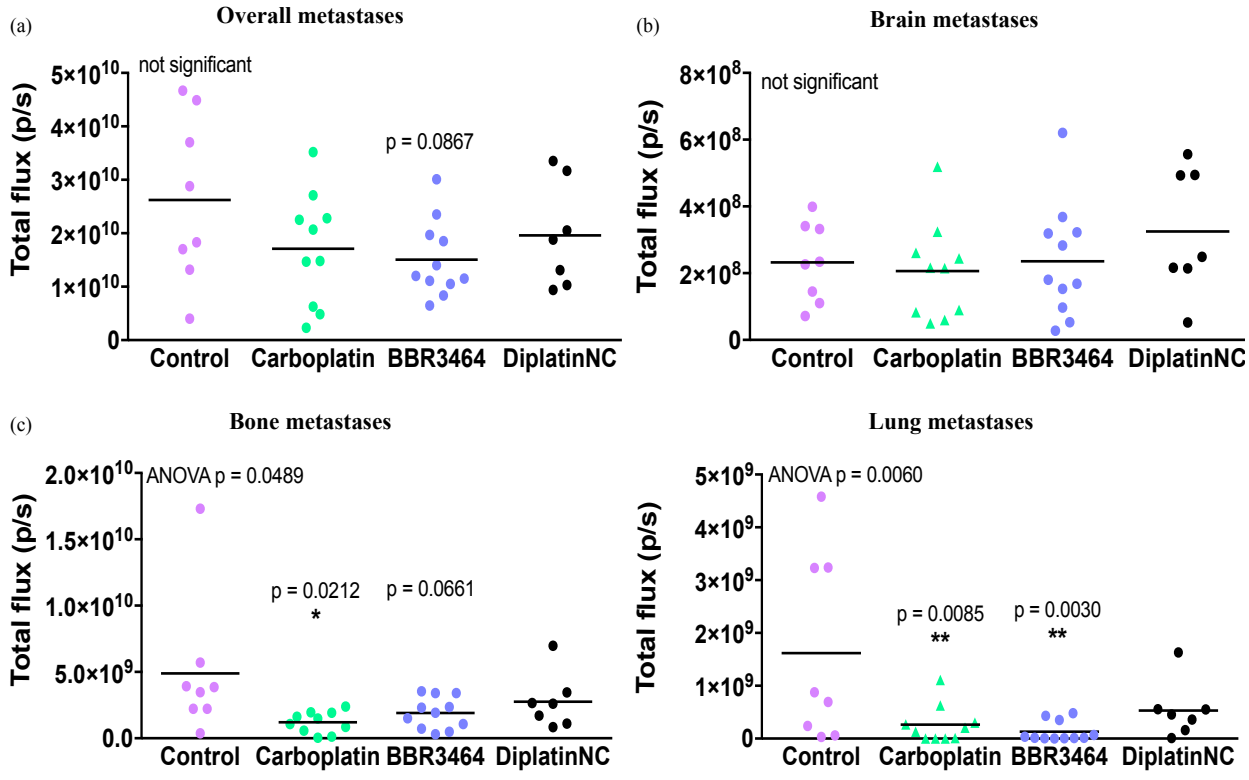

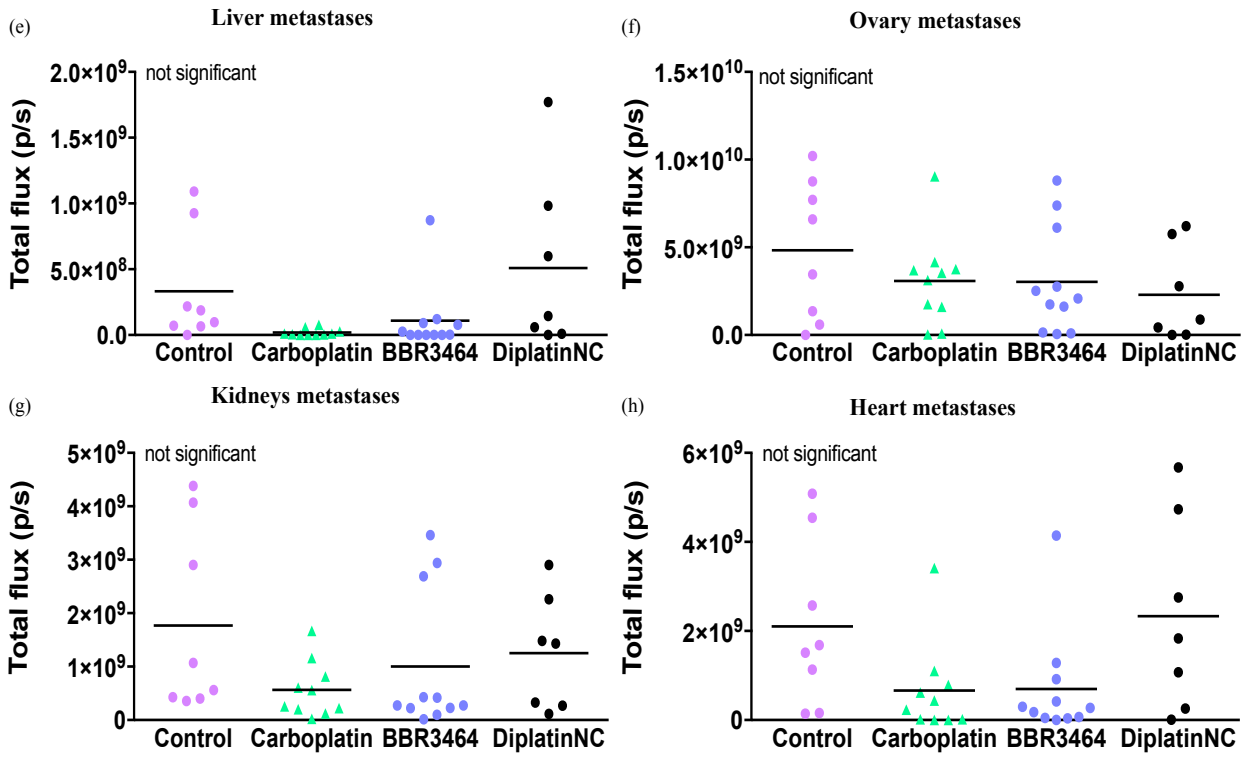

Figure 5.14. *In vivo* experiment 5. BBR3464 (Triplatin) significantly reduced lung metastases in female BALB/c mice that were intracardiac injected with murine mammary carcinoma 4T1-*luc* cells (day 0). Mice were treated with BBR3464 (0.3 mg/kg), DiplatinNC (40 mg/kg), carboplatin (40 mg/kg), or saline on days 1, 5, and 9 by i.p. injections. (a) On day 13, BBR3464 diminished the overall metastases. Once organs were harvested, *ex vivo* images by IVIS were used to quantify metastases in (b) brain, (c) bone, (d) lung, (e) liver, (f) ovary, (g) kidneys, and (h) heart. Each group had 10 mice.

5.4 Summary.

In the orthotopic models (done in Dr. Takabe Lab) secondary tumors are usually confined to the surrounding organs (lung, lymph node).[117] Therefore, the next *in vivo* experiments have further explored PPCs anti-metastatic role through intracardiac injection delivery route. Both NSG and BALB/c mice were intracardiac injected with either the human TNBC MDA-MB-231-BrM2-*luc*

cells or the 4T1-*luc* cells respectively for a confirmation of PPC anti-metastatic activity. However, both models have their caveats. NSG mice lack a functional immune system and thus neglects the critical immune interplay with metastasis progression[141] and possible therapeutic resistance.[142] However, tumors of mouse origin (required for immunocompetent mice) are problematic for development of species-specific biological agents and the tumors tend to exhibit very rapid growth. The 4T1 cells rapid growth was a constant problem for mice to survive long enough for tumors to developed and then treated for a completed treatment regimen. As a result, metastases appeared in the heart – their clumpy nature during the intracardiac injection may have contributed as well – and liver metastases had a low occurrence making this system a poor liver metastases model. Intriguingly, the NSG mice intracardiac injected with the MDA-MB-231-BrM2-*luc* cells had highest tumor in the liver and had widespread metastases to other organs most notably the bone. Moreover, liver metastases from intracardiac injection were not reported for this brain trophic cell line in nude mice[132] and the parental cell line MDA-MB-231-*luc* usually has low[143] or high[131] liver metastases occurrence.

Variations in drug toxicity were observed between the MTD studies and the TNBC models, which may be explained by the former using 8-week-old males and the latter using 6-week-old females. This difference in body weight could result in the heavier males tolerating the chemotherapies easier than the smaller and younger females.

Triplatin and BBR3571 efficacy in metastatic TNBC mouse models suggested better anti-metastatic targeting than the currently used platinum agent carboplatin. Moreover, Triplatin had prolonged survival compared to another clinically used platinum agent cisplatin and had increased

life span by 60%. Considering this MDA-MB-231-BrM2-*luc* cell-intracardiac injected NSG mouse model had significantly high metastases burden in the liver than anywhere else, Triplatin and BBR3571 significant suppression of metastases in the liver may indicate a potential for targeting high tumor burden areas. This hypothesis is verified by Triplatin accumulation mainly occurring in the kidney, heart, and lung.[139]

Future directions include Triplatin compared to carboplatin and saline control in breast cancer PDX models in collaboration with Dr. Harrell. Some of these breast cancer PDX lines were not sensitive to carboplatin[144] which may provide a therapeutic niche for PPCs.

Data was published in:

- Katner, S.J., *et al. Proc. AACR Chicago, IL.* Abstract **#3941** (2018)
- Katner, S.J., *et al. Proc. AACR Washington, DC.* Abstract **#17** (2017)
- Katsuta, E., Peterson, E.J., Katner, S.J., *et al. AACR Washington, DC.* Abstract **#5117** (2017)
- Katsuta, E., Demasi, S., Katner, S., *et al. Proc. AACR New Orleans, LA.* Abstract **#3064** (2016)

5.5 Experimental.

Cell lines and cell culture

MDA-MB-231-BrM2-*luc* cells and MDA-MB-231 -*luc* cells were provided by Dr. Koblinski and were cultured in DMEM media (Invitrogen) with 10% FBS, 1% L-glutamine, and 1% penicillin/streptomycin (Gibco). 4T1-*luc* cells were provided by Dr. Koblinski and were cultured

in RPMI media with 10% FBS and 1% penicillin/streptomycin. All cells were grown in a humidified atmosphere at 37°C with 5% CO_2.

MTT cell viability assay

MDA-MB-231-BrM2-*luc* cells were seeded in 96-well plates (3×10^3 cells/well) in supplemented media (100 μL). After incubation overnight, the cells were treated with varying concentrations of the indicated Pt compound, in sets containing 4 replicates for each concentration. After drug exposure for 24 h, 1 mM MTT (3-(4,5-dimethylthiazol-2-yl)-2,5-diphenyltetrazolim bromide) (Sigma) was added to each well and incubated for 4 h. The MTT reagent was removed, and 100 μL of DMSO was added to each well to lyse the cells and dissolve the purple formazan. All incubations were performed at 37°C with 5% CO_2. Spectrophotometric readings were determined at 570 nm using a microplate reader (Bio-Tek instruments). Percentage cell survival was determined as treated/untreated controls × 100. Data are reported as the average of 2 independent experiments ± SD.

In vivo studies

Virginia Commonwealth University Institutional Animal Care and Use Committee (IACUC) approval was obtained for all experiments. NSG mice were purchased from the Cancer Mouse Models Core at VCU Massey Cancer Center.

Maximum Tolerated Dose Determination in Mice - 1

NOD-SCID-IL2R-Gamma null (NSG) male 6-8-week-old mice were intraperitoneal (i.p.) injected with DiplatinNC (20, 40, and 60 mg/kg), BBR3571NC (50 and 70 mg/kg), or saline control on

days 1, 5, 9. Overall health and body weight were observed in mice until day 15 when the mice were euthanized. (n = 5)

Maximum Tolerated Dose Determination in Mice - 2

NSG male 6-8-week-old mice were intravenous (i.v.) injected with DiplatinNC (40, 20, and 10 mg/kg), or saline control on days 1, 5, 9. Overall health and body weight were observed in mice until day 12 when the mice were euthanized. (n = 5)

Maximum Tolerated Dose Determination in Mice - 3

NSG male 6-8-week-old mice were i.p. injected with TriplatinNC (20, 15, and 10 mg/kg), BBR3571NC (0.1, 0.2, and 0.3 mg/kg), or saline control on days 1, 5, 9. Overall health and body weight were observed in mice until day 15 when the mice were euthanized. (n = 3)

Animal Model Experiment 1

NSG female 6-8-week-old mice were injected into the left cardiac ventricle with $1x10^5$ human breast cancer MDA-MB-231-BrM2-*luc* cells (in 200 µL PBS) on day 0. For the intracardiac injection, mice were anesthetized using 2.5% isoflurane at 1 L/min oxygen flow, while cells were mixed with luciferin to permit immediate IVIS (*in vivo* imaging system, Xenogen IVIS 200) imaging for verification of widespread seeding of tumor cells. Mice were randomized on day 10 based on total flux values and body weight into 3 groups (DiplatinNC, Triplatin, control). Then the mice were treated by i.p. with DiplatinNC (40 mg/kg), Triplatin (0.3 mg/kg), or saline control on days 10, 14, and 18. Tumor burden was quantified by bioluminescence (radiance/sec) emitted from the MDA-MB-231-BrM2-*luc* cells after a 200 µL subcutaneous injection of luciferin (150

mg/kg diluted in PBS) allowing for live *in vivo* imaging using IVIS and Living Image® software (Caliper Life Sciences, Hopkinton, MA). On day 21, mice were euthanized and organs (kidneys, heart, lung, ovaries, liver, brain, and skeleton) were harvested for *ex vivo* imaging with an additional luciferin incubation. These tissues were also collected for histology. (n = 10)

Animal Model Experiment 2

NSG female 6-8-week-old mice were injected into the left cardiac ventricle with $1x10^4$ human breast cancer MDA-MB-231-BrM2-*luc* cells (in 200 µL PBS) on day 0. Intracardiac injection was previously described in *Experiment 1*. Tumor burden was quantified by bioluminescence (radiance/sec) emitted from the MDA-MB-231-BrM2-*luc* cells after a 200 µL subcutaneous injection of luciferin (150 mg/kg diluted in PBS) allowing for live *in vivo* imaging using IVIS and Living Image® software. On days 10, 19, and 35, mice were euthanized and organs (kidneys, heart, lung, ovaries, liver, brain, and skeleton) were harvested for *ex vivo* imaging with an additional luciferin incubation. These tissues were also collected for histology. (n = 2)

Animal Model Experiment 3

NSG female 6-8-week-old mice were injected into the left cardiac ventricle with $1x10^4$ human breast cancer MDA-MB-231-BrM2-*luc* cells (in 200 µL PBS) on day 0. Intracardiac injection was previously described in *Experiment 1*. Mice were randomized on day 10 based on total flux values and body weight into 4 groups (DiplatinNC, Triplatin, cisplatin, control). Then the mice were treated by i.p. with DiplatinNC (40 mg/kg), Triplatin (0.3 mg/kg), cisplatin (3 mg/kg), or saline control on days 10, 14, and 18. Tumor burden was quantified by bioluminescence (radiance/sec) emitted from the MDA-MB-231-BrM2-*luc* cells after a 200 µL subcutaneous injection of luciferin

(150 mg/kg diluted in PBS) allowing for live *in vivo* imaging using IVIS and Living Image® software. On day 21, mice were euthanized and organs (kidneys, heart, lung, ovaries, liver, brain, and skeleton) were harvested for *ex vivo* imaging with an additional luciferin incubation. These tissues were also collected for histology. (n = 10)

Animal Model Experiment 4

NSG female 6-8-week-old mice were injected into the left cardiac ventricle with $1x10^5$ human breast cancer MDA-MB-231-BrM2-*luc* cells (in 200 µL PBS) on day 0. Intracardiac injection was previously described in *Experiment 1*. Mice were randomized on day 10 based on total flux values and body weight into 4 groups (TriplatinNC, BBR3571, carboplatin, control). Then the mice were treated by i.p. with TriplatinNC (20 mg/kg), BBR3571 (0.3 mg/kg), carboplatin (40 mg/kg), or saline control on days 10, 14, and 18. Tumor burden was quantified by bioluminescence (radiance/sec) emitted from the MDA-MB-231-BrM2-*luc* cells after a 200 µL subcutaneous injection of luciferin (150 mg/kg diluted in PBS) allowing for live *in vivo* imaging using IVIS and Living Image® software. On day 21, mice were euthanized and organs (kidneys, heart, lung, ovaries, liver, brain, and skeleton) were harvested for *ex vivo* imaging with an additional luciferin incubation. These tissues were also collected for histology. (n = 11)

Animal Model Experiment 5

BALB/c female 6-8-week-old mice were injected into the left cardiac ventricle with $4x10^4$ murine breast cancer 4T1-*luc* cells (in 200 µL PBS) on day 0. Intracardiac injection was previously described in *Experiment 1*. Mice were randomized on day 1 based on total flux values and body weight into 4 groups (DiplatinNC, Triplatin, carboplatin, control). Then the mice were treated by

i.p. with DiplatinNC (40 mg/kg), Triplatin (0.3 mg/kg), carboplatin (40 mg/kg), or saline control on days 1, 5, and 9. Tumor burden was quantified by bioluminescence (radiance/sec) emitted from the MDA-MB-231-BrM2-*luc* cells after a 200 µL subcutaneous injection of luciferin (150 mg/ kg diluted in PBS) allowing for live *in vivo* imaging using IVIS and Living Image® software. On day 19 (24 hours after last dose), 3 mice from each control and Triplatin groups were euthanized and organs (kidneys, lung, ovaries, liver, brain, and skeleton) were collected for imaging and histology. On day 21, mice were euthanized and organs (kidneys, heart, lung, ovaries, liver, brain, and skeleton) were harvested for *ex vivo* imaging with an additional luciferin incubation. These tissues were also collected for histology. (n = 10)

Histology

All tissues were fixed in 10% neutral buffered formalin for at least 5 days before paraffin embedding and sectioning. Liver tissues were either stained with hematoxylin and eosin (H&E) staining, or immunohistochemistry (IHC) with a hematoxylin counter stain. For IHC, human leukocyte antigen (HLA) primary antibody (Abcam, clone EMR8-5, 1:50 dilution) followed by horse radish peroxidase (HRP) conjugated secondary antibody incubations were used to detect the human cancer cells from the mice tissue. The tissue slides were visualized with a Vectra® Polaris™ Automated Quantitative Pathology Imaging System (PerkinElmer) using whole-slide scanning at 10x to 40x range in brightfield. Phenochart Whole Slide Contextual Viewer (PerkinElmer) was used to visualize the scans. Liver metastases were quantified by metastases cell number identified by the HLA staining using Cell Counter on ImageJ and then normalized to total liver area measured in ImageJ. (n = 5)

Statistical analysis

Ordinary one-way analysis of variances (ANOVA) and Dunnett's multiple comparisons tests were performed among the control and treatment groups to determine statistical significance using the combined (dorsal and ventral) total flux values from photon emission. Tukey's multiple comparisons tests were performed to compare across all groups (*in vivo* experiment 2). Unpaired t-tests were performed only for the first *in vivo* experiment because there were only 2 groups (control and Triplatin). Kaplan-Meier survival plots were generated and changes in survival were analyzed by the log-rank test. All analyses were calculated in GraphPad PRISM 7 software and data with p values < 0.05 were considered significant.

Chapter 6. Extension to Gliomas

Briefly, previous studies have demonstrated PPCs potent cytotoxicity in neuroblastoma[122] and glioblastoma[121] models that may also be explained by glycan targeting in these tumors. Syndecans are expressed in glioma tumor cells[145] with syndecan 1 expression associated with poor prognosis.[146] Also, since breast cancer metastasizes to the brain, especially in TNBC patients having the worst overall survival,[112,147] PPC may have an effect on brain metastases considering their anti-metastatic activity in breast cancer mouse models (Chapter 5).

6.1 PPC pass through the blood brain barrier

To access the PPCs effect on the BBB integrity and determine PPC ability to cross the BBB, PPC cytotoxicity profiles were evaluated in human Ty10 brain endothelial cells and human astrocytes. The PPCs observed lower cytoxicity than cisplatin in Ty10 endothelial cells and human astrocytes (Figure 6.1). Based on these cytoxicity profiles, treatments of 10 μM were considerd non-cytotoxic concentrations in the *in vitro* BBB format especially considering the treatments would first be administrated through the top insert where the Ty10 endothelial cells are located (Figure 6.2), and then diluted into the astrocyte media once the treatments have crossed the BBB. Therefore, the astrocytes would receive diluted treatment concentrations in this set up.

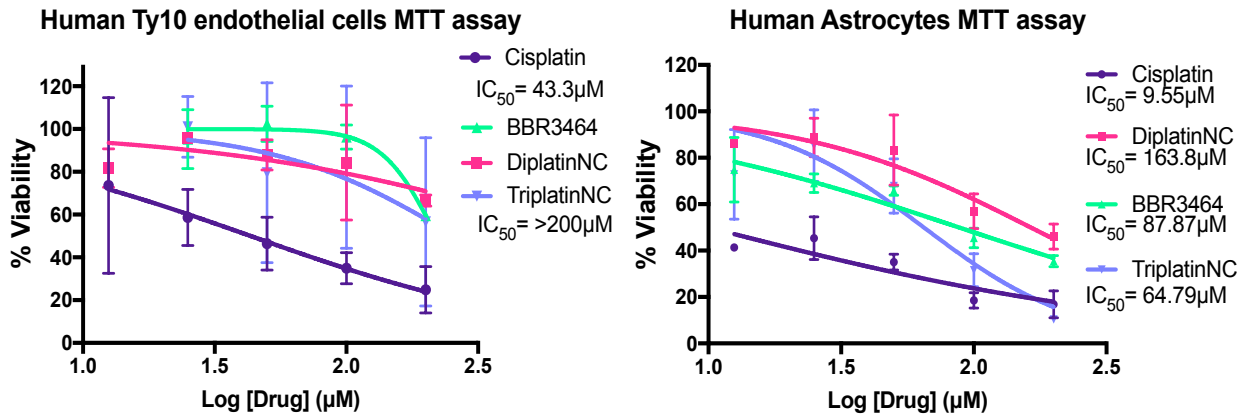

Figure 6.1. MTT cytotoxicity assays of PPCs in human Ty10 brain endothelial cells (left) and human astrocytes (right) after 24-hour treatments. Data generated was a co-effort with myself and Megan Sayyad from Dr. Koblinski's lab. Error bars represent the mean ± SD of at least 2 independent experiments (each with 3 replicates).

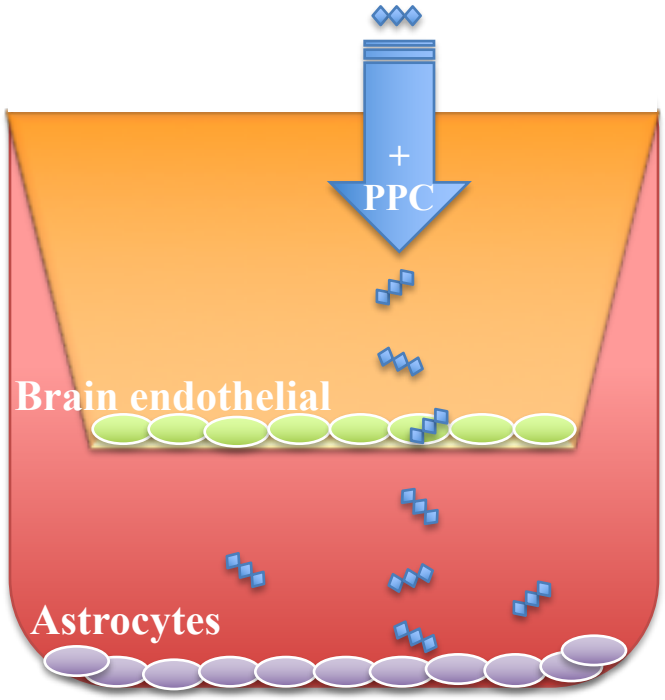

Figure 6.2. *In vitro* BBB model with human Ty10 brain endothelial cells and human astrocytes treated with non-cytotoxic concentrations of PPCs.

Transendothelial electrical resistance (TEER) was used to measure the barrier integrity of the Ty10 endothelial monolayer on the insert of the *in vitro* BBB system. However, to avoid dislodging the cells from the insert or wells, the volthommeter's electrodes were held slightly above the cells causing differences in the depth to which the electrode tips were immersed and thus differences in apparent fluid resistance occurred making the readings variable (Appendix V Figure 1).[148] Also, the TEER readings required the cells sit out at room temperature for a long period of time and thus the human astrocytes began to peel off the plate.

Therefore, we switched to using the RTCA xCELLigence to measure Ty10 endothelial cell monolayer impedance. Human astrocytes were seeded into an E-plate filter insert to support endothelial cell-cell contact and barrier tightness through release of paracrine factors, and endothelial cells (Ty10 cells) were seeded in the bottom E-plate compartment. When the endothelial cells lose their barrier tightness, the impedance readout decreases[149] such as observed for TNF-alpha-treated cells (Figure 6.3), whereas PPC treated cell, the impedance readouts are similar to the control (Figure 6.3). Cisplatin had high impedence readouts, which is commonly observed for cisplatin and may be related to changes in morphology.[150] Therefore, PPCs do not affect the BBB barrier permeability in RTCA xCELLigence *in vitro* BBB system.

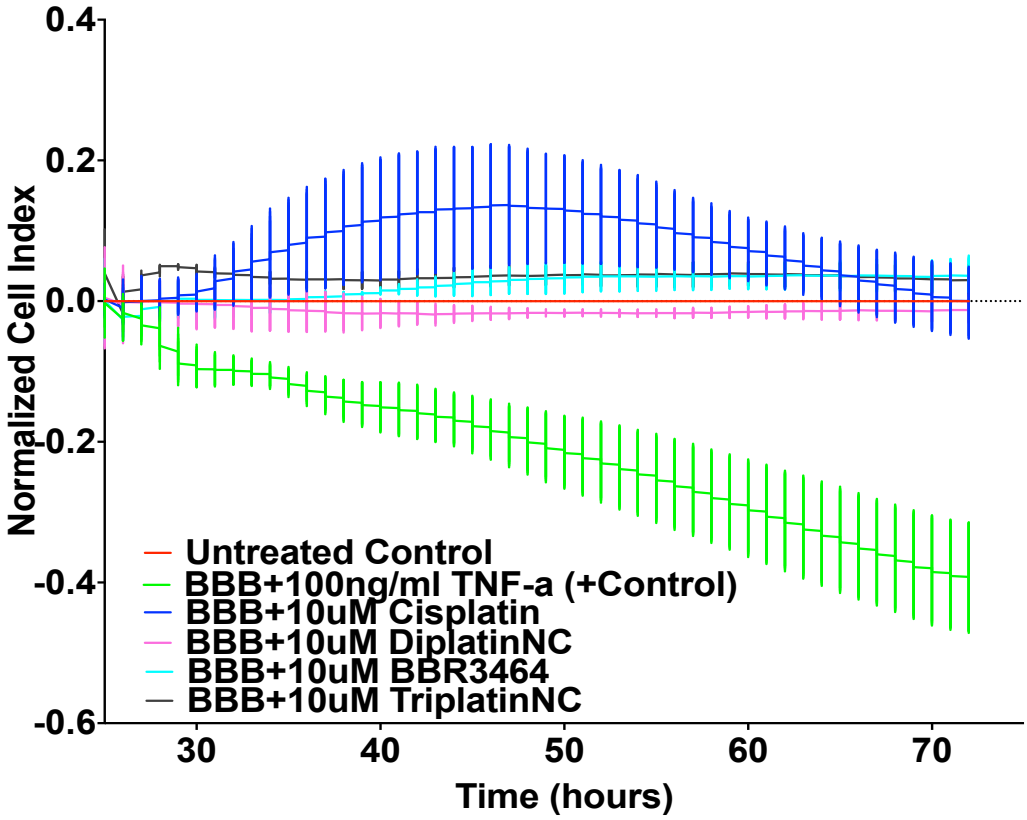

Figure 6.3. PPCs and cisplatin (10 μM) effects on BBB integrity with RTCA xCELLigence to measure Ty10 endothelial cell monolayer impedance. Data generated was a co-effort with myself and Megan Sayyad from Dr. Koblinski's lab. Error bars represent the mean ± SD of at least 3 independent experiments (each with 2 replicates).

To confirm that PPCs do not disrupt the BBB, we stained for tight junction proteins (Claudin-5 and ZO-1) present in the Ty10 endothelial cells *in vitro* BBB format. In the BBB, Claudin-5 and ZO-1 staining are major indications of barrier strength and integrity.[151152] Here the Ty10 endothelial cells were seeded in the insert while the human astrocytes were seeded in the feeder tray bellow[153] as in Figure 6.2. The BBB system was treated with PPCs, cisplatin, or TNF-alpha control for disruption, into the insert containing Ty10 endothelial cells (Figure 6.4) for 24 hours.

Then Ty10 endothelial cells were stained for Claudin-5 or ZO-1 and imaged on the Zeiss LSM 710 confocal. Claudin-5 revealed PPCs (50 µM) similar BBB integrity as the untreated, while cisplatin (50 µM) had some disruption (Appendix V Figure 2). Using 5-fold less treatment doses, we observed similar BBB integrity for all of the treatments (10 µM) as the untreated control for the ZO-1 staining (Figure 6. 4). Therefore, PPCs do not affect the *in vitro* BBB integrity.

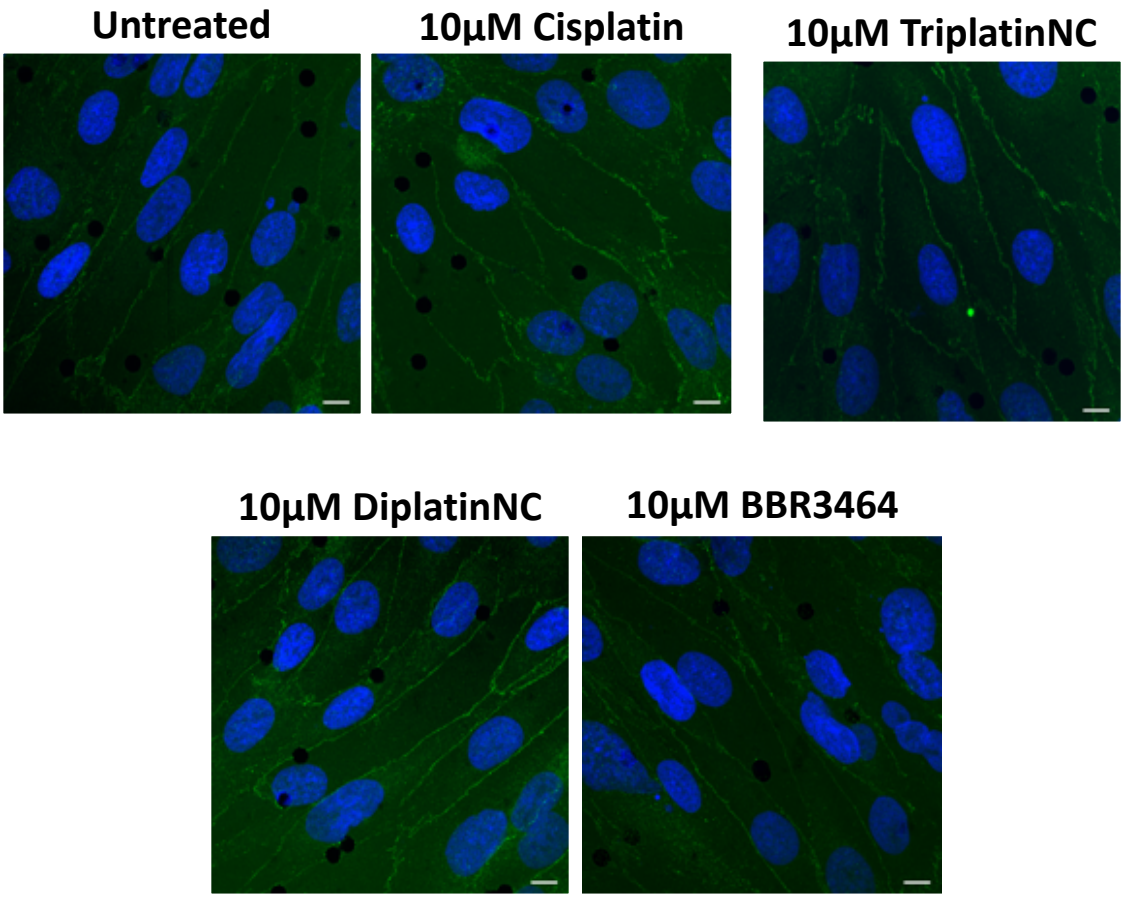

Figure 6.4. PPCs and cisplatin (10 µM) effects on BBB integrity with ZO-1 staining (green) and DAPI (blue). Data generated was a co-effort with myself and Megan Sayyad from Dr. Koblinski's lab. Images are representative of 3 independent experiments (each with 2 replicates).

Before tight junction protein staining, the media and the human astrocytes in the feeder tray wells from the BBB system in Figure 6.2 were removed after the 24-hour treatments and analyzed on the ICP-MS for Pt content. Samples were normalized to drug Pt centers to determine the % of PPC or cisplatin penetration through the *in vitro* BBB. PPCs and cisplatin we observed to penetrate the BBB with TriplatinNC and cisplatin having the highest passage (Figure 6.5). Overall the data suggests that PPCs can cross the in vitro BBB barrier and not affect BBB integrity.

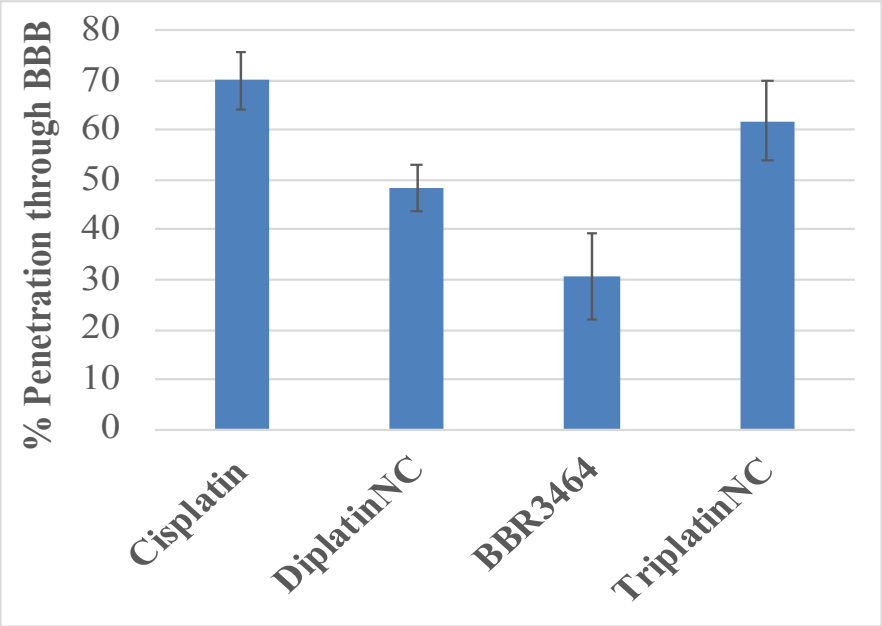

Figure 6.5. PPCs and cisplatin (10 µM) % penetration through the *in vitro* BBB determined by ICP-MS. Data generated was a co-effort with myself and Megan Sayyad from Dr. Koblinski's lab. Error bars represent the mean ± SD of at least 3 independent experiments (each with 2 replicates).

6.2 PPC cytotoxicity in PDX glioblastoma cells

PPCs cytotoxicity profiles were determined in patient-derived glioblastomas cells using proliferation assays. The covalent compounds (BBR3610 &Triplatin) were more cytotoxic in

primary astrocytes (non-cancerous cells) than non-covalent series (TriplatinNC, DiplatinNC, and AH44) (Figure 6.6). TriplatinNC had the most potency across the patient-derived glioblastomas cells cells (Figure 6.7). U3047GM (purple in Figure 6.7) was the most sensitive cell line overall, but no trend has emerged. Possibly through other experiments like cell migration, trends may develop.

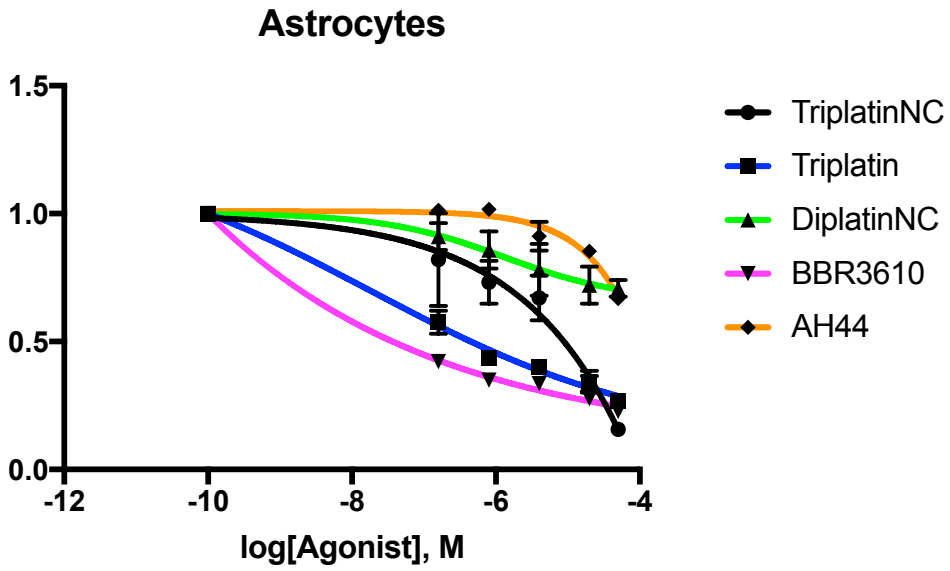

Figure 6.6. PPC cytotoxicity profile in human astrocytes. Data generated from collaboration with Dr. Karin Forsberg Nilsson.

IC50	TriplatinNC	Triplatin	DiplatinNC	BBR3610	AH44
"Cell lines"	1-5uM	0.1-0.5uM	25uM	0.1uM	25uM
U3213MG	0,95uM	1,15uM	2,45uM	0,41uM	8,26uM
U3071MG	9,21uM	NA	NA	NA	NA
U3299MG	0,35uM	1,22uM	2,83uM	0,95uM	4,04uM
U3047MG	0,19uM	0,44uM	0,81uM	0,13uM	3,23uM

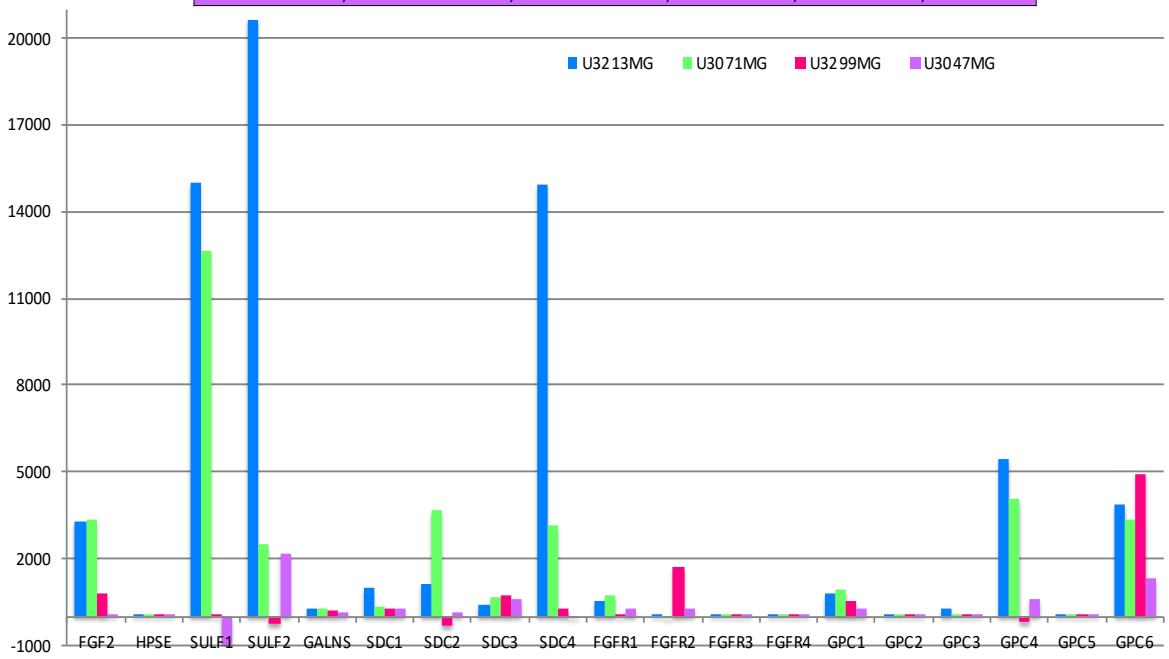

Figure 6.7. PPCs were evaluated for cytotoxicity in patient derived glioblastoma cells (top) and the mRNA expression of proteoglycans, growth factors, and sulfatases. Data generated from collaboration with Dr. Karin Forsberg Nilsson.

6.3 Summary

The *in vitro* BBB results of PPCs crossing the *in vitro* BBB barrier and not affecting the BBB integrity further emphasizes the PPCs potential in targeting breast cancer brain metastases and glioblastomas. However, cisplatin is generally consider to have low penetration through the BBB with neurotoxicity[154] which may suggest an error in the *in vitro* BBB assay. Although, recent studies have emerged using chemotherapies for treating brain metastases considering the

metastasis process breaks down the BBB and may allow low penetrating chemotherapies through.[155]

6.4 Experimental.

Cell cultures

Ty10 brain endothelial cells generated by Dr. Takashi Kanda (Yamagucchi University Graduate School of Medicine) and Primary human astrocytes (ScienCell Research Laboratories) were both from the Dr. Koblinski lab and cultured as previously described.[153]

MTT cell viability assay

Ty10 brain endothelial cells (1×10^4 cells/well) or human astrocytes (5×10^3 cells/well) were seeded in 96-well plates in supplemented media (100 μL). After incubation overnight, the cells were treated with varying concentrations of the indicated Pt compound, in sets containing 4 replicates for each concentration. After drug exposure for 24 h, 1 mM MTT (3-(4,5-dimethylthiazol-2-yl)-2,5-diphenyltetrazolim bromide) (Sigma) was added to each well and incubated for 4 h. The MTT reagent was removed, and 100 μL of DMSO was added to each well to lyse the cells and dissolve the purple formazan. All incubations were performed at 37°C with 5% CO_2. Spectrophotometric readings were determined at 570 nm using a microplate reader (Bio-Tek instruments). Percentage cell survival was determined as treated/untreated controls × 100. Data are reported as the average of 2 independent experiments ± SD.

In vitro BBB model set up

Standard 24-well plates were coated with Poly-L-Lysine and incubated for 30 minutes at 37°C before 1 mL of human astrocytes ($1.25x10^5$ cells/mL) were added to each feeder tray well. Astrocytes were allowed to attach to plate for 2-3 hours at 37°C. 24-well filter plate containing 8 μm pore PET tissue culture inserts (HTS fluoroBlok Multiwell Insert System, BD Falcon) were coated with rat tail collagen I diluted in 1x PBS and incubated for 30 minutes at 37°C before 300 μL of Ty10 endothelial cells ($4.25x10^4$ cells/well) were added to each insert placed in the astrocytes feeder tray "BBB" system. The BBB system was incubated for 48 hours at 37°C undisturbed. Note that % penetration control wells did not contain any cells. Astrocyte media was removed and replaced with fresh media. Endothelial media was removed and replaced with fresh media or media containing PPC (50 μM or 10 μM), 5% EtOH, or 100 ng/ml TNF-alpha. BBB system was incubated for additional 24 hours at 37°C.

Transendothelial electrical resistance (TEER)

TEER readings were conducted by using a Voltohmmeter with one electrode in the insert and the other in the well of the feeder tray. Each well was measured in ohms and recorded before treatment (day 4) and after treatment (day 5). Resistance of blanks (no cells) were subtracted from wells containing cells and were corrected for filter surface area.

Staining Ty10 endothelial cells from in vitro BBB system

Inserts were fixed in 4% paraformaldehyde on ice (then permeabilize with 0.3% Triton-X-100 1xPBS for 10 minutes at room temperature) for ZO-1 staining or in methanol for Claudin-5 staining. Cells were blocked with 3-5% BSA in 1xPBS for 1 hour at room temperature. Primary

antibodies Ant-Claudin-5 (1:200) or Anti-ZO-1 (1:400) were added for 1 hour at room temperature in a humidified chamber. Cells were washed 3 times with 1xPBS. Donkey anti-mouse Alexa-488 secondary antibodies (1:1000) were incubated for 1 hour at room temperature. Cell were washed 3 times with 1xPBS with the third wash containing DAPI (1:30,000), and then the filters were cut out and mounted onto slides. Claudin-5 or ZO-1 (Alexa-488) staining was image on the Zeiss LSM 710 confocal at 63x with oil immersion.

RTCA xCELLigence System

E-plates were prepared similar to in vitro BBB set up except with Ty10 endothelial cells in the bottom plate and human astrocytes in the inserts. E-plates were placed in the RTCA DP Analyzer inside the incubator at 37^{o}C. After the formation of tight junction (24 hours), wells were treated with 150 µL of fresh media or media containing either 100 ng/ml of TNF-alpha, or 10 µM PPCs/cisplatin. E-plates were placed back in the RTCA DP Analyzer inside the incubator at 37^{o}C and measurements were recorded for 48-72 hours at intervals of 15 minutes. Measurements were analyzed using RTCA software.

% PPC penetration through BBB by ICP-MS

Feeder tray media was collected in 15 mL tubes, and then astrocytes were collected in 150 µL of trypsin. The collected cell and media mixtures were frozen with liquid nitrogen and lyophilized overnight. Solids were digested in 0.5 mL of nitric acid for 48 hours and diluted with 1 mL of diH_2O. The solutions were filtered through a 0.45 GHP filter and ran on the Varian 820 ICP-MS to determine the concentration of platinum in each sample. The standards were prepared with K_2PtCl_4 in concentration of 1, 5, 10, 50, 100, 150, and 250ppb. Blank was 7% nitric acid.

Chapter 7. TPA Compounds in Ovarian Cancer

7.1 Rationale.

Second and third generations of platinum anticancer agents, carboplatin and oxaliplatin, were developed to solve cisplatin's pharmacokinetic instability by substituting liable chloride with more stable carboxylate leaving groups.[156] This increased stability limited interactions with sulfur containing molecules that caused drug inactivation, resistance, and toxic side effects.[157] However, pharmacokinetic problems are not the only obstacle that platinum anticancer agents face. Since carboplatin forms the same DNA adducts as cisplatin, both compounds are susceptible to recognition and repair of cisplatin-DNA adducts[158] – another cisplatin resistant mechanism. Cisplatin's *cis* derivatives generally share this resistant mechanism since they form similar adducts with DNA. Yet, oxaliplatin is less susceptible to recognition of its DNA adducts due to the additional steric hindrance provided by the diamocyclohexane (DACH) carrier ligand.[158–162] Therefore, it is necessary to develop compounds that create unique DNA-drug adducts while stable enough to avoid metabolic inactivation.

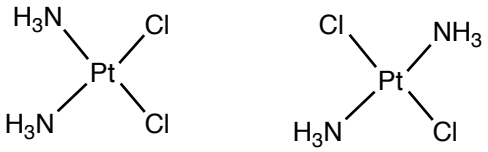

Cisplatin Transplatin

Figure 7.1. Structures of cisplatin and transplatin.

Since the discovery of cisplatin, platinum(II) compounds in the *cis* arrangement have been extensively studied for antitumor activity. Following these early structure activity relationships

platinum compounds were in the *cis* configuration of the two leaving groups (chlorides) for binding to DNA resulting in antitumor activity, whereas leaving groups in the *trans* configuration have been clinically inactive (Figure 7.1).[163,164] Cisplatin's *trans*-isomer, transplatin, is inactive because of the transinfluence from its leaving groups (chlorides) being in the *trans* position making transplatin more reactive than a *cis*-isomer and thus potentially increasing its susceptibility to inactivation by sulfur containing nucleophiles. Furthermore, transplatin is also inactive due to its inability to perturb the DNA structure.[165] Currently, there exists several *trans*-platinum compounds that form unique DNA adducts with many of them having activity in both cisplatin- and oxaliplatin-resistant cells by replacing of one or both NH_3 groups.[166–168] Substituting the amine group with a planar heterocylic ligand gives a discrete class of *trans*-platinum planar amine (TPA) compounds, trans-$[PtX_2(L)(L')]$ where L or L' are pyridine, thiazole, quinolone, or isoquinoline carrier ligands and X as the leaving group.[168,169]

TPA compounds had a unique cytotoxicity profile across the NCI tumor panel and were active in cisplatin- and oxaliplatin-resistant cell lines.[169] Replacement of the labile chloride leaving group with carboxylate ligands enhanced the compound's stability due to weak transinfluence of carboxylate leaving groups and ultimately reduced the metabolic inactivation.[170] This carboxylate stabilizing strategy was used in carboplatin and later generations of platinum anticancer agents. The use of the carboxylate ligands also resulted in good aqueous solubility, sustained cytotoxicity, and increased cellular accumulation.[171,172] Additionally, TPA compounds can be modulated in regard to their reactivity through modification of the carboxylate leaving group, while the formation of its DNA adduct can be manipulated by the carrier ligand – exemplified in oxaliplatin. In previous studies, the nature of the carboxylate ligand affected the cytotoxicity, cellular

accumulation, and metabolic stability of the TPA compounds.[170] Further studies showed the isoquinoline carrier ligand resulted in the highest cytotoxicity compared to picoline or pyridine ligands.[173,174] Therefore, we examined the structure activity relationships of three TPA compounds with the isoquinoline or thiazole carrier ligands and varying carboxylate leaving groups (acetate, hydroxyacetate, and lactate) as shown in Figure 7.2. These compounds were extensively analyzed *in vitro* beforehand and thus, discussed here are their *in vivo* activity.

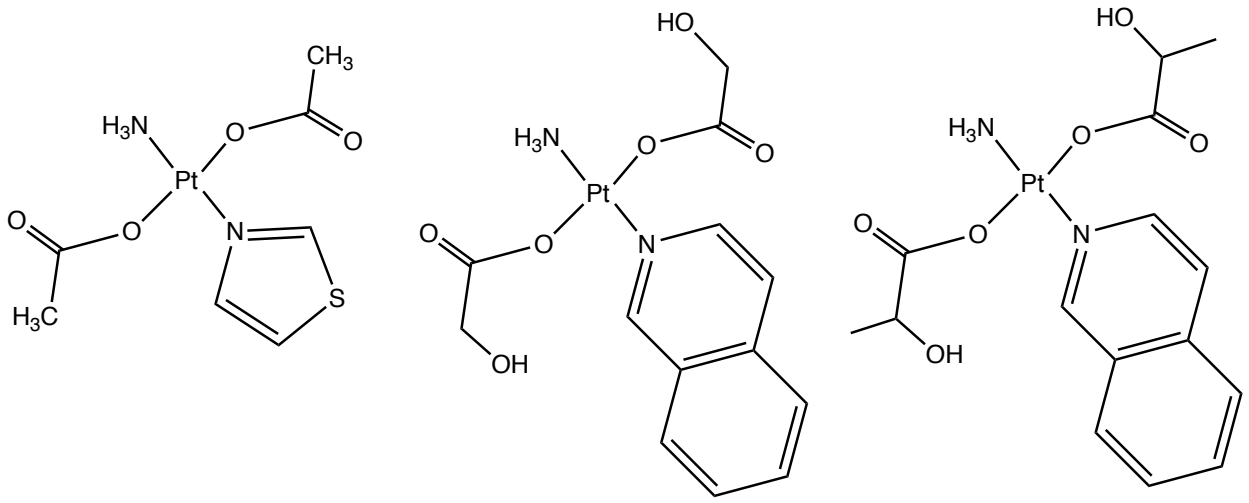

TPA Thiazole TPA hydroxyacetate TPA lactate

Figure 7.2. Structures of *trans*-platinum planar amine (TPA) carboxylate compounds studied in human ovarian cancer mouse models.

Under Dr. Koblinski's and Dr. Hu's supervision, I was trained throughout these experiments to handle mice, observe overall health of mice, administrate treatments, run IVIS for imaging proposes, euthanize mice, and dissect mice for harvesting organs (brain, lung, liver, kidneys, ovary, heart, and skeleton), and analyze all of the data.

7.2 TPA compounds activity in vivo.

To determine the maximum tolerated dose of the TPA compounds in mice, NOD-SCID-IL2R-Gamma null (NSG) mice were intraperitoneal (i.p.) injected with TPA compounds on day 1, 5, 9 and observed until day 15 (Figure 7.3). TPA compounds were selected for *in vivo* studies based on their activity *in vitro* studies. All of mice had gained weight with good overall health at high 100 mg/kg doses with the exception for TPA Thiazole 100mg/kg that had minimal body weight loss (<4%) as shown in Figure 7.3. Therefore, the TPA compounds can be administrated at least 100 mg/kg via i.p. route for NSG mice.

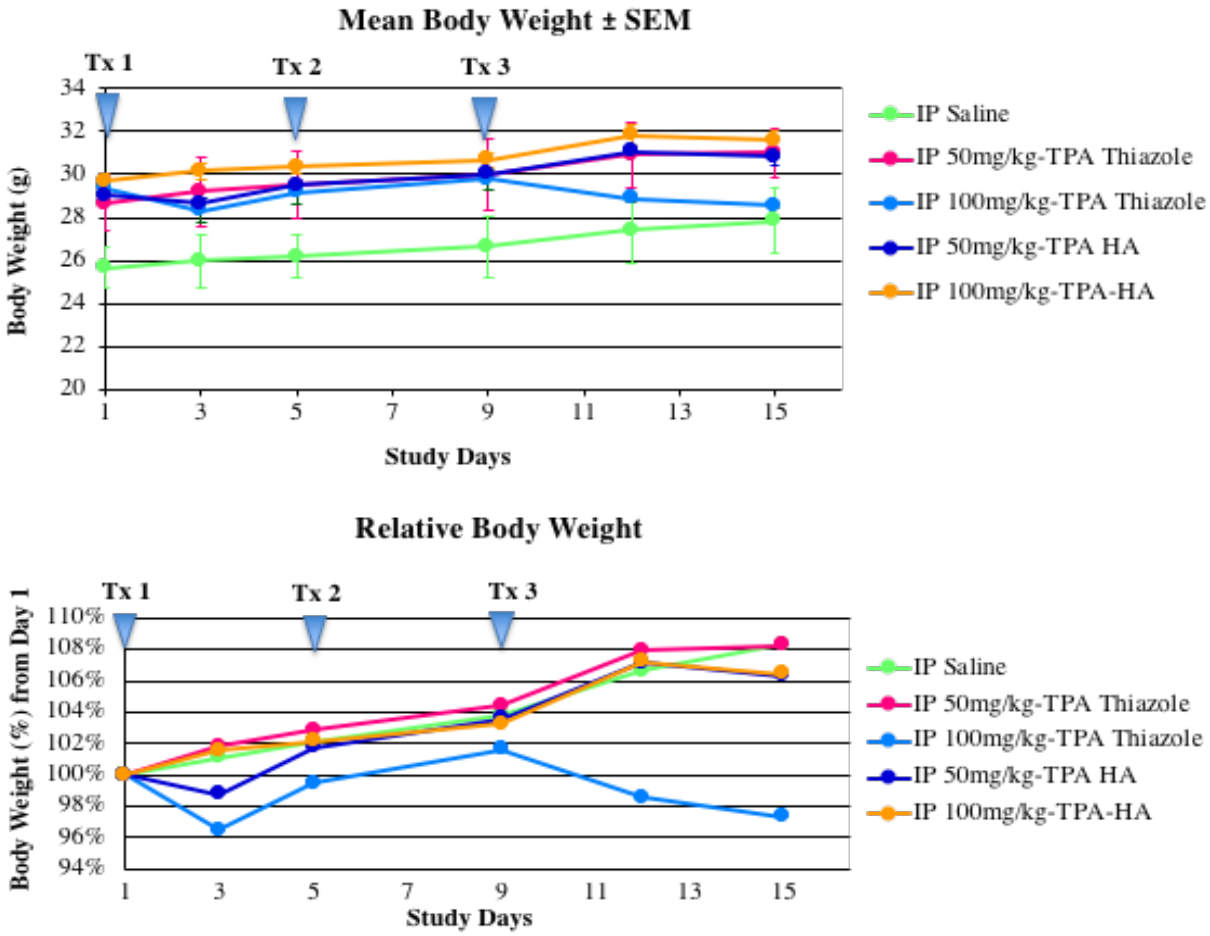

Figure 7.3. Maximum tolerated dose of TPA compounds *in vivo*. NSG mice were treated on days 1, 5, and 9 with saline control, TPA thiazole (50 and 100 mg/kg), or TPA hydroxyacetate (HA, 50

and 100 mg/kg). (top) The mean body weight and (bottom) % body weight from day 1 were observed until day 15 when the mice were euthanized. Each group had 3 mice.

Next, we investigated the TPA compounds activity *in vivo* by using a human ovarian mouse model. NSG mice were selected for their complete lack of a proper immune system as compared to other breeds available. NSG immunocompromised condition allows for xenografts (human cells in this case) to establish and spread at injection site for high tumor burden. NSG female mice were intraperitoneal (i.p.) injected with human ovarian carcinoma A2780-*luc* cells to simulate ovarian cancer progression in the peritoneal cavity and monitored by bioluminescent imaging from the luciferase transfected cells when the mice were given luciferin injections. The next day, the mice were treated with TPA thiazole (100 mg/kg), TPA hydroxyacetate (100 mg/kg), cisplatin (3 mg/kg), or saline control every 4 days as described in Figure 7.4a. The dosage of the TPA compounds were determined by the previous maximum tolerated dose studies in NSG mice (Figure 7.3). A range of 1-6 mg/kg is commonly used dosage for cisplatin throughout the literature[122] and given the frequency of the treatments we chose 3 mg/kg dose. The drugs were administrated by i.p. which is a reasonable treatment approach for ovarian cancer because of the cancer's peritoneal spread, chemotherapeutics can directly target it at high concentrations.[175] Kaplan-Meier analysis demonstrated that both TPA compounds had not improved survival, while cisplatin dramatically extended survival for all of the cisplatin treated mice and significantly reduced overall cancer progression where the mice had little to no bioluminescent signal (Figure 7.4 b). Cisplatin's dramatic suppression of tumor growth *in vitro* and *in vivo* is commonly observed in the cisplatin sensitive A2780 cell line.

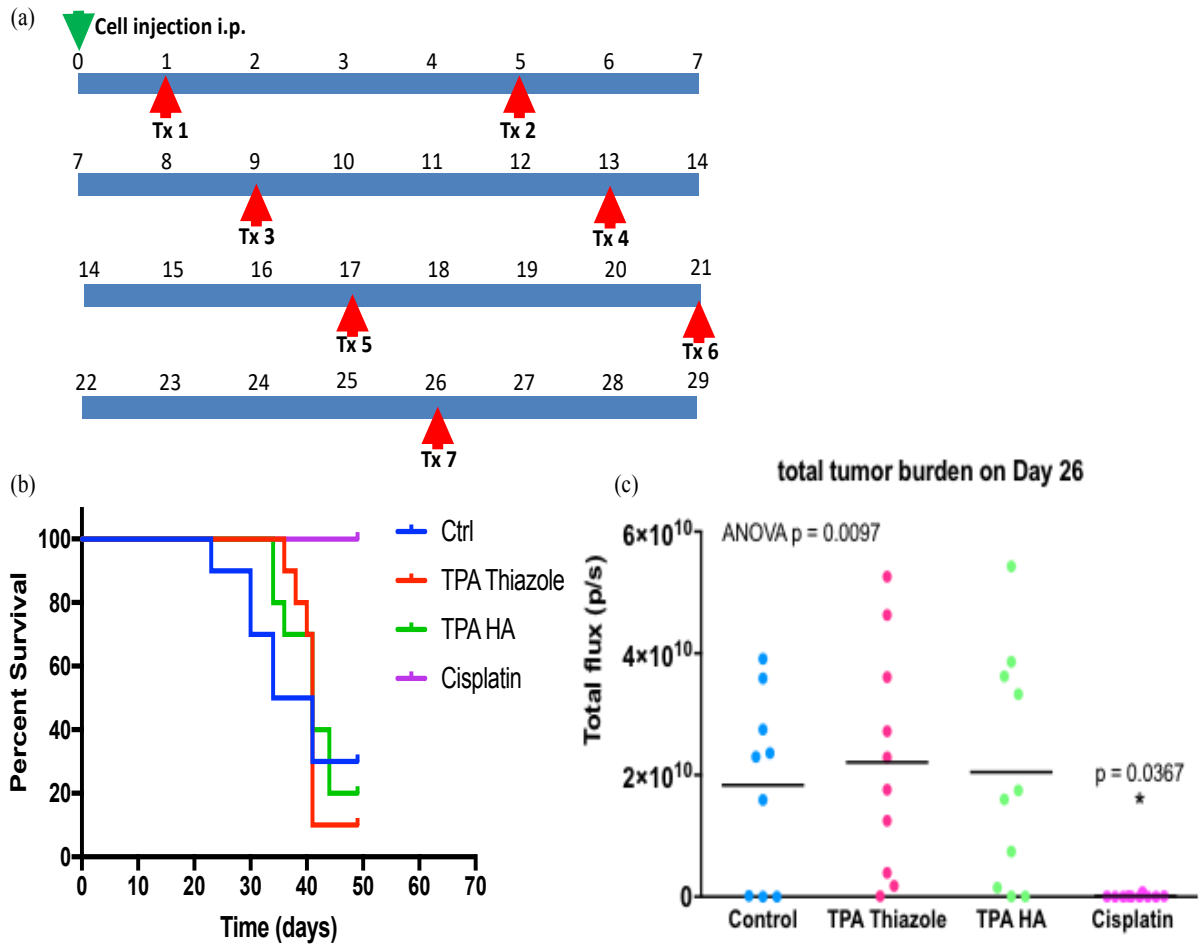

Figure 7.4. TPA compounds activity *in vivo*. (a) NSG mice were treated on days 1, 5, 9, 13, 17, 21, 26 days after A2870-luc cells injection with saline control, TPA Thiazole (100 mg/kg), TPA hydroxyacetate (HA, 100 mg/kg), or Cisplatin (3 mg/kg). (b) Prolong survival was only observed for Cisplatin treatments and (b) had a reduced tumor burden on the last day of treatment (day 26). Asterisks denote significance with $p < 5$. Each group had 10 mice.

Subsequently, we decided to increase TPA hydroxyacetate dose from 100 to 200 mg/kg and evaluate TPA lactate *in vivo* using the same previous human ovarian mouse model and treatment schedule as shown in Figure 7.4. Both of these TPA compounds were reevaluated and selected for this *in vivo* study because of their success *in vitro*. NSG female mice were i.p. injected with A2780-

luc cells and then treated with TPA hydroxyacetate (200 mg/kg), TPA lactate (100 mg/kg), or saline control. The dosage of the TPA compounds were determined by maximum tolerated dose studies in NSG mice (Figure 7.3) but TPA hydroxyacetate dose was doubled to observe a possible dose response. Our rationale for 200mg/kg was based on similar compounds ability to be tolerated at high doses such as the well-known carboplatin high dosing schedule, and also TPA hydroxyacetate's current tolerability at 100 mg/kg dose. Indeed, the mice experienced no weight loss or differences in overall health at high 200 mg/kg doses indicating that the TPA compounds are well tolerated. Kaplan-Meier analysis demonstrated that both TPA hydroxyacetate and lactate had significantly improved survival (Figure 7.5 a). On last day of treatment (day 26 post cell injection), overall tumor burden was substantially reduced in TPA lactate treated mice which might have contributed to its increased survival (Figure 7.5 b). The median survival and percent increase in life span were calculated in Table 7.1, with an increased life span of 19.35% and 32.26% for TPA hydroxyacetate and lactate respectively.

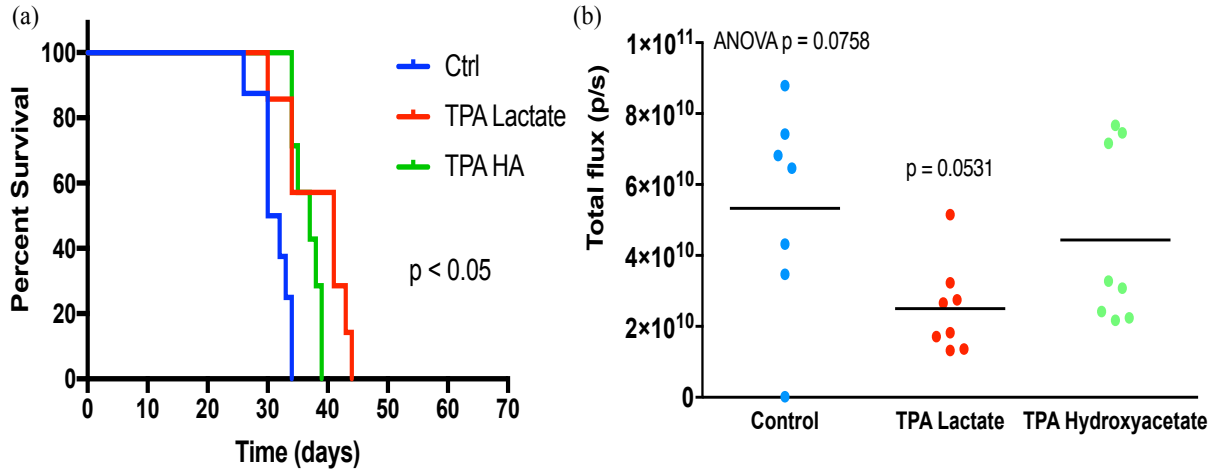

Figure 7.5. TPA compounds activity *in vivo*. NSG mice were treated on days 1, 5, 9, 13, 17, 21, 26 days after A2870-luc cells injection with saline control, TPA lactate (100 mg/kg), or TPA

hydroxyacetate (200 mg/kg). (b) Prolong survival was observed for both TPA treatments and (b) TPA lactate had a reduced tumor burden on the last day of treatment (day 26). Each group had 10 mice.

	MEDIAN SURVIVAL (DAYS)	INCREASE IN LIFE SPAN (%)
TPA HYDROXYACETATE	37	19.35
TPA LACTATE	41	32.26
CONTROL	31	

Table 7.1. The median survival and percent increase in life span (treated (T) over control (C) mice (T x 100/C) – 100) were calculated from the *in vivo* studies.

Few trans-Pt(II) complexes have been evaluated *in vivo*. Transplatin analogs containing a 3-hydroxymethylpyridine,[176] iminoether,[177,178] or 4-piperidinopiperidine[179] carrier ligands in place of a NH_3 group, all had antitumor efficacy *in vivo*. Although these transplatin analogs had efficacy comparable to that of cisplatin, they all contained the chloride leaving groups. Having these liable ligands exposes the compounds to inactivation by thiol-containing nucleophiles, whereas our TPA carboxylate compounds are more stable.[170] Here, we are the first to report TPA carboxylate compounds activity *in vivo* and together emphasize the need to further examine trans-platinum compounds for antitumor efficacy.

7.3 Summary.

It is interesting that a single substitution of an amine for a sterically hindering amine in transplatin results in the transformation of an inactive to an active anticancer agent. The use of these bulky

amines in the *trans*-platinum geometry is expansive and many of these complexes have cytotoxicity equivalent to that of cisplatin.[169] The cytotoxicity profiles of *trans*-platinum planar amine compounds are distinct from that of cisplatin and its analogs.[168] From our previous *in vitro* studies *(manuscript in preparation as indicated below)*, demonstrated a correlation with higher reactivity (TPA hydroxyacetate) to increased cytoxicity and cellular accumulation. However, this trend was not observed for cisplatin, thereby suggesting that the reactivity of carboxylate leaving groups influences metabolic stability, cellular accumulation, and cytotoxicity; as well as increases the TPA compound's overall aqueous solubility. These results reflect the balance between cytotoxicity and metabolic stability previously confirmed.[170] Intriguingly, TPA lactate was more active *in vivo* than the more reactive TPA hydroxyacetate for both tumor burden reduction and prolong survival. Also given that TPA hydroxyacetate 2-fold increase in dose over TPA lactate suggests a benefit in a less reactive, more metabolically stable TPA compound for an *in vivo* response.

Although the TPA compounds were not comparable to cisplatin in the cisplatin sensitive A2780 cells, these compounds (especially TPA lactate) should be evaluated in cisplatin resistant cell lines both *in vitro* and *in vivo*. There exist several ovarian carcinoma cells that have acquired resistance. A2780cisR cells encompass a variety of major mechanisms of resistance to cisplatin: decreased uptake, enhanced DNA repair/tolerance, and elevated GSH levels.[180] The TPA compounds unique DNA adducts and pharmacokinetic stability compared to cisplatin may prove efficacious in cisplatin resistant cells.

Data was published in:

- Lee, D.E., Menon, V., Peterson, E.J. Katner, S.J., Koblinski, J.E., Farrell, N.P. Metabolic stability and distinct cytotoxic profile of trans-platinum planar amine compounds. *-in preparation for submission*

7.4 Experimental.

Maximum Tolerated Dose Determination in Mice

Virginia Commonwealth University Institutional Animal Care and Use Committee (IACUC) approval was obtained for all experiments. NOD-SCID-IL2R-Gamma null (NSG) male 6-8-week-old mice were intraperitoneal (i.p.) injected with TPA thiazole (50 and 100 mg/kg), TPA hydroxyacetate (50 and 100 mg/kg), or saline control on days 1, 5, 9. Overall health and body weight were observed in mice until day 15 when the mice were euthanized. (n = 3)

Animal Model Experiment 1

NSG female 6-8-week-old mice were i.p. injected with $1x10^6$ human ovarian cancer A2780-*luc* cells (in 100 µL PBS) on day 0. Mice were randomized on day 1 based on total flux values and body weight. Then mice were treated with by i.p. TPA thiazole (100 mg/kg), TPA hydroxyacetate (100 mg/kg), or saline control on days 1, 5, 9, 13, 17, 21, and 26. Tumor burden was quantified by bioluminescence (radiance/sec) emitted from the A2780-*luc* cells after a 200 µL subcutaneous injection of luciferin (150 mg/ kg diluted in PBS) allowing for the live *in vivo* imaging using IVIS (*in vivo* imaging system, Xenogen IVIS 200) and Living Image® software (Caliper Life Sciences, Hopkinton, MA). Kaplan-Meier survival analyses were performed with Prism software. (n = 10)

Animal Model Experiment 2

NSG female 6-8-week-old mice were i.p. injected with $1x10^6$ human ovarian cancer A2780-*luc* cells (in 100 µL PBS) on day 0. Mice were randomized on day 1 based on total flux values and body weight. Then mice were treated with by i.p. TPA lactate (100 mg/kg), TPA hydroxyacetate (200 mg/kg), or saline control on days 1, 5, 9, 13, 17, 21, and 26. Tumor burden was quantified by bioluminescence (radiance/sec) emitted from the A2780-*luc* cells after a 200 µL subcutaneous injection of luciferin (150 mg/kg diluted in PBS) allowing for the live *in vivo* imaging using IVIS and Living Image® software. Kaplan-Meier survival analyses were performed with Prism software. (n = 10)

Statistical analysis

Ordinary one-way analysis of variances (ANOVA) and Dunnett's multiple comparisons tests were performed among the control and treatment samples to determine statistical significance using the combined (dorsal and ventral) total flux values from photon emission. Kaplan-Meier survival plots were generated and changes in survival were analyzed by the log-rank test. All analyses were calculated in GraphPad PRISM 7 software and data with p values < 0.05 were considered significant.

Conclusions

PPCs are dual-function agents through their interactions with both nucleic acids and HS. The novel Pt-HS interaction opens up new areas of metalloglycomics and potential anti-angiogenic activity. Here, we report PPC interactions with HS-like models: Fondaparinux (FPX)[44] (Chapter 2) and heparin[45] (Chapter 3). We demonstrate TriplatinNC high affinity to heparin in biophysical studies and compare HS interactions with DNA and HS using competition assays.[44,45] these approaches may be extended to a range of metal-ammine compounds[45] (Chapter 3). The biological consequences of PPC-HS interactions include modulation of heparanase cleavage, growth factor binding to HS, and growth factor-induced migration and signaling in breast cancer and endothelial cells (Chapter 4), as potential anti-metastatic and anti-angiogenic effects *in vivo*. We report proof-of-principle of strong *in vivo* anti-metastatic activity of PPCs in triple negative breast cancer (TNBC) models[46–48] (Chapter 5). Impressively, PPCs reduce overall tumor metastases with emphasis in lung, bone, and liver locations in both immunocompetent and immunosuppressive mouse models (Chapter 5). PPCs demonstrated permeability through the blood brain barrier (BBB) implying further applications for PPCs (Chapter 6), while other platinum compounds demonstrate *in vivo* efficacy (Chapter 7). The focus of my thesis was to emphasize the dual-functional nature of these compounds and to highlight their therapeutic potential for targeting HSPG in metastatic breast cancer and triple negative breast cancer (TNBC).

Appendix I – Chapter 2

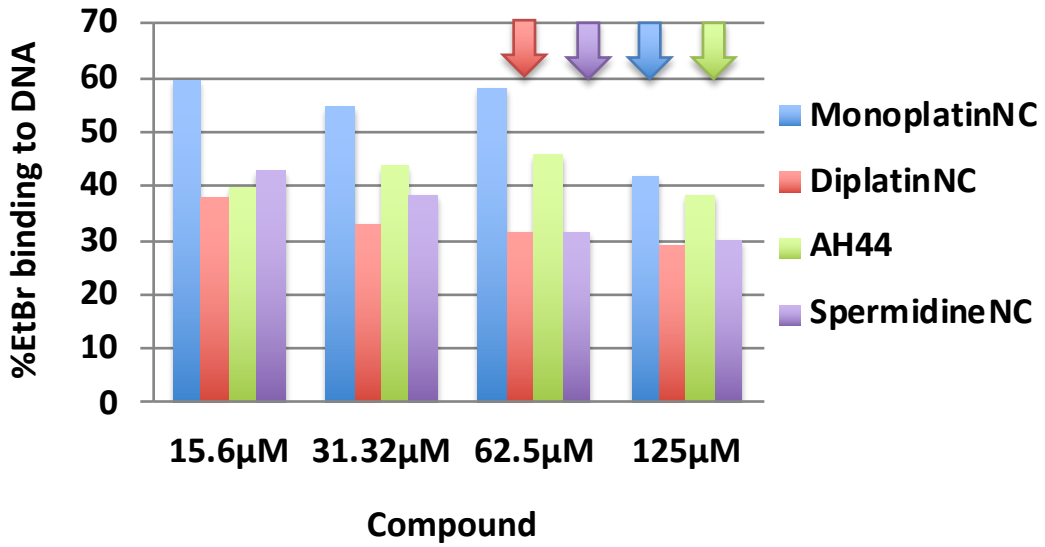

Appendix I Figure 1. The concentration of PPC required to reduce fluorescent >50% by displacing EtBr from DNA to was determined for each compound. Arrows indicate concentration chosen for the EtBr reporter assays in Chapter 2.

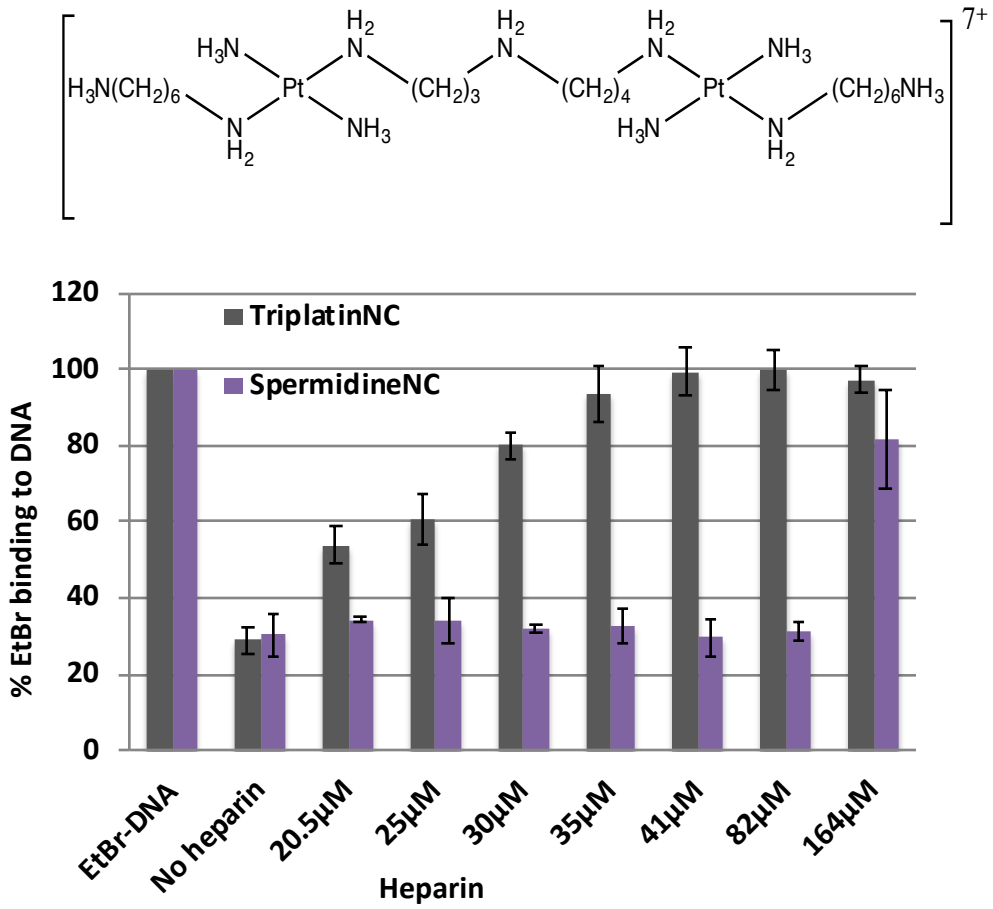

Appendix I Figure 2. SpermindineNC (structure, top) compared to TriplatinNC for heparin sequestration in the EtBr reporter assay. Error bars represent the mean ± SD of at least 2 independent experiments (each with 3 replicates).

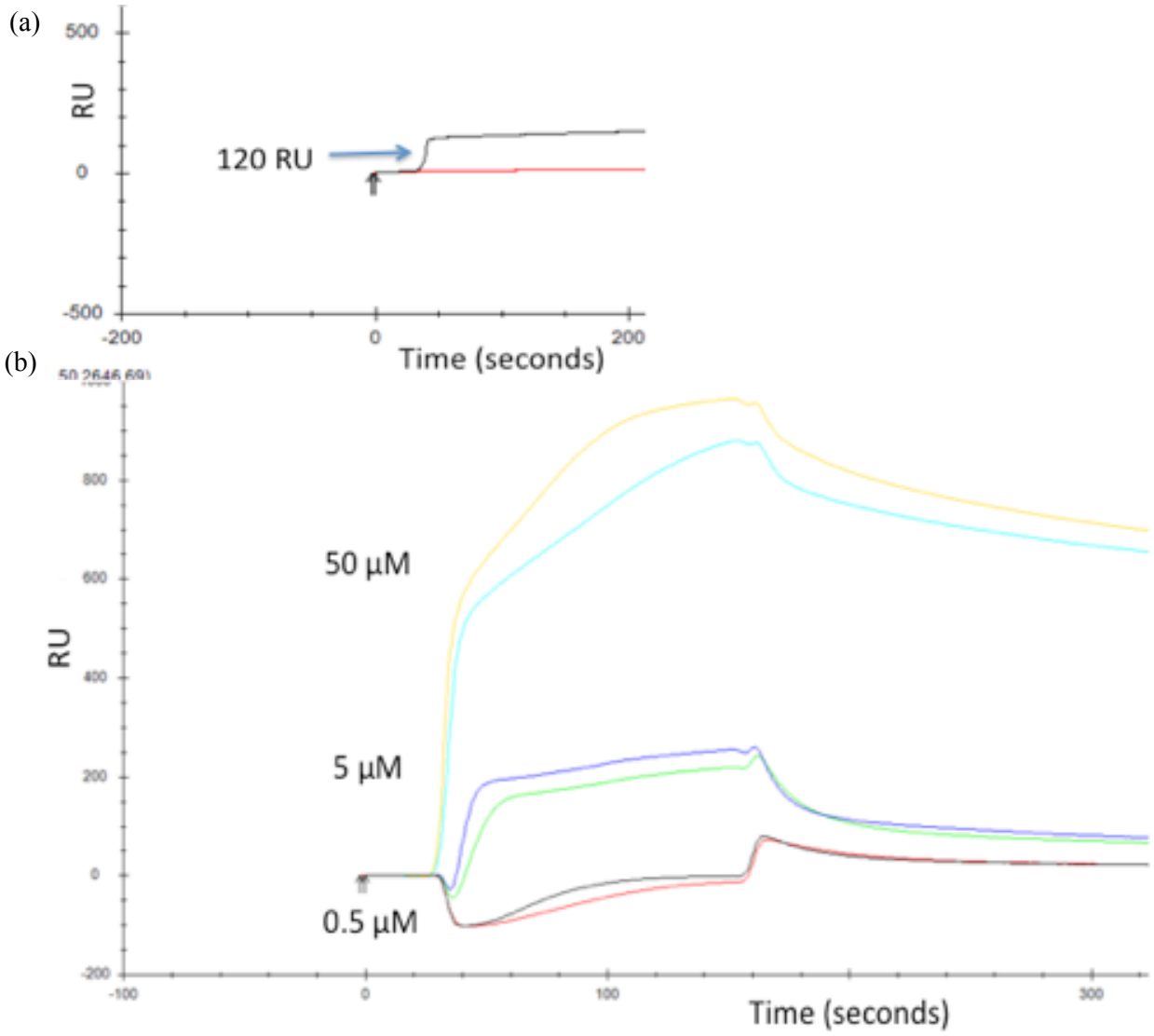

Appendix II Figure 1. *SPR trial 2.* Determination of the TriplatinNC–heparin binding affinity by SPR. (a) Biotinylated heparin (MW ~15000) was immobilized to Streptavidin on a CMD chip blocked with ethanol amine. (b) After injection of 50, 5, and 0.5 µM of TriplatinNC, the solution was allowed to flow over the chip for 5 min to allow binding; a buffer was then injected, and after flowing for 5 min, dissociation was assessed. Significant non-specific binding from TriplatinNC was observed in the reference channel (no heparin) indicated by the bottom curve for each concentration.

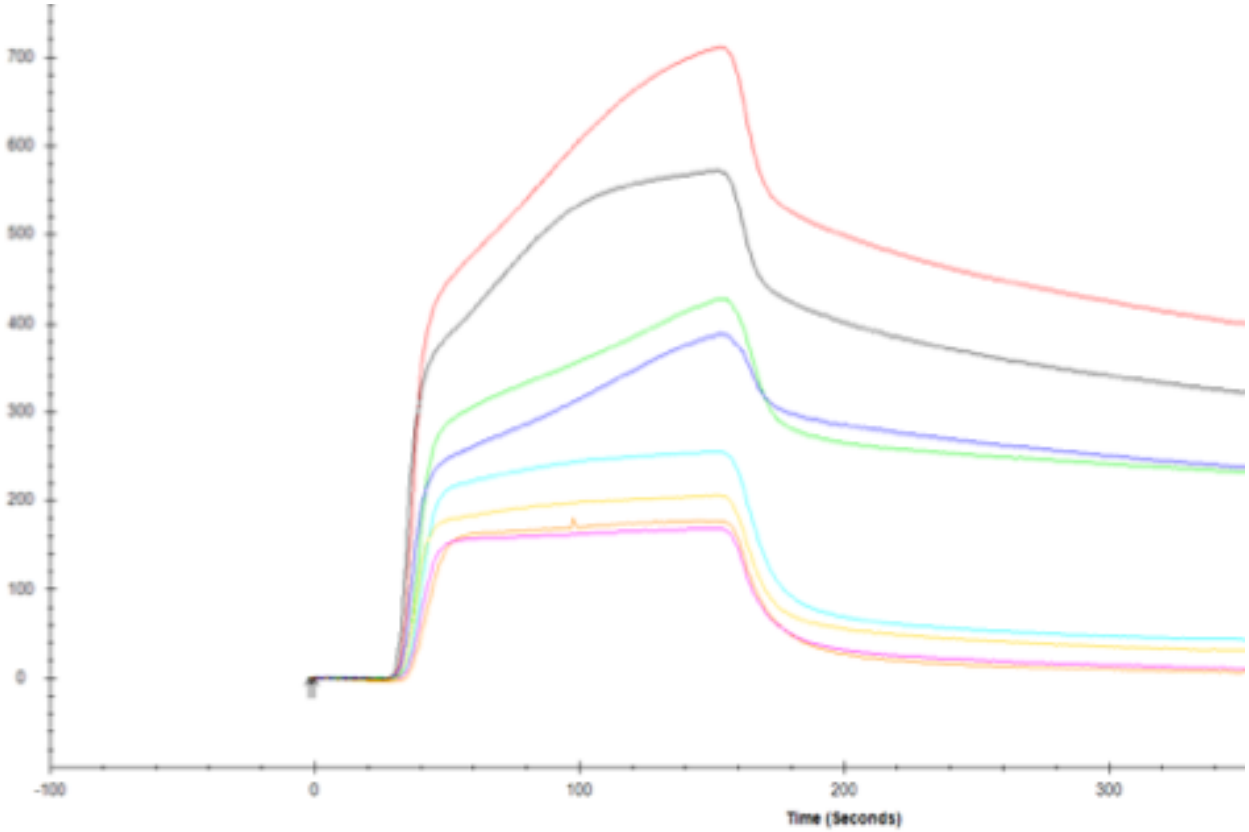

Appendix II Figure 2. *SPR trial 2-3.* Determination of the TriplatinNC–heparin binding affinity by SPR using a biotinylated heparin (MW ~15000) immobilized to Streptavidin on a CMD chip blocked with ethylene diamine. After injection of 50, 5, and 0.5 μM of TriplatinNC, the solution was allowed to flow over the chip for 5 min to allow binding; a buffer was then injected, and after flowing for 5 min, dissociation was assessed. Significant non-specific binding from TriplatinNC was observed in the reference channel (no heparin) indicated by the bottom curve for each concentration.

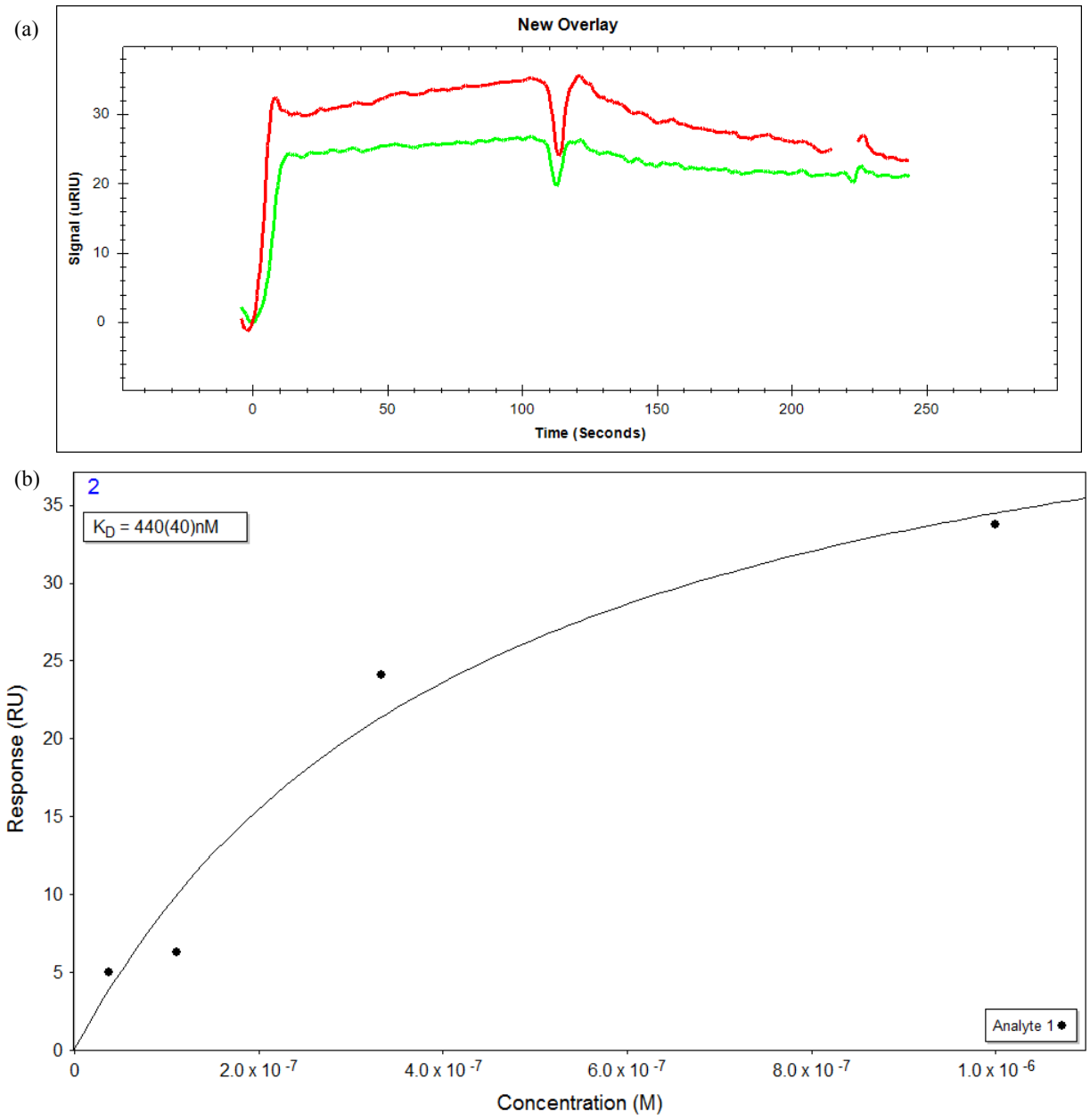

Appendix II Figure 3. *SPR trial 5.* Determination of the TriplatinNC−heparin binding affinity by SPR using a biotinylated heparin (MW ∼15000) immobilized to Neutravidin on a planar mSAM chip. (a) After injection of 5, 1, 0.333, and 0.111 μM of TriplatinNC, the solution was allowed to flow over the chip for 5 min to allow binding; a buffer was then injected, and after flowing for 5 min, dissociation was assessed. (b) The amount of TriplatinNC bound at equilibrium was corrected for background and plotted versus input TriplatinNC concentration. Analysis by equilibrium parameters using a 1:1 binding model yielded a K_d value of 440±40nM.

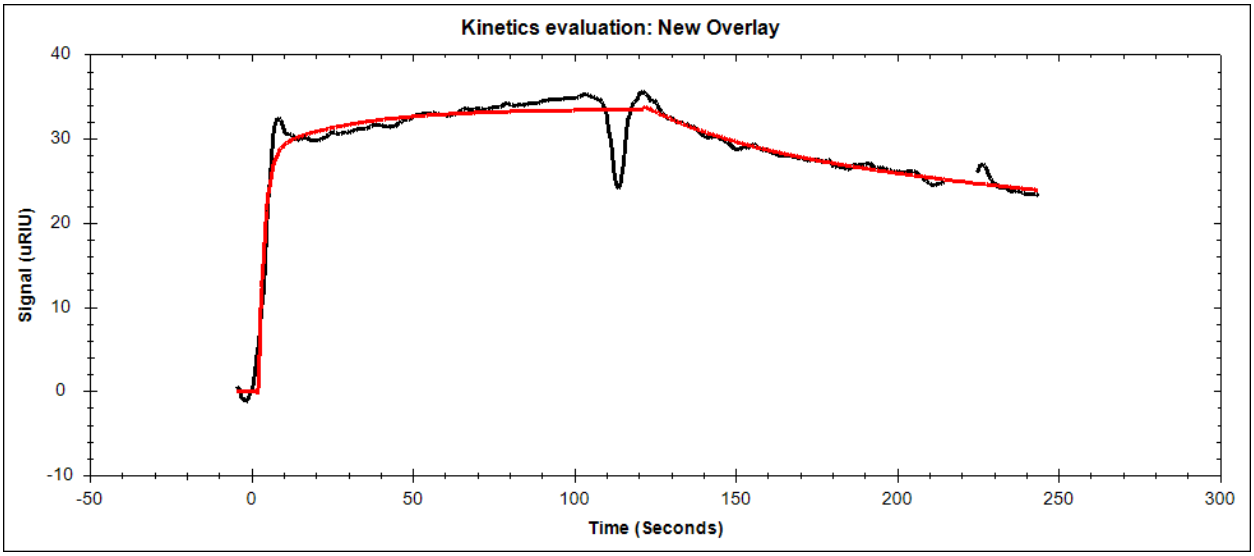

Appendix II Figure 4. *SPR trial 5.* A two-site model for TriplatinNC-heparin binding by SPR. The 1μM TriplatinNC injection gave the best curve and fit to a two-site model with immobilized heparin.

Appendix III – Chapter 4

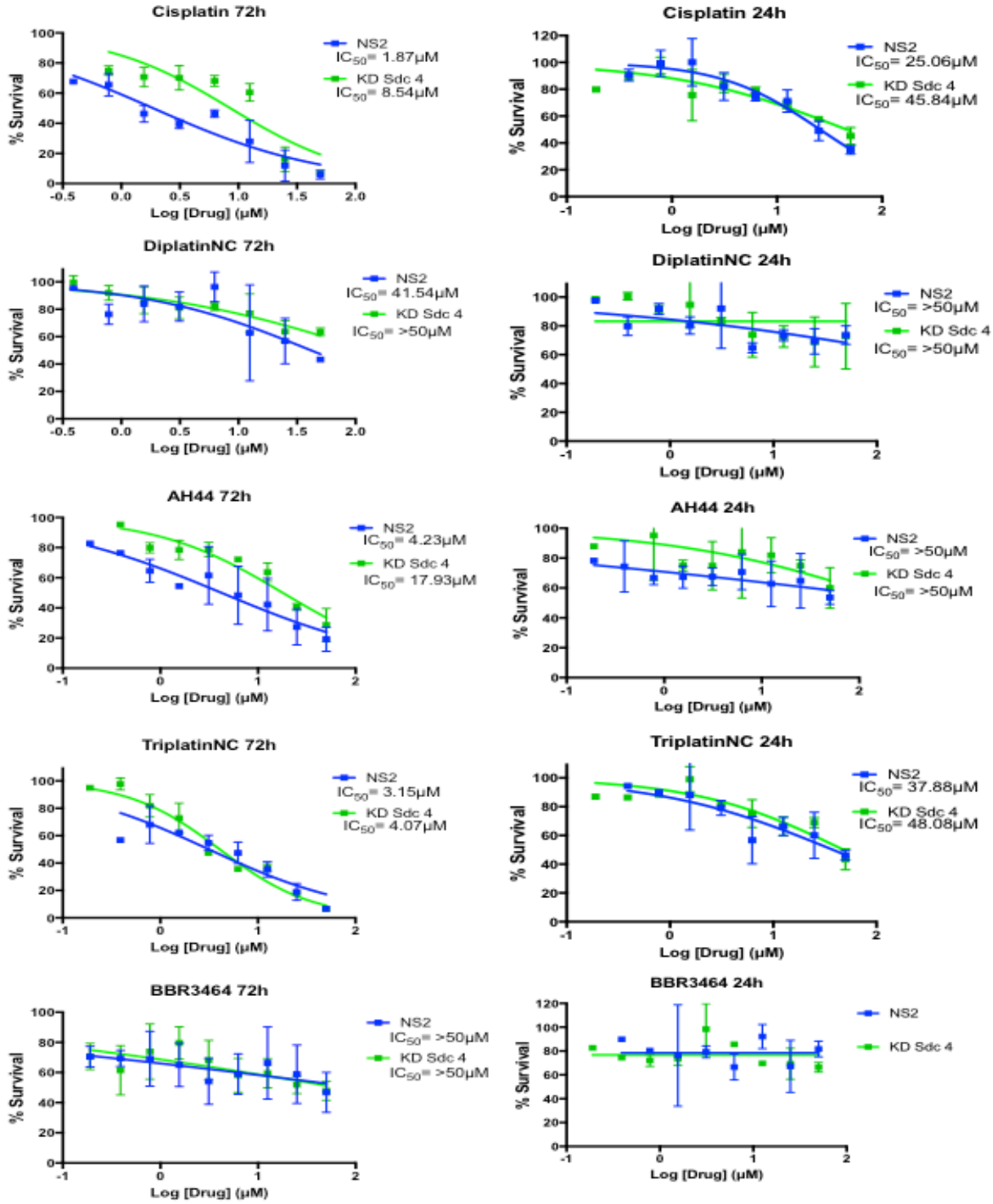

Appendix III Figure 1. PPC cytotoxicity with modified syndecan expression. PPCs and cisplatin were incubated for 72 hour (left) and 24 hour (right) in control empty vector NS2 MDA-MB-231 cells and KD Sdc4 MDA-MB-231 cells. IC_{50} values ± SD of at least 2 independent experiments (each with 4 replicates) were calculated in Graphpad Prism 7.

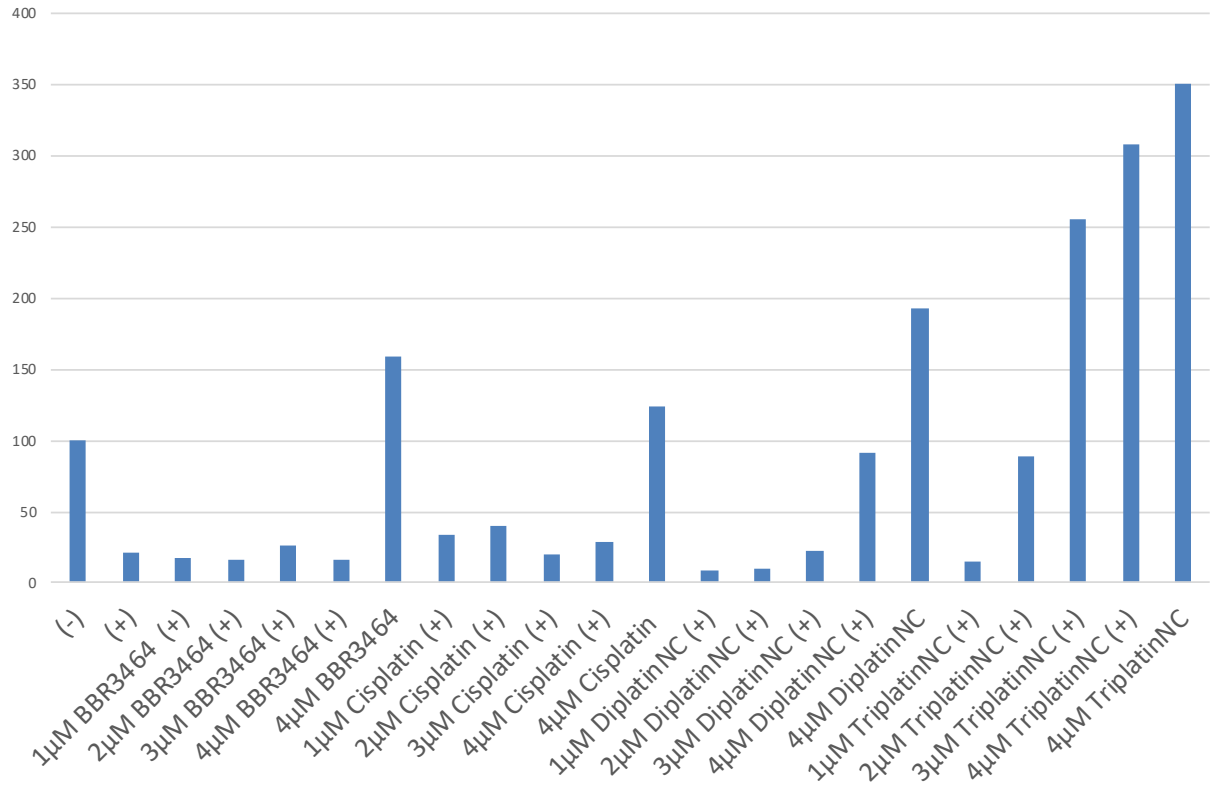

Appendix III Figure 2. Treatment with bacterial heparinase (+) had low % intact HS, while increasing PPC concentrations interacted with HS and thus prevented the heparinase degradation in CHO-K1 cells. Cisplatin did not appear to protect the HS from heparinase cleavage. Intact HS were detected by a labeled-HS specific antibody using flow cytometry.

Appendix IV – Chapter 5

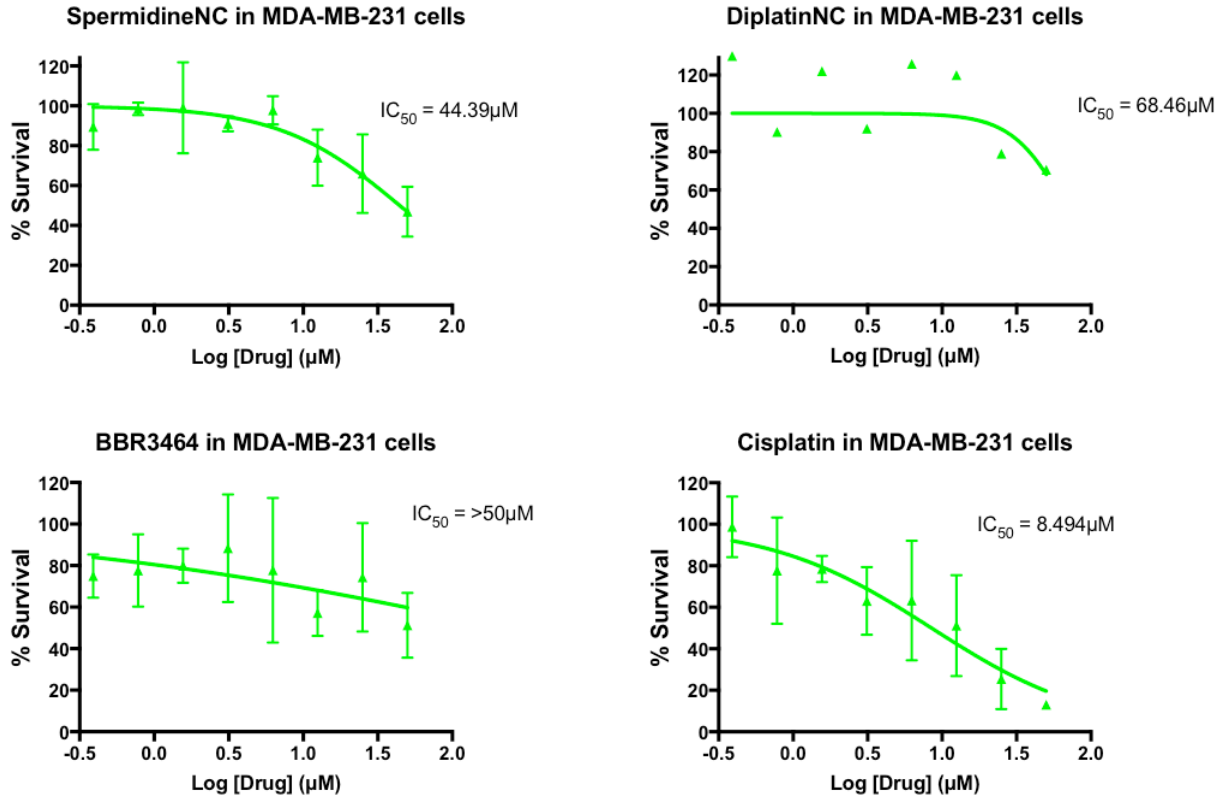

Appendix IV Figure 1 Cytotoxicity of PPCs in MDA-MB-231-luc cells after 72h drug treatment. IC_{50} values ± SD of at least 2 independent experiments (each with 4 replicates) were calculated in GraphPad Prism 7.

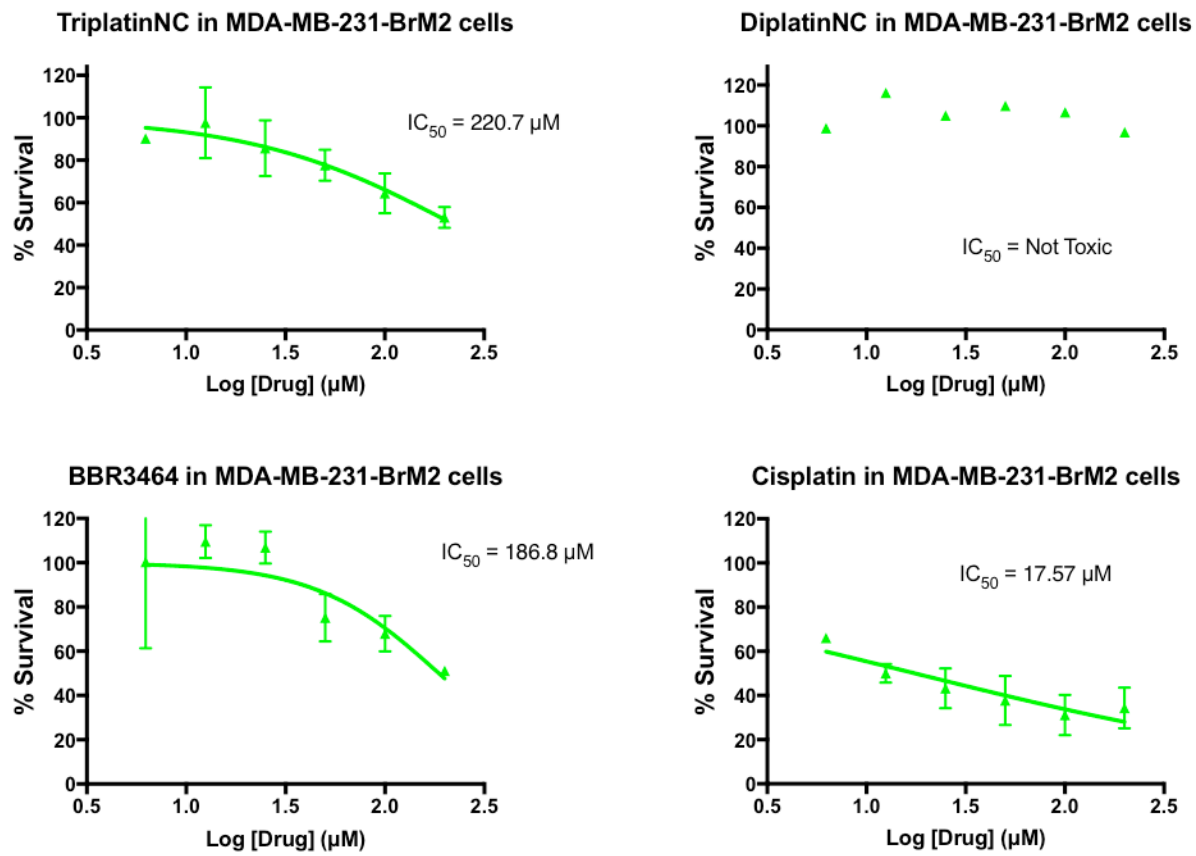

Appendix IV Figure 2. Plots of Table 5.1. Cytotoxicity of PPCs in MDA-MB-231-BrM2-luc cells after 24h drug treatment. IC_{50} values ± SD of at least 2 independent experiments (each with 4 replicates) were calculated in GraphPad Prism 7.

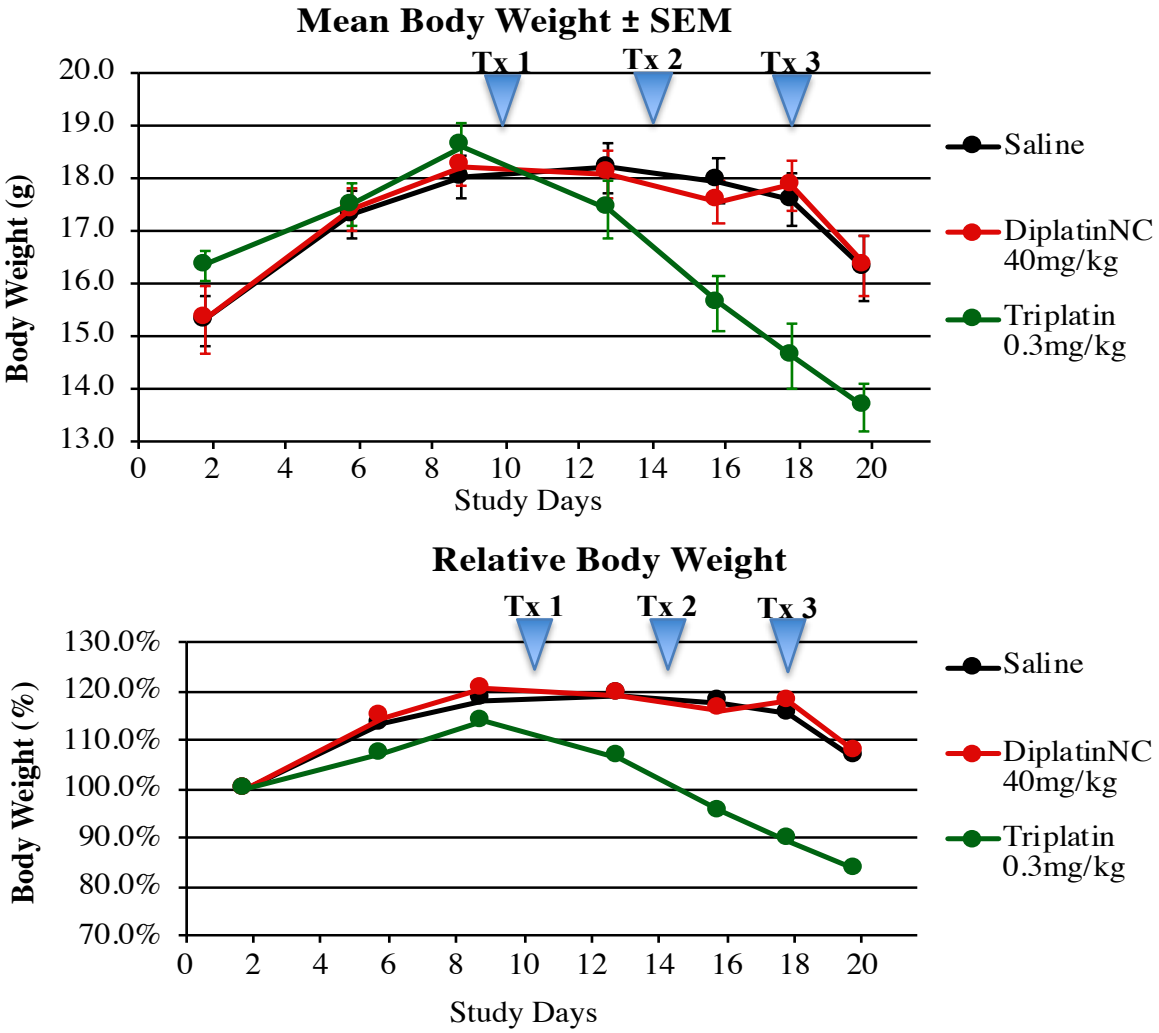

Appendix IV Figure 2. Body weight was measured throughout *in vivo* experiment 1. Each group had 10 mice.

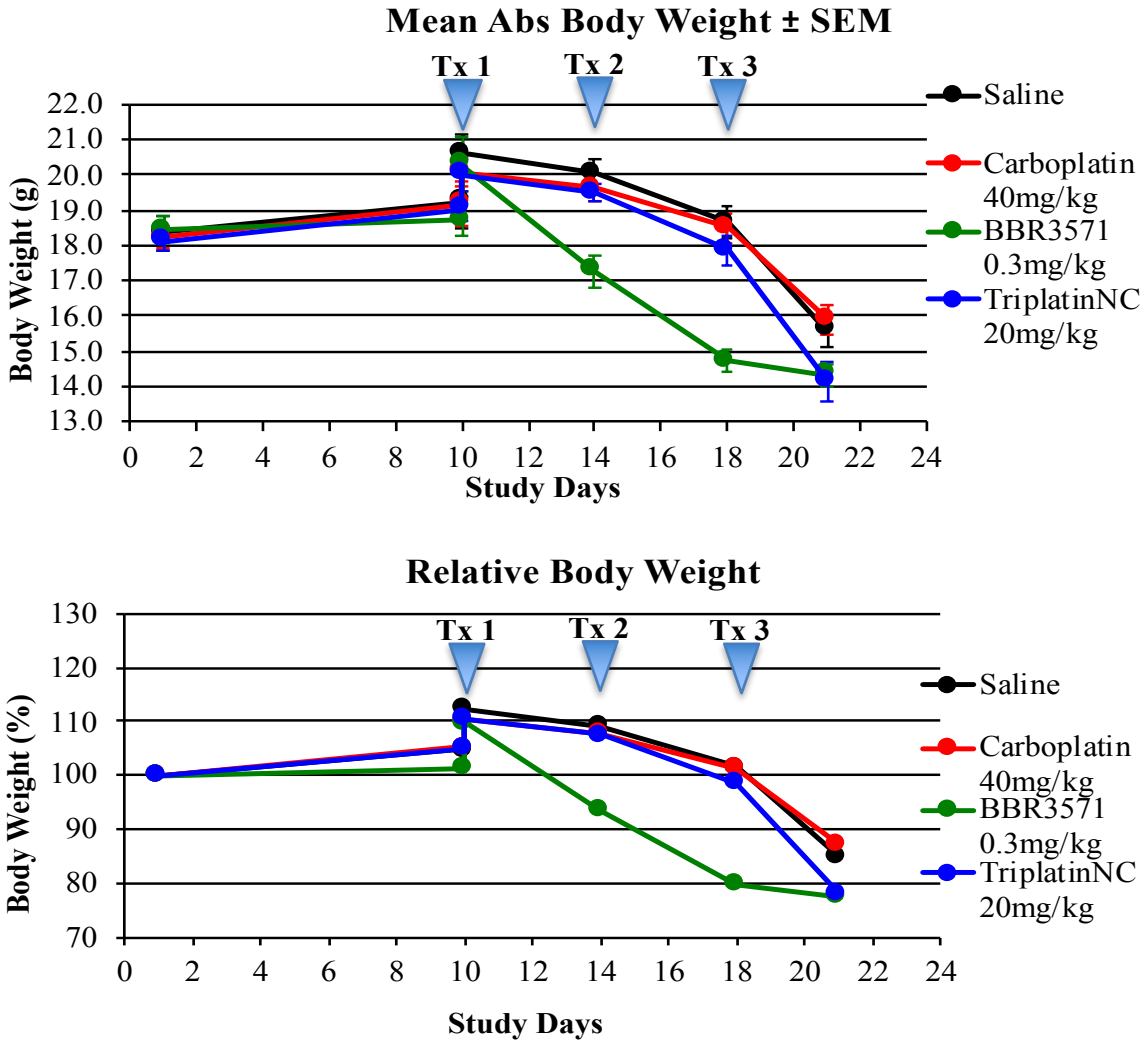

Appendix IV Figure 3. Body weight was measured throughout *in vivo* experiment 4. Each group had 10 mice.

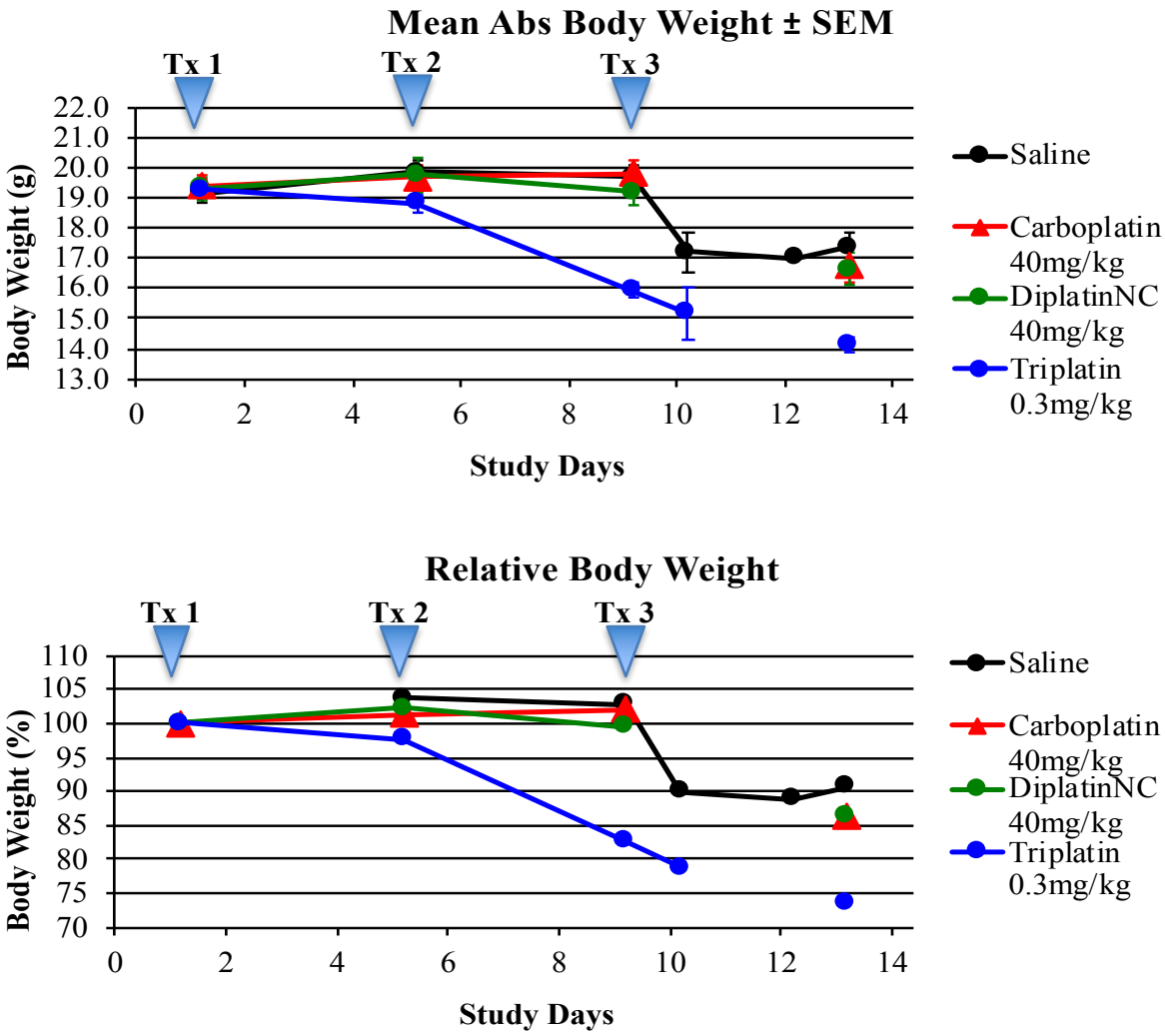

Appendix IV Figure 4. Body weight was measured throughout *in vivo* experiment 5. Each group had 11 mice.

Appendix V – Chapter 6

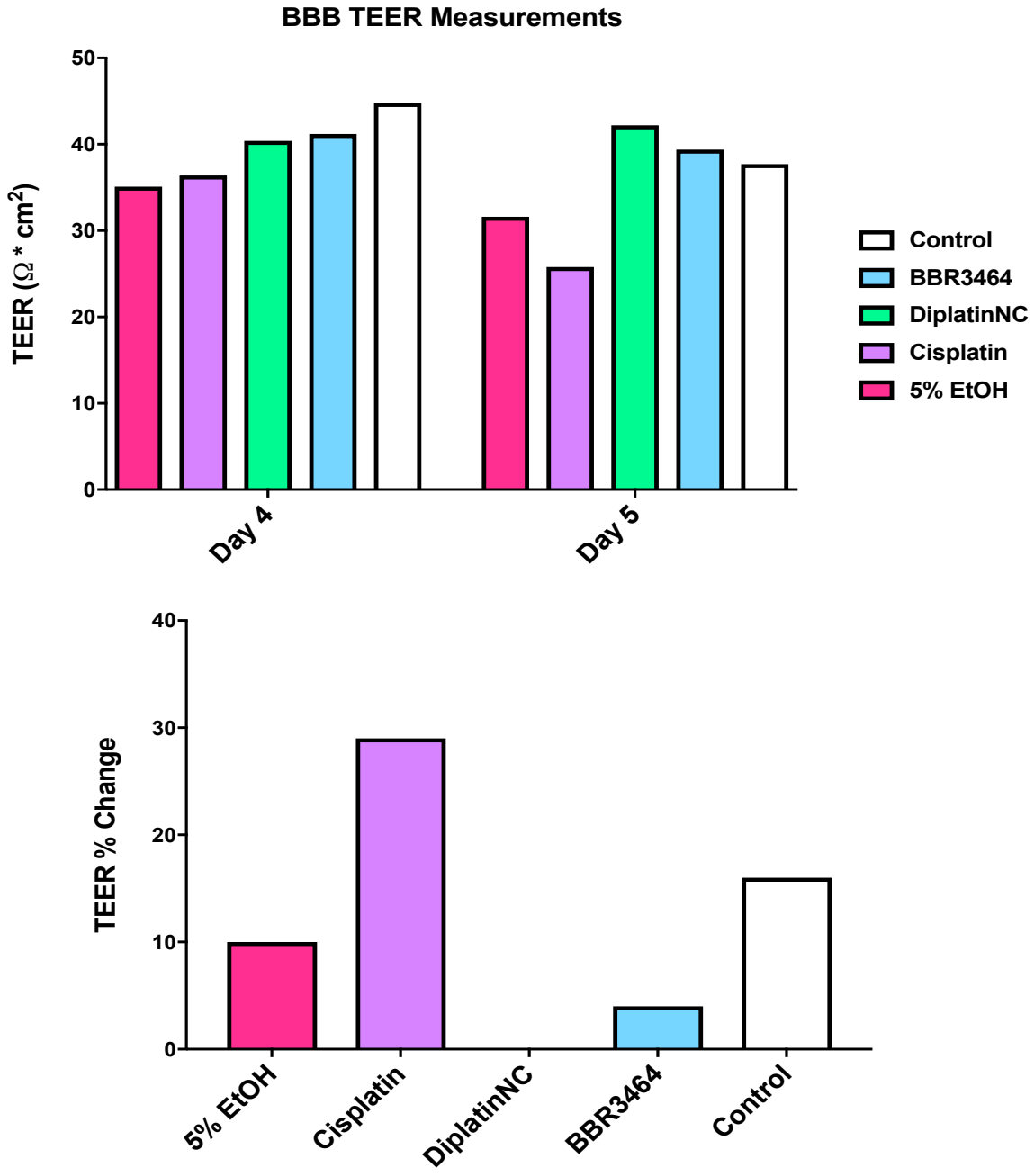

Appendix V Figure 1. PPCs and cisplatin (50 µM) effects on BBB integrity with TEER (top) and the % change in TEER from day 4 to day 5. Data generated was a co-effort with myself and Megan Sayyad from Dr. Koblinski's lab.

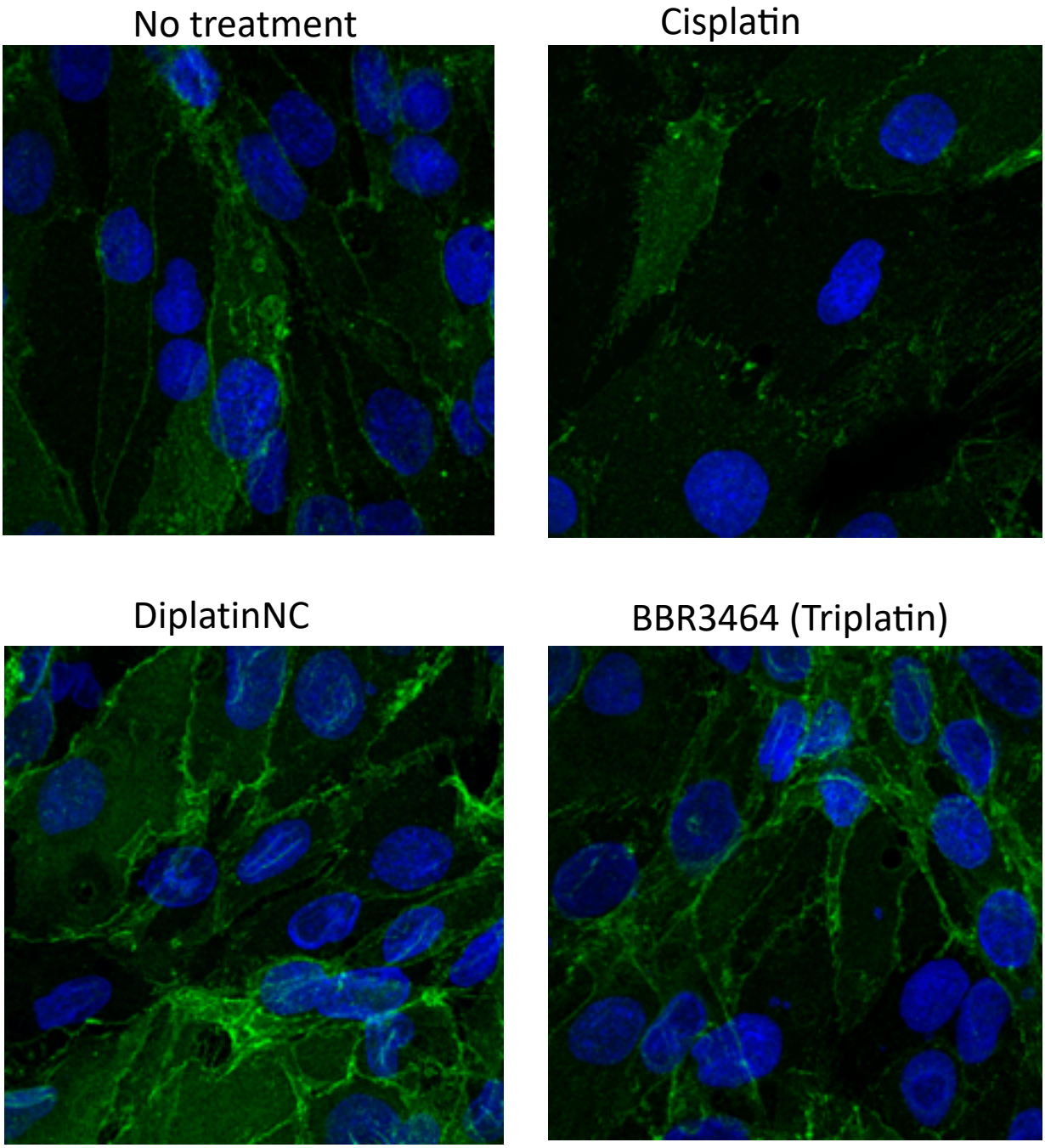

Appendix V Figure 2. PPCs and cisplatin (50 μM) effects on BBB integrity with Claudin-5 staining (green) and DAPI (blue). Data generated was a co-effort with myself and Megan Sayyad from Dr. Koblinski's lab. Images are representative of 3 independent experiments (each with 2 replicates).

References

1. Siegel, R. L., Miller, K. D. & Jemal, A. Cancer statistics. *CA Cancer J Clin* **66,** 7–30 (2016).
2. Ludwig, J. A. & Weinstein, J. N. Biomarkers in cancer staging, prognosis and treatment selection. *Nat. Rev. Cancer* **5,** 845–856 (2005).
3. Clarke, R., Tyson, J. J. & Dixon, J. M. Endocrine resistance in breast cancer--An overview and update. *Mol. Cell. Endocrinol.* **418 Pt 3,** 220–34 (2015).
4. Martelotto, L. G., Ng, C. K., Piscuoglio, S., Weigelt, B. & Reis-Filho, J. S. Breast cancer intra-tumor heterogeneity. *Breast Cancer Res.* **16,** R48 (2014).
5. Lehmann, B. D. & Pietenpol, J. A. Clinical implications of molecular heterogeneity in triple negative breast cancer. *Breast* **24 Suppl 2,** S36-40 (2015).
6. Babayan, A. *et al.* Heterogeneity of Estrogen Receptor Expression in Circulating Tumor Cells from Metastatic Breast Cancer Patients. *PLoS One* **8,** 1–11 (2013).
7. Zeichner, S. B. *et al.* Defining the Survival Benchmark for Breast Cancer Patients with Systemic Relapse. *Breast Cancer Basic Clin. Res.* **9,** 9–17 (2015).
8. Atchley, D. P. *et al.* Clinical and pathologic characteristics of patients with BRCA-positive and BRCA-negative breast cancer. *J. Clin. Oncol.* **26,** 4282–4288 (2008).
9. Gucalp, A. *et al.* Phase II Trial of Bicalutamide in Patients with Androgen Receptor–Positive, Estrogen Receptor–Negative Metastatic Breast Cancer. *Clin. Cancer Res.* **19,** 5505–5512 (2013).
10. Linderholm, B. K. *et al.* Significantly higher levels of vascular endothelial growth factor (VEGF) and shorter survival times for patients with primary operable triple-negative breast cancer. *Ann. Oncol.* **20,** 1639–1646 (2009).
11. Sorlie, T. *et al.* Repeated observation of breast tumor subtypes in independent gene expression data sets. *Proc. Natl. Acad. Sci.* **100,** 8418–8423 (2003).
12. Sikov, W. M. *et al.* Impact of the addition of carboplatin and/or bevacizumab to neoadjuvant once-per-week paclitaxel followed by dose-dense doxorubicin and cyclophosphamide on pathologic

complete response rates in stage II to III triple-negative breast cancer: CALGB 40603 (A. *J. Clin. Oncol.* **33,** 13–21 (2015).

13. Carey, L. A. *et al.* TBCRC 001: Randomized phase II study of cetuximab in combination with carboplatin in stage IV triple-negative breast cancer. *J. Clin. Oncol.* **30,** 2615–2623 (2012).
14. Galluzzi, L. *et al.* Molecular mechanisms of cisplatin resistance. *Oncogene* **31,** 1869–1883 (2012).
15. Eckstein, N. Platinum resistance in breast and ovarian cancer cell lines. *J. Exp. Clin. Cancer Res.* **30,** 91 (2011).
16. Perego, P. *et al.* A novel trinuclear platinum complex overcomes cisplatin resistance in an osteosarcoma cell system. *Mol. Pharmacol.* **55,** 528–534 (1999).
17. Pratesi, G. *et al.* A novel charged trinuclear platinum complex effective against cisplatin-resistant tumours: hypersensitivity of p53-mutant human tumour xenografts. *Br. J. Cancer* **80,** 1912–9 (1999).
18. Manzotti, C. *et al.* BBR 3464: A novel triplatinum complex, exhibiting a preclinical profile of antitumor efficacy different from cisplatin. *Clin. Cancer Res.* **6,** 2626–2634 (2000).
19. Gourley, C. *et al.* A phase I study of the trinuclear platinum compound, BBR 3464, in combination with protracted venous infusional 5-fluorouracil in patients with advanced cancer. *Cancer Chemother. Pharmacol.* **53,** 95–101 (2004).
20. Oehlsen, M. E., Qu, Y. & Farrell, N. Reaction of polynuclear platinum antitumor compounds with reduced glutathione studied by multinuclear (1H, 1H,- 15N gradient heteronuclear single-quantum coherence, and 195Pt) NMR spectroscopy. *Inorg. Chem.* **42,** 5498–5506 (2003).
21. Harris, A. L. *et al.* Synthesis, characterization, and cytotoxicity of a novel highly charged trinuclear platinum compound. Enhancement of cellular uptake with charge. *Inorg. Chem.* **44,** 9598–9600 (2005).
22. Harris, A. L., Ryan, J. J. & Farrell, N. Biological Consequences of Trinuclear Platinum Complexes:Comparison of [{trans-PtCl(NH3)2}2 -(trans-Pt(NH3)2(H2N(CH2)6- NH2)2)]4+ (BBR3464) with Its Noncovalent Congeners. *Mol. Pharmacol.* **69,** 666–672 (2006).

23. Komeda, S. *et al.* A third mode of DNA binding: Phosphate clamps by a polynuclear platinum complex. *J. Am. Chem. Soc.* **128,** 16092–16103 (2006).

24. Komeda, S. *et al.* The phosphate clamp: A small and independent motif for nucleic acid backbone recognition. *Nucleic Acids Res.* **39,** 325–336 (2011).

25. Calnan, B. J., Biancalana, S., Hudson, D. & Frankel, A. D. Analysis of arginine-rich peptides from the HIV Tat protein reveals unusual features of RNA-protein recognition. *Genes Dev.* **5,** 201–210 (1991).

26. Fuchs, S. M. & Raines, R. T. Internalization of cationic peptides: The road less (or more?) traveled. *Cell. Mol. Life Sci.* **63,** 1819–1822 (2006).

27. Fuchs, S. M. & Raines, R. T. Pathway for Polyarginine Entry into Mammalian Cells. *Biochemistry* **43,** 2438–2444 (2004).

28. Chiodelli, P., Bugatti, A., Urbinati, C. & Rusnati, M. Heparin/heparan sulfate proteoglycans glycomic interactome in angiogenesis: Biological implications and therapeutical use. *Molecules* **20,** 6342–6388 (2015).

29. Silva, H. *et al.* Heparan sulfate proteoglycan-mediated entry pathway for charged tri-platinum compounds. Differential cellular accumulation mechanisms for platinum. *Mol. Pharmacol.* **9,** 1795–1802 (2012).

30. Peterson, E. J. *et al.* Antiangiogenic platinum through glycan targeting. *Chem. Sci.* **8,** 241–252 (2017).

31. Farrell, N. P. Multi-platinum anti-cancer agents. Substitution-inert compounds for tumor selectivity and new targets. *Chem. Soc. Rev.* **44,** 8773–8785 (2015).

32. Mangrum, J. B. *et al.* A new approach to glycan targeting: enzyme inhibition by oligosaccharide metalloshielding. *Chem. Commun. (Camb).* **50,** 4056–8 (2014).

33. Peterson, E. J. *et al.* Nucleolar targeting by platinum: P53-independent apoptosis follows rRNA inhibition, cell-cycle arrest, and DNA compaction. *Mol. Pharm.* **12,** 287–297 (2015).

34. Xu, D. & Esko, J. D. Demystifying heparan sulfate-protein interactions. *Annu. Rev. Biochem.* **83,**

129–57 (2014).

35. Zhou, W.-Y., Zheng, H., Du, X. & Yang, J. Characterization of FGFR signaling pathway as therapeutic targets for sarcoma patients. *Cancer Biol. Med.* **13,** 260–8 (2016).

36. Jia, L. & Ma, S. Recent advances in the discovery of heparanase inhibitors as anti-cancer agents. *Eur. J. Med. Chem.* **121,** 209–220 (2016).

37. Baraz, L., Haupt, Y., Elkin, M., Peretz, T. & Vlodavsky, I. Tumor suppressor p53 regulates heparanase gene expression. *Oncogene* **25,** 3939–3947 (2006).

38. Maxhimer, J. B. *et al.* Heparanase-1 expression is associated with the metastatic potential of breast cancer. *Surgery* **132,** 326–333 (2002).

39. Heyman, B. & Yang, Y. Mechanisms of heparanase inhibitors in cancer therapy. *Exp. Hematol.* **44,** 1002–1012 (2016).

40. Vlodavsky, I. *et al.* Mammalian heparanase: gene cloning, expression and function in tumor progression and metastasis. *Nat. Med.* **5,** 793–802 (1999).

41. Pisano, C., Vlodavsky, I., Ilan, N. & Zunino, F. The potential of heparanase as a therapeutic target in cancer. *Biochem. Pharmacol.* **89,** 12–19 (2014).

42. Wedlock, L. E. *et al.* NanoSIMS multi-element imaging reveals internalisation and nucleolar targeting for a highly-charged polynuclear platinum compound. *Chem Commun* **49,** 6944–6946 (2013).

43. Hammond, E., Khurana, A., Shridhar, V. & Dredge, K. The Role of Heparanase and Sulfatases in the Modification of Heparan Sulfate Proteoglycans within the Tumor Microenvironment and Opportunities for Novel Cancer Therapeutics. *Front. Oncol.* **4,** 195 (2014).

44. Gorle, A. K. *et al.* Substitution-Inert Polynuclear Platinum Complexes as Metalloshielding Agents for Heparan Sulfate. *Chem. Eur. J* (2018). doi:10.1002/chem.201706030

45. Katner, S. J., Johnson, W. E., Peterson, E. J., Page, P. & Farrell, N. P. Comparison of Metal–Ammine Compounds Binding to DNA and Heparin. Glycans as Ligands in Bioinorganic Chemistry. *Inorg. Chem.* acs.inorgchem.7b03043 (2018). doi:10.1021/acs.inorgchem.7b03043

46. Katsuta, E., Peterson, E. J., Katner, S. J., Farrell, N. P. & Takabe, K. Triplatin preferably suppress lung metastasis of breast cancer, and peritoneal carcinomatosis of colon and pancreatic cancer. *Proc. AACR Washingt. D.C.* Abstract #5117 (2017).

47. Katner, S. J. *et al.* Heparan sulfate , a new target for platinum in metastatic TNBC. *Proc. AACR Chicago,* Abstract #3941 (2018).

48. Katner, S. J. *et al.* Anti-metastatic platinum through glycan targeting in breast cancer. *Proc. AACR Washingt. D.C.* Abstract #17 (2017).

49. Brabec, V. *et al.* DNA modifications by a novel bifunctional trinuclear platinum Phase I anticancer agent. *Biochemistry* **38,** 6781–6790 (1999).

50. Zehnulova, J., Kasparkova, J., Farrell, N. & Brabec, V. Conformation, Recognition by High Mobility Group Domain Proteins, and Nucleotide Excision Repair of DNA Intrastrand Cross-links of Novel Antitumor Trinuclear Platinum Complex BBR3464. *J. Biol. Chem.* **276,** 22191–22199 (2001).

51. Kasparkova, J., Zehnulova, J., Farrell, N. & Brabec, V. DNA interstrand cross-links of the novel antitumor trinuclear platinum complex BBR3464. Conformation, recognition by high mobility group domain proteins, and nucleotide excision repair. *J. Biol. Chem.* **277,** 48076–48086 (2002).

52. Fuster, M. M. & Esko, J. D. The sweet and sour of cancer: Glycans as novel therapeutic targets. *Nat. Rev. Cancer* **5,** 526–542 (2005).

53. Lidholt, K. *et al.* A Single Mutation Affects Both N-Acetylglucosaminyltransferase and Glucuronosyltransferase Activities in a Chinese Hamster Ovary Cell Mutant Defective in Heparan Sulfate Biosynthesis. *Proc. Natl. Acad. Sci.* **89,** 2267–2271 (1992).

54. Esko, J. D., Stewart, T. E. & Taylor, W. H. Animal cell mutants defective in glycosaminoglycan biosynthesis. *Proc. Natl. Acad. Sci. U. S. A.* **82,** 3197–3201 (1985).

55. Burger, H. *et al.* Drug transporters of platinum-based anticancer agents and their clinical significance. *Drug Resist. Updat.* **14,** 22–34 (2011).

56. Hall, M. D., Okabe, M., Shen, D.-W., Liang, X.-J. & Gottesman, M. M. The Role of Cellular

Accumulation in Determining Sensitivity to Platinum-Based Chemotherapy. *Annu. Rev. Pharmacol. Toxicol.* **48,** 495–535 (2008).

57. Howell, S. B., Safaei, R., Larson, C. A. & Sailor, M. J. Copper transporters and the cellular pharmacology of the platinum-containing cancer drugs. *Mol. Pharmacol.* **77,** 887–894 (2010).

58. Kabolizadeh, P., Ryan, J. & Farrell, N. Differences in the cellular response and signaling pathways of cisplatin and BBR3464 ([{trans-PtCl(NH3)2}2??-(trans-Pt(NH3)2(H2N(CH2)6-NH2)2)]4+) influenced by copper homeostasis. *Biochem. Pharmacol.* **73,** 1270–1279 (2007).

59. Capila, I. & Linhardt, R. J. Heparin - Protein Interactions. *Angew. Chemie - Int. Ed.* **41,** 390–412 (2015).

60. Prisecaru, A. *et al.* The phosphate clamp: Sequence selective nucleic acid binding profiles and conformational induction of endonuclease inhibition by cationic Triplatin complexes. *Nucleic Acids Res.* **42,** 13474–13487 (2014).

61. Qu, Y., Kipping, R. G. & Farrell, N. P. Solution studies on DNA interactions of substitution-inert platinum complexes mediated via the phosphate clamp. *Dalt. Trans.* **44,** 3563–3572 (2015).

62. Carte, N. *et al.* Determination by electrospray mass spectrometry of the outersphere association constants of DNA/platinum complexes using 20-mer oligonucleotides and ([Pt(NH3)4]2+, 2C-) or ([Pt(py)4]2+, 2Cl-). *Anal. Biochem.* **284,** 77–86 (2000).

63. Malina, J., Farrell, N. P. & Brabec, V. Substitution-inert trinuclear platinum complexes efficiently condense/aggregate nucleic acids and inhibit enzymatic activity**. *Angew. Chemie - Int. Ed.* **53,** 12812–12816 (2014).

64. Varki, A. *et al. Essentials of Glycobiology.* (Cold Spring Harbor Laboratory Press, 2009).

65. Cummings, R. D. & Pierce, J. M. The Challenge and Promise of Glycomics. *Chem. & Biol.* **21,** 1–15 (2014).

66. Humphries, D. E. *et al.* Heparin is essential for the storage of specific granule proteases in mast cells. *Nature* **400,** 769–772 (1999).

67. Meneghetti, M. C. Z. *et al.* Heparan sulfate and heparin interactions with proteins. *J. R. Soc.*

Interface **12,** 20150589 (2015).

68. Hudak, J. E. & Bertozzi, C. R. Glycotherapy: New advances inspire a reemergence of glycans in medicine. *Chem. Biol.* **21,** 16–37 (2014).

69. Zhang, F., Liang, X., Beaudet, J. M., Lee, Y. & Linhardt, R. J. The effects of metal ions on heparin / heparin sulfate-protein interactions. OBJ OBJ OBJ OBJ OBJ OBJ *J Biom Tech Res* **1,** 6000101 (2014).

70. Seo, Y., Schenauer, M. R. & Leary, J. A. Biologically Relevant Metal-Cation Binding Induces Conformational Changes in Heparin Oligosaccharides as Measured by Ion Mobility Mass Spectrometry. *Int J Mass Spectrom.* **303,** 191–198 (2011).

71. Stevic, I., Parmar, N., Paredes, N., Berry, L. R. & Chan, A. K. C. Binding of Heparin to Metals. *Cell Biochem. Biophys.* **59,** 171–178 (2011).

72. Chenghua, S. *et al.* Crystallographic Analysis of Calcium-dependent Heparin Binding to Annexin A2*. *J. Biol. Chem.* **281,** 31689–31695 (2006).

73. Xie, H. & Kang, Y. J. Role of copper in angiogenesis and its medicinal implications. *Curr. Med. Chem.* **16,** 1304–1314 (2009).

74. D'Andrea, L. D., Romanelli, A., Di Stasi, R. & Pedone, C. Bioinorganic aspects of angiogenesis. *Dalt. Trans.* **39,** 7625 (2010).

75. Rudd, T. R. *et al.* Site-specific interactions of copper(II) ions with heparin revealed with complementary (SRCD, NMR, FTIR and EPR) spectroscopic techniques. *Carbohydr. Res.* **343,** 2184–2193 (2008).

76. Hung, K.-W. *et al.* Solution Structure of the Ligand Binding Domain of the Fibroblast Growth Factor Receptor: Role of Heparin in the Activation of the Receptor † , ‡. *Biochemistry* **44,** 15787–15798 (2005).

77. Waller, L. N., Fox, N., Fox, K. F., Fox, A. & Price, R. L. Ruthenium red staining for ultrastructural visualization of a glycoprotein layer surrounding the spore of Bacillus anthracis and Bacillus subtilis. *J. Microbiol. Methods* **58,** 23–30 (2004).

78. Rozenberg, G. I. *et al.* Heparan sulfate, heparin, and heparinase activity detection on polyacrylamide gel electrophoresis using the fluorochrome tris (2, 2'-bipyridine) ruthenium (II). *Electrophoresis* **22,** 3–11 (2001).

79. Cheng, T.-T. *et al.* A new fluorescence 'switch on' assay for heparin detection by using a functional ruthenium polypyridyl complex. *Analyst* **138,** 3483 (2013).

80. Du, X. *et al.* Insights into Protein-Ligand Interactions: Mechanisms, Models, and Methods. *Int. J. Mol. Sci.* **17,** 144 (2016).

81. Schasfoort, R. B. & Tudos, A. J. Introduction to Surface Plasmon Resonance. in *Handbook of Surface Plasmon Resonance* 1–14 (2008).

82. Gaus, K. & Hall, E. A. H. Surface Modification Method for Adhesion of Gels. *J. Colloid Inerface Sci.* **194,** 373–378 (1997).

83. Osmond, R. I. W., Kett, W. C., Skett, S. E. & Coombe, D. R. Protein-heparin interactions measured by BIAcore 2000 are affected by the method of heparin immobilization. *Anal. Biochem.* **310,** 199–207 (2002).

84. Cochran, S., Li, C. P. & Ferro, V. A surface plasmon resonance-based solution affinity assay for heparan sulfate-binding proteins. *Glycoconj. J.* **26,** 577–587 (2009).

85. Powell, A. K., Yates, E. A., Fernig, D. G. & Turnbull, J. E. Interactions of heparin/heparan sulfate with proteins: Appraisal of structural factors and experimental approaches. *Glycobiology* **14,** (2004).

86. Biver, T. Stabilisation of non-canonical structures of nucleic acids by metal ions and small molecules. *Coord. Chem. Rev.* **257,** 2765–2783 (2013).

87. Bharanidharan, D., Thiyagarajan, S. & Gautham, N. Hexammineruthenium(III) ion interactions with Z-DNA. *Acta Crystallogr. Sect. F Struct. Biol. Cryst. Commun.* **63,** 1008–1013 (2007).

88. Matulis, D., Rouzina, I. & Bloomfield, V. A. Thermodynamics of DNA binding and condensation: isothermal titration calorimetry and electrostatic mechanism. *J. Mol. Biol.* **296,** 1053–1063 (2000).

89. Deng, H. & Bloomfield, V. A. Structural effects of cobalt-amine compounds on DNA

condensation. *Biophys. J.* **77,** 1556–1561 (1999).

90. Kankia, B. I., Buckin, V. & Bloomfield, V. A. Hexamminecobalt(III)-induced condensation of calf thymus DNA: circular dichroism and hydration measurements. *Nucleic Acids Res.* **29,** 2795–2801 (2001).

91. Suda, Y. *et al.* Immobilization and clustering of structurally defined oligosaccharides for sugar chips: An improved method for surface plasmon resonance analysis of protein-carbohydrate interactions. *Bioconjug. Chem.* **17,** 1125–1135 (2006).

92. Ruhaak, L. R. *et al.* Glycan labeling strategies and their use in identification and quantification. *Anal. Bioanal. Chem.* **397,** 3457–3481 (2010).

93. Baba, F. *et al.* Syndecan-1 and syndecan-4 are overexpressed in an estrogen receptor-negative, highly proliferative breast carcinoma subtype. *Breast Cancer Res. Treat.* **98,** 91–98 (2006).

94. Ferrara, N. & Kerbel, R. S. Angiogenesis as a therapeutic target. *Nature* **438,** 967–974 (2005).

95. Robinson, C. J., Mulloy, B., Gallagher, J. T. & Stringer, S. E. VEGF165-binding sites within heparan sulfate encompass two highly sulfated domains and can be liberated by K5 lyase. *J. Biol. Chem.* **281,** 1731–1740 (2006).

96. Spivak-Kroizman, T. *et al.* Heparin-induced oligomerization of FGF molecules is responsible for FGF receptor dimerization, activation, and cell proliferation. *Cell* **79,** 1015–1024 (1994).

97. Van Wijk, X. M. *et al.* Interfering with UDP-GlcNAc metabolism and heparan sulfate expression using a sugar analogue reduces angiogenesis. *ACS Chem. Biol.* **8,** 2331–2338 (2013).

98. Limaverde-Sousa, G., Sternberg, C. & Ferreira, C. G. Antiangiogenesis beyond VEGF inhibition: A journey from antiangiogenic single-target to broad-spectrum agents. *Cancer Treat. Rev.* **40,** 548–557 (2014).

99. Koch, S. & Claesson-Welsh, L. Signal transduction by vascular endothelial growth factor receptors. *Cold Spring Harb. Perspect. Med.* **2,** 1–21 (2012).

100. Ferrara, N. Role of vascular endothelial growth factor in regulation of physiological angiogenesis. *Am. J. Physiol. Cell Physiol.* **280,** C1358-1366 (2001).

101. Liang, C. C., Park, A. Y. & Guan, J. L. In vitro scratch assay: A convenient and inexpensive method for analysis of cell migration in vitro. *Nat. Protoc.* **2,** 329–333 (2007).

102. Huang, S.-W., Lien, J.-C., Kuo, S.-C. & Huang, T.-F. Antiangiogenic mechanisms of PJ-8, a novel inhibitor of vascular endothelial growth factor receptor signaling. *Carcinogenesis* **33,** 1022–30 (2012).

103. Arnaoutova, I. & Kleinman, H. K. In vitro angiogenesis: Endothelial cell tube formation on gelled basement membrane extract. *Nat. Protoc.* **5,** 628–635 (2010).

104. Kleinman, H. K. & Martin, G. R. Matrigel: Basement membrane matrix with biological activity. *Semin. Cancer Biol.* **15,** 378–386 (2005).

105. Reiland, J. *et al.* Heparanase degrades syndecan-1 and perlecan heparan sulfate: Functional implications for tumor cell invasion. *J. Biol. Chem.* **279,** 8047–8055 (2004).

106. Zhang, L., Ngo, J. A., Wetzel, M. D. & Marchetti, D. Heparanase mediates a novel mechanism in lapatinib-resistant brain metastatic breast cancer. *Neoplasia* **17,** 101–113 (2015).

107. Zhang, L., Sullivan, P., Suyama, J. & Marchetti, D. Epidermal Growth Factor-Induced Heparanase Nucleolar Localization Augments DNA Topoisomerase I Activity in Brain Metastatic Breast Cancer. *Mol. Cancer Res.* **8,** 278–290 (2010).

108. Mani, K. *et al.* The heparan sulfate-specific epitope 10E4 is NO-sensitive and partly inaccessible in glypican-1. *Glycobiology* **14,** 599–607 (2004).

109. Mani, K., Belting, M. & Ellervik, U. Tumor attenuation by 2 (6-hydroxynaphthyl) - b - D - xylopyranoside requires priming of heparan sulfate and nuclear targeting of the products. *Glycobiology* **14,** 387–397 (2004).

110. Jones, A. L., Hulett, M. D. & Parish, C. R. Histidine-rich glycoprotein binds to cell-surface heparan sulfate via its N-terminal domain following Zn2+ chelation. *J. Biol. Chem.* **279,** 30114–30122 (2004).

111. Rautela, J. *et al.* Loss of Host Type-I IFN Signaling Accelerates Metastasis and Impairs NK-cell Antitumor Function in Multiple Models of Breast Cancer. *Cancer Immunol. Res.* **3,** 1207–1217

(2015).

112. Leone, J. P. & Leone, B. A. Breast cancer brain metastases : the last frontier. *Exp. Hematol. Oncol.* **4,** 1–10 (2015).

113. Dent, R. *et al.* Pattern of metastatic spread in triple-negative breast cancer. *Breast Cancer Res. Treat.* **115,** 423–428 (2009).

114. Lin, N. U. *et al.* Sites of Distant Recurrence and Clinical Outcomes in Patients With Metastatic Triple-negative Breast Cancer. *Cancer* **113,** 2638–2645 (2008).

115. Tseng, L. M. *et al.* Distant metastasis in triple-negative breast cancer. *Neoplasia* **60,** 290–294 (2013).

116. Tarhan, M. O. *et al.* The clinicopathological evaluation of the breast cancer patients with brain metastases : predictors of survival. *Clin Exp Metastasis* **30,** 201–213 (2013).

117. Iorns, E. *et al.* A New Mouse Model for the Study of Human Breast Cancer Metastasis. *PLoS One* **7,** (2012).

118. Lambert, A. W., Pattabiraman, D. R. & Weinberg, R. A. EMERGING BIOLOGICAL PRINCIPLES OF METASTASIS. *Cell* **168,** 670–691 (2017).

119. Rehemtulla, A. *et al.* Rapid and quantitative assessment of cancer treatment response using in vivo bioluminescence imaging. *Neoplasia* **2,** 491–495 (2000).

120. Negrin, R. S. & Contag, C. H. In vivo imaging using bioluminescence: A tool for probing graft-versus-host disease. *Nat. Rev. Immunol.* **6,** 484–490 (2006).

121. Billecke, C. *et al.* Polynuclear platinum anticancer drugs are more potent than cisplatin and induce cell cycle arrest in glioma. *Neuro Oncol* **8,** 215–226 (2006).

122. Riccardi, A. *et al.* In vitro and in vivo antitumor activity of the novel trinuclear platinum complex BBR 3464 in neuroblastoma. *Cancer Chemother. Pharmacol.* **47,** 498–504 (2001).

123. Nagahashi, M. *et al.* Sphingosine-1-phosphate produced by sphingosine kinase 1 promotes breast cancer progression by stimulating angiogenesis and lymphangiogenesis. *Cancer Res.* **72,** 726–735 (2012).

124. Rashid, O. M. *et al.* An Improved Syngeneic Orthotopic Murine Model of Human Breast Cancer Progression. *Breast Cancer Res. Treat.* **147,** 501–512 (2014).

125. Rashid, O. M. *et al.* Resection of the Primary Tumor Improves Survival in Metastatic Breast Cancer by Reduction of Overall Tumor Burden Conclusions—Decreasing overall tumor burden through resection of the primary breast tumor decreased MDSCs, increased CD4 and CD8 cells, and i. *Surgery* **153,** 771–778 (2013).

126. Shultz, L. D. *et al.* Human Lymphoid and Myeloid Cell Development in NOD/LtSz-scid IL2Rynull Mice Engrafted with Mobilized Human Hemopoietic Stem Cells. *J. Immunol.* 6477–6489 (2005).

127. Shultz, L. D. *et al.* Multiple defects in innate and adaptive immunologic function in NOD / LtSz-scid mice. *J. Immunol.* 180–191 (1995). doi:10.4049/jimmunol.179.1.89

128. Sellers, R. S., Clifford, C. B., Treuting, P. M. & Brayton, C. Immunological variation between inbred laboratory mouse strains: Points to consider in phenotyping genetically immunomodified mice. *Vet. Pathol.* **49,** 32–43 (2012).

129. Market, E. & Papavasiliou, F. N. V(D)J recombination and the evolution of the adaptive immune system. *PLoS Biol.* **1,** 24–27 (2003).

130. Cao, X. *et al.* Defective lymphoid development in mice lacking expression of the common cytokine receptor γ chain. *Immunity* **2,** 223–238 (1995).

131. Puchalapalli, M. *et al.* NSG mice provide a better spontaneous model of breast cancer metastasis than athymic (nude) mice. *PLoS One* **11,** 1–15 (2016).

132. Bos, P. D. *et al.* Genes that mediate breast cancer metastasis to the brain. *Nature* **459,** 1005–1009 (2009).

133. Blagosklonny, M. V. Cell cycle arrest is not senescence. *Aging (Albany. NY).* **3,** 94–101 (2011).

134. Cruz-Muñoz, W. & Kerbel, R. S. Preclinical approaches to study the biology and treatment of brain metastases. *Semin. Cancer Biol.* **21,** 123–130 (2011).

135. Adkins, C. E. *et al.* A novel preclinical method to quantitatively evaluate early-stage metastatic

events at the murine blood-brain barrier. *Cancer Prev. Res.* **8,** 68–76 (2015).

136. Miyagi, Y. *et al.* Intraperitoneal carboplatin infusion may be a pharmacologically more reasonable route than intravenous administration as a systemic chemotherapy. A comparative pharmacokinetic analysis of platinum using a new mathematical model after intraperitoneal vs. i. *Gynecol. Oncol.* **99,** 591–596 (2005).

137. Teefey, P. *et al.* Factors associated with improved toxicity and tolerability of intraperitoneal chemotherapy in advanced-stage epithelial ovarian cancers. *Am. J. Obstet. Gynecol.* **208,** 501.e1-501.e7 (2013).

138. Kim, S. W. *et al.* The feasibility of carboplatin-based intraperitoneal chemotherapy in ovarian cancer. *Eur. J. Obstet. Gynecol. Reprod. Biol.* **152,** 195–199 (2010).

139. Sessa, C. *et al.* Clinical and pharmacological phase I study with accelerated titration design of a daily times five schedule of BBR3464, a novel cationic triplatinum complex. *Ann. Oncol.* **11,** 977–983 (2000).

140. White, P., Liebhaber, S. A. & Cooke, N. E. 129X1/SvJ Mouse Strain Has a Novel Defect in Inflammatory Cell Recruitment. *J. Immunol.* **168,** 869–874 (2002).

141. Bos, P. D., Nguyen, D. X. & Massagué, J. Modeling metastasis in the mouse. *Curr. Opin. Pharmacol.* **10,** 571–577 (2010).

142. Ruffell, B. & Coussens, L. M. Cancer Cell Perspective Macrophages and Therapeutic Resistance in Cancer. *Cancer Cell* **27,** 1–11 (2015).

143. Bondavera, A. *et al.* The lysyl oxidase inhibitor, β-aminopropionitrile, diminishes the metastatic colonization potential of circulating breast cancer cells. *PLoS One* **4,** (2009).

144. Turner, T. *et al.* Characterizing the efficacy of cancer therapeutics in patient-derived xenograft models of metastatic breast cancer. *Breast Cancer Res. Treat.* (2018). doi:10.1007/s10549-018-4748-4

145. Watanabe, A. *et al.* Expression of syndecans, a heparan sulfate proteoglycan, in malignant gliomas: Participation of nuclear factor-κB in upregulation of syndecan-1 expression. *J.*

Neurooncol. **77,** 25–32 (2006).

146. Xu, Y., Yuan, J., Zhang, Z., Lin, L. & Xu, S. Syndecan-1 expression in human glioma is correlated with advanced tumor progression and poor prognosis. *Mol. Biol. Rep.* **39,** 8979–8985 (2012).

147. Saraf, A. *et al.* Breast cancer subtype and stage are prognostic of time from breast cancer diagnosis to brain metastasis development. *J. Neurooncol.* **0,** 0 (2017).

148. Srinivasan, B. *et al. TEER measurement techniques for in vitro barrier model systems*. **20,** (2015).

149. Atienzar, F. A., Gerets, H., Tilmant, K., Toussaint, G. & Dhalluin, S. Evaluation of impedance-based label-free technology as a tool for pharmacology and toxicology investigations. *Biosensors* **3,** 132–156 (2013).

150. Gumulec, J. *et al.* Cisplatin-resistant prostate cancer model: Differences in antioxidant system, apoptosis and cell cycle. *Int. J. Oncol.* **44,** 923–933 (2014).

151. Abbott, N. J., Rönnbäck, L. & Hansson, E. Astrocyte – endothelial interactions at the blood – brain barrier. *Nature* **7,** 41–53 (2006).

152. Li, G. *et al.* Permeability of Endothelial and Astrocyte Cocultures: In Vitro Blood–Brain Barrier Models for Drug Delivery Studies. *Ann Biomed Eng.* **38,** 2499–2511 (2010).

153. Winger, R. C., Koblinski, J. E., Kanda, T., Ransohoff, R. M. & Muller, W. A. Rapid Remodeling of Tight Junctions During Paracellular Diapedesis in a Human Model of the Blood-Brain Barrier. *J. Immunol.* **193,** 2427–2437 (2014).

154. McWhinney, S. R., Goldberg, R. M. & McLeod, H. L. Platinum Neurotoxicity Pharmacogenetics. *Mol Cancer Ther.* **8,** 10–16 (2009).

155. Fidler, I. J. The role of the organ microenvironment in brain metastasis. *Semin. Cancer Biol.* **21,** 107–112 (2011).

156. Knox, R. J., Friedlos, F., Lydall, D. A. & Roberts, J. J. Mechanism of Cytotoxicity of Anticancer Platinum Drugs : Evidence That cis-Diamminedichloroplatinum (II) and cis-Diammine-(1,1-cyclobutanedicarboxylato)platinum(II) Differ Only in the Kinetics of Their Interaction with DNA

Mechanism of Cytotoxicity of. *Cancer Res.* **46,** 1972–1979 (1986).

157. Barnham, K. J., Djuran, M. I., Murdoch, P. del S., Ranford, J. D. & Sadler, P. J. Ring-Opened Adducts of the Anticancer Drug Carboplatin with Sulfur Amino Acids. *Inorg. Chem.* **35,** 1065–1072 (1996).

158. Rixe, O. *et al.* Oxaliplatin, tetraplatin, cisplatin, and carboplatin: Spectrum of activity in drug-resistant cell lines and in the cell lines of the National Cancer Institute's Anticancer Drug Screen panel. *Biochem. Pharmacol.* **52,** 1855–1865 (1996).

159. Reardon, J. T., Vaisman, A., Chaney, S. G. & Sancar, A. Efficient Nucleotide Excision Repair of Cisplatin , Oxaliplatin , and Bis-aceto- ammine-dichloro-cyclohexylamine-platinum (IV) (JM216) Platinum Intrastrand DNA Diadducts. *Cancer Res.* **59,** 3968–3971 (1999).

160. Vaisman, A. *et al.* The role of hMLH1, hMSH3, and hMSH6 defects in cisplatin and oxaliplatin resistance: Correlation with replicative bypass of platinum-DNA adducts. *Cancer Res.* **58,** 3579–3585 (1998).

161. Chaney, S. G. *et al.* Protein interactions with platinum-DNA adducts: From structure to function. *J. Inorg. Biochem.* **98,** 1551–1559 (2004).

162. Hector, S., Bolanowska-Higdon, W., Zdanowicz, J., Hitt, S. & Pendyala, L. In vitro studies on the mechanisms of oxaliplatin resistance. *Cancer Chemother. Pharmacol.* **48,** 398–406 (2001).

163. Reedijk, J. Improved understanding in platinum antitumor chemistry. *J. Chem. Soc. Chem. Commun.* 801–806 (1996).

164. Braddock, P. D. *et al.* Structure and activity relationships of platinum complexes with anti-tumour activity. *Chem. Biol. Interact.* **11,** 145–161 (1975).

165. Eastman, A. The formation, isolation and characterization of DNA adducts produced by anticancer platinum complexes. *Pharmacol. Ther.* **34,** 155–166 (1987).

166. Marini, V. *et al.* Conformation, protein recognition and repair of DNA interstrand and intrastrand cross-links of antitumor trans-[PtCl2(NH3)(thiazole)]. *Nucleic Acids Res.* **33,** 5819–5828 (2005).

167. Farrell, N., Kelland, L. R., Roberts, J. D. & Vanbeusichem, M. Activation of the Transgeometry in

Platinum Antitumor Complexes - a Survey of the Cytotoxicity of Transcomplexes Containing Planar Ligands in Murine-L1210 and Human Tumor Panels and Studies on Their Mechanism of Action. *Cancer Res.* **52,** 5065–5072 (1992).

168. Fojo, T. *et al.* Identification of non-cross-resistant platinum compounds with novel cytotoxicity profiles using the NCI anticancer drug screen and clustered image map visualizations. *Crit. Rev. Oncol. Hematol.* **53,** 25–34 (2005).

169. Aris, S. M. & Farrell, N. P. Towards Antitumor Active trans-Platinum Compounds. *Eur. J. Inorg. Chem.* **10,** 1293–1302 (2009).

170. Benedetti, B. T., Quintal, S. & Farrell, N. P. Modulation of drug activation profiles through carboxylate ligand modification in cytotoxic trans-platinum planar amine compounds. *Dalt. Trans.* **40,** 10983–8 (2011).

171. Ma, E. S. F. *et al.* Enhancement of Aqueous Solubility and Stability Employing a Trans Acetate Axis in Trans Planar Amine Platinum Compounds while Maintaining the Biological Profile. *J. Med. Chem.* **48,** 5651–5654 (2005).

172. Quiroga, A. G., Perez, J. M., Alonso, C., Navarro-ranninger, C. & Farrell, N. Novel Transplatinum (II) Complexes with [N 2 O 2] Donor Sets. Cellular Pharmacology and Apoptosis Induction in Pam 212- ras Cells. *J. Med. Chem.* **49,** 224–231 (2006).

173. Bulluss, G. H. *et al.* trans-Platinum Planar Amine Compounds with [N 2 O 2] Ligand Donor Sets : Effects of Carboxylate Leaving Groups and Steric Hindrance on Chemical and Biological Properties. *Inorg. Chem. Commun.* **45,** 5733–5735 (2006).

174. Aris, S. M., Knott, K. M., Yang, X., Gewirtz, D. A. & Farrell, N. P. Modulation of transplanaramine platinum complex reactivity by systematic modification of carrier and leaving groups. *Inorganica Chim. Acta* **362,** 929–934 (2009).

175. Fujiwara, K., Armstrong, D., Morgan, M. & Markman, M. Principles and practice of intraperitoneal chemotherapy for ovarian cancer. *Int. J. Gynecol. Cancer* **17,** 1–20 (2007).

176. Grabner, S. *et al.* Cytotoxic trans-platinum(II) complex with 3-hydroxymethylpyridine: Synthesis,

X-ray structure and biological activity evaluation. *J. Inorg. Biochem.* **161,** 40–51 (2016).

177. Coluccia, M. *et al.* Platinum (II) complexes containing iminoethers : a trans platinum antitumour agent. *Chem. Biol. Interact.* **98,** 251–266 (1995).

178. Leng, M. *et al.* Replacement of an NH(3) by an iminoether in transplatin makes an antitumor drug from an inactive compound. *Mol. Pharmacol.* **58,** 1525–35 (2000).

179. Najajreh, Y. *et al.* Cationic nonsymmetric transplatinum complexes with piperidinopiperidine ligands. Preparation, characterization, in vitro cytotoxicity, in vivo toxicity, and anticancer efficacy studies. *J. Med. Chem.* **49,** 4665–4673 (2006).

180. Behrens, B. C. *et al.* Characterization of a cis -Diamminedichloroplatinum (II) -resistant human ovarian cancer cell line and its use in evaluation of platinum analogues human ovarian cancer cell line and its use in evaluation of platinum analogues. *Cancer Res.* **47,** 414–418 (1987).